

Cone-beam CT-guidance in Interventional Radiology

Sicco J. Braak

Cone-beam CT-guidance in Interventional Radiology

Thesis, Utrecht University, The Netherlands

Copyright © by S.J. Braak, 2012

ISBN	978-90-393-5848-1
Printed by	Printsupport4u, Meppel
Lay out	Roy Sanders, Utrecht
Cover design	Sicco J Braak & Roy Sanders

Publication of this thesis was financially supported by:

Philips Healthcare, C.R. Bard inc., Guerbet Group, Bayer BV, ZGT (raad van bestuur), AZN (raad van bestuur), Microtek Medical BV, Galil-medical, MML-medical, Apriomed AB, iSYS Medizintechnik GmbH, Neorad AS.

The sponsors, who are gratefully acknowledged, had no involvement in any stage of the study design, data collection, data-analysis, interpretation of the study results or the decision to publish study results.

Cone-beam CT-guidance in Interventional Radiology

Cone-beam CT-geleiding in de Interventie Radiologie

(met een samenvatting in het Nederlands)

Proefschrift

ter verkrijging van de graad van doctor aan de Universiteit Utrecht
op gezag van de rector magnificus, prof.dr. G.J. van der Zwaan,
ingevolge het besluit van het college voor promoties in het openbaar te
verdedigen op dinsdag 23 oktober 2012 des middags te 4.15 uur

door

Sicco Jurjen Braak
geboren op 16 juni 1978 te Utrecht.

Promotor: Prof. dr. W.P.Th.M. Mali

Co-promotoren: Dr. M.J.L. van Strijen
Dr. J.P.M. van Heesewijk

To whom this may concern

Contents

General introduction and thesis outline.	11
--	----

Part 1: CBCT-guidance: Phantom studies

Chapter 1	Accuracy Study of Needle Placement in Percutaneous Vertebroplasty: Cone-beam CT-Guidance versus Conventional Fluoroscopy.	19
------------------	---	----

S.J. Braak, K.Zuurmond, Hans C.J. Aerts, M. van Leersum, T.Th.C. Overtoom, J.P.M. van Heesewijk, M.J.L. van Strijen. Accepted pending revision CVIR.

Chapter 2	Cone-beam CT guidance Provides Superior Accuracy for Complex Needle Paths Compared to CT guidance.	35
------------------	--	----

WMH Busser, SJ Braak, MJ Arntz, WKJ Renema, JJ Futterer, MJL van Strijen, YL Hoogeveen, F de Lange, LJ SchultzeKool. Submitted AJR.

Part 2: Clinical application of CBCT-guidance

Chapter 3	Real-Time 3D Fluoroscopy Guidance during Needle Interventions: Technique, Accuracy, and Feasibility.	49
------------------	--	----

S.J. Braak, M.J.L. van Strijen, M. van Leersum, H.W. van Es, J.P.M. van Heesewijk. AJR 2010; 194:W445-451.

Chapter 4	Pulmonary Masses: Initial Results of Cone-beam CT Guidance with Needle Planning Software for Percutaneous Lung Biopsy.	67
------------------	--	----

S.J. Braak, J. Herder, J.P.M. van Heesewijk, M.J.L. van Strijen. CVIR 2011; online 7 December 2011 epub ahead of print; DOI 10.1007/s00270-011-0302-z

Chapter 5	3D Cone-beam CT guidance, a Novel Technique in Renal Biopsy: Results in 41 Patients with Suspected Renal Masses.	83
------------------	--	----

S.J. Braak, H.H.E. van Melick, M.G. Onaca, J.P.M. van Heesewijk,

M.J.L. van Strijen. European Radiology. 2 June 2012 epub ahead of print;

DOI 10.1007/s00330-012-2498-y

Chapter 6	Type II Endoleak Embolization after Endovascular Abdominal Aortic Aneurysm Repair with Use of Real-time Three-dimensional Fluoroscopic Needle Guidance.	99
------------------	---	----

S.J. Braak, L. van Bindsbergen*, M.J.L. van Strijen, J.P.P.M. de Vries. JVIR*

2010; 21:1443-1447 (=contributed equally)*

Part 3: Radiation dose of CBCT-guidance

Chapter 7	Effective Dose during Needle Interventions: Cone-beam CT Guidance Compared with Conventional CT Guidance.	113
------------------	---	-----

S.J. Braak, M.J.L. van Strijen, H.W. van Es, R.A.J. Nievelstein,

J.P.M. van Heesewijk. JVIR 2011; 22:455-461

Chapter 8	Operator Radiation Exposure in Cone-beam CT guidance.	129
------------------	---	-----

S.J. Braak, M.J.L. van Strijen, E. Meijer, J.P.M. van Heesewijk, W.P.Th.M. Mali.

Submitted JVIR.

Part 4: Clinical considerations

Chapter 9	Quantification of Kidney Movement from Supine to Prone Position	149
------------------	---	-----

D. Meek, S.J. Braak, M.J.L. van Strijen, H.W. van Es, J.P.M. van Heesewijk.

Submitted European Radiology

Chapter 10	Cone-beam CT and Real Time 3D Needle Guidance for Biopsy and Needle Interventions: a Pictorial of the Technique and Clinical Indications. <i>M.J.L. van Strijen, S.J. Braak. Submitted for publication</i>	167
	Summary, General Discussion, Implications	183
Appendix	Samenvatting (summary in Dutch)	193
	Authors and affiliations	199
	Review committee	203
	List of publications	207
	Acknowledgements (dankwoord)	213
	Curriculum Vitae	219



General Introduction and
Thesis Outline

Introduction

The development of Cone-beam CT-guidance (CBCT-guidance) started as any other 'X-ray-using-technique' with the fundamental discovery of the X-ray in 1895 by Wilhelm Conrad Röntgen [1].

In angiographic interventions the introduction of the floating table in 1973 was one step in the process of viewing different parts of the patient, but the major change came when tube and image intensifier angulation was further improved by also enabling rotation. This eventually resulted via the U-arm in the C-arm in 1989 with full rotation and angulation around the patient now being possible.

For angiography the development of digital subtractions angiography (DSA) was very important [2,3] and for image-guided treatment many new possibilities followed quickly like bolus chase, road mapping and eventually rotational angiography (RA) in 1989. This technique was perfected resulting in 3D-rotational angiography (3D-RA), introduced around 1998 [4]. With this technique the images of the region of interest are acquired in multiple directions by rotating the C-arm over 180 degrees. With 'back projection' a volume of the contrast-rich structures was reconstructed making it possible to view the data from any angle [5,6].

The next great leap was the development and introduction of the flat panel detector (FPD) in 1995 [3]. The image intensifier with television was replaced by a solid-state detector with direct production of a digital electronic signal [7,8]. Because of the construction of the FPD the fluoroscopy images were not subjected to distortion, as was the case in image intensifier systems. Further advantages were the smaller size of the equipment setup, the more reliable operation and the direct production of the electronic signal. Potentially the radiation dose was lower than in image intensifier systems and is not different in the different Field of View's (FOV) [3,7,8-11]. Among the disadvantages of FPD systems is the fact that the separate elements of the FPD can degrade, resulting in decreased image quality. Also FPD systems are more sensitive to temperature changes and mechanical shocks. The spatial resolution of the FPD systems is directly influenced by the size of the separate elements of the FPD [7].

One of the latest evolutions to the modern FPD fluoroscopy systems is

rotational soft tissue cone-beam imaging. Evolving from 3D-RA there was also an increasing need for viewing low-contrast structures in a 3D volume and having CT-like imaging available. In the early days an angio-CT system was developed, combining the conventional angiographic system with an in-room CT-scanner. This system never became popular because of the high costs [12]. A better solution was offered by rotating conventional angiographic systems >180 degrees. In this way the cone-beam shaped X-ray could be reconstructed in a 3D CT-volume (cone beam CT imaging, CBCT). Feldkamp et al. [13] were the first to describe a CBCT system. This system however used an image intensifier, which had a very limited spatial resolution. With the introduction of FPD's, that have significantly better contrast and spatial resolution, a cone-beam CT with sub millimeter isotropic volume reconstructions after a single rotation around the patient was available [14]. This CBCT proved to have additional clinical value to conventional angiographic fluoroscopy for example in suspected intracranial hemorrhage, visualisation of highly flexible, minimal radiopacity stents and in the perfusion of organs [15-17]. The further development of CBCT and its clinical use is still an ongoing process. Where the first CBCT's took 20 seconds to acquire, these rotations are now possible in less than 6 seconds. The low-contrast detectability of CBCT is now around 5 Hounsfield Units (HU) [18]. As stated by Orth et al. [12] and Hirota et al. [17], CBCT has a potential impact on interventional radiology by allowing all types of interventional procedures to be performed in the interventional suite, especially with the addition of dedicated needle guidance software (navigation) to the interventional angiographic C-arm fluoroscopy system in 2007: **Cone-beam CT-guidance!**

Using CBCT-guidance in a routine clinical setting has many advantages. The availability of real-time fluoroscopic overlay makes it possible to biopsy moving targets more accurately than with step-and-shoot modalities. For difficult to reach lesions (e.g. lesions in the lower thoracic regions, in subphrenic locations or in the upper pole of the kidneys) CBCT-guidance offers a competitive (perhaps even better) method, compared to existing methods, to perform the needle procedure. Using conventional CT-guidance for needle interventions is of course possible but this often requires longer fluoroscopy times, larger volumes to scan in order to follow the needle path, and good 3D insight of the operator. Furthermore the workspace is much better in CBCT-guidance

compared to CT-guidance (even when there is a dedicated large bore CT). Over the past few years interventional radiology has seen a considerable shift toward non-vascular interventions and especially toward interventional oncology. For positioning biopsy needles but also for needle interventions in ablation procedures there is an increasing need for reliable and accurate image guidance in interventional procedures.

Thesis Outline

This thesis is divided in four parts. Part I focuses on the evaluation of Cone-beam CT-guidance in percutaneous needle interventions in phantoms with a comparison to conventional fluoroscopy (**Chapter 1**) and a comparison to conventional CT-guidance (**Chapter 2**). In these chapters we mainly focused on the accuracy, procedure-time, fluoroscopy-time and Dose-area Product (DAP). The second part of this thesis describes the technique, accuracy and feasibility in a clinical setting (**Chapter 3**), with special focus on percutaneous transthoracic needle guidance (**Chapter 4**), kidney interventions (**Chapter 5**) and the use of cone-beam CT-guidance in the treatment of type II endoleaks (**Chapter 6**).

Part III of this thesis highlights the radiation burden of this system when using CBCT-guidance. In **Chapter 7** the effective radiation dose for the patient was investigated and compared to the resulting dose when using conventional CT-guidance. **Chapter 8** describes the results of the scatter radiation dose measurements during Cone-beam CT-guidance procedures for the operator and the effect of shielding on the scatter radiation dose.

The last part of this thesis outlines some important clinical features of the navigation software. Since it is possible to import previously acquired CT- or MRI data, the problem of the shift of major upper abdominal organs arises when initially a supine position is used in these imported scans and a prone position is needed for performing the intervention. The software enabling the needle path planning was used to quantify specifically the movement of the kidney between prone and supine patient positions (**Chapter 9**). In the last **chapter (10)** this technique is evaluated in different types of procedures and different anatomic locations and tips and tricks are provided based on our experience in over 600 procedures performed.

References:

1. Röntgen W. C. : Ueber eine neue Art von Strahlen. Mitteilung 1. Sitzungsberichte d. phys.-med. Gesellsch. z. Würzburg., 1895, pp. 132-141. English translation in Science, Feb. 14, 1896.
2. Harrington DP, Boxt LM, Murray PD. Digital Subtraction Angiography: Overview of Technical Principles. *AJR Am J Roentgenol* 1982; 139:781-786.
3. Körner M, Weber CH, Wirth S, Pfeifer KJ, Reiser MF, Treitl M. Advances in digital radiography: Physical principles and system overview. *Radiographics* 2007; 27:675-686.
4. Anxionnat R, Bracard S, Macho J, Da Costa E, Vaillant R, Launay L, Troussat Y, Romeas R, Picard L. 3D angiography clinical interest. First applications in interventional neuroradiology. *J Neuroradiol* 1998; 25:251-262.
5. Hofman JAM. The art of medical imaging: Philips and the evolution of medical x ray technology. *Medicamundi* 2010; 54(1):5-21.
6. Bridcut RR, Winder RJ, Workman A, Flynn P. Assessment of distortion in a three-dimensional rotational angiography system. *BJR* 2002; 75:266-270.
7. Nickelhoff EL. The AAPM/RSNA Physics Tutorial for Residents: Physics of flat-panel fluoroscopy systems. *Radiographics* 2011; 31:591-602.
8. Cowen AR, Davies AG, Sivananthan MU. The design and imaging characteristics of dynamic, solid-state, flat-panel x-ray image detectors for digital fluoroscopy and fluorography. *Clin Radiol* 2008; 63:1073-1085.
9. Suzuki S, Furui S, Kobayashi I et al. Radiation dose to patients and radiologists during transcatheter arterial embolization: comparison of a digital flat-panel system and conventional unit. *AJR Am J Roentgenol* 2005; 185:855-859
10. Vano E, Geiger B, Schreiner A et al. Dynamic flat panel detector versus image intensifier in cardiac imaging: dose and image quality. *Phys Med Biol* 2005; 50:5731-5742
11. Trianni A, Bernardi G, Padovani R. Are new technologies always reducing patient doses in cardiac procedures? *Radiat Prot Dosimetry* 2005; 117:97-101.
12. Orth RC, Wallace MJ, Kuo MD. C-arm Cone-beam CT- General Principles and Technical Considerations for Use in Interventional Radiology. *J Vasc Interv Radiol* 2008; 19:814-821.
13. Feldkamp LA, Davis LC, Kress JW. Practical cone-beam algorithm. *J Opt Soc Am* 1984; 1(6):612-619.
14. Ning R, Chen B, Yu R, Conover D, Tang X, Ning Y. Flat panel detector-based cone-beam volume CT angiography imaging- system evaluation. *IEEE trans med imaging* 2000; 19(9):949-963.
15. Fahrig R, Dixon R, Payne T, Morin RL, Ganguly A, Strobel N. Dose and image quality for a cone-beam C-arm CT system. *Med Phys* 2006; 33:4541-4550

16. Benndorf et al. Angiographic CT in cerebrovascular stenting. *Am J of Neuroradiol* 2005; 26:1813-1818.
17. Hirota S, Nakao N, Yamatomo S, Kobayashi K, Maeda H, Ishikura R, Miura K, Sakamoto K, Ueda K, Baba R. Cone-Beam CT with Flat-Panel-Detector Digital Angiographic system early experience in abdominal interventional procedures. *Cardiovasc Interv Radiol* 2006; 29:1034-1038.
18. Gupta R, Grasruck M, Suess C, Bartling SH, Schmidt B, Stierstorfer K, Popescu S, Brady T, Flohr T. Ultra-high resolution flat-panel volume CT: fundamental principles, design architecture, and system characterization. *Eur Rad* 2006; 16:1191-1205.



Sicco J. Braak¹ • Kirsten Zuurmond² • Hans C.J. Aerts² • Marc van Leersum¹ • Timotheus T.Th Overtoom¹ • Johannes P.M. van Heesewijk¹ • Marco J.L. van Strijen¹

¹Department of Radiology, St Antonius Hospital, Nieuwegein, The Netherlands

²Department of Clinical Development Philips Medical, Best, The Netherlands

Accepted pending revision Cardiovasc Intervent Radiol

Chapter 1

Accuracy Study of Needle Placement in
Percutaneous Vertebroplasty:

Cone-beam CT-Guidance versus Conventional Fluoroscopy

Abstract

Objective:

To investigate the accuracy, procedure-time, fluoroscopy-time and dose-area-product (DAP) in needle placement in percutaneous vertebroplasty (PVP) between CBCT-guidance and fluoroscopy.

Summary of Background Data:

Accurate needle placement in PVP is crucial and conventionally performed using fluoroscopy. More accurate needle placement technique can possibly reduce complications and increase success rate of PVP. Recently, a sophisticated technique to guide needles has been developed. This is achieved by a combination of cone-beam CT (CBCT), navigation software and real-time fluoroscopy.

Materials and Methods:

On four spine phantoms with 11 vertebrae (Th7-L5), four interventional radiologists (two experienced CBCT-guidance and two non-experienced) punctured all vertebrae bipedicular. Each side was randomized between CBCT-guidance and fluoroscopy. The placement of the needle had to be to a specific target point. After the procedure a CBCT was performed to determine the accuracy, procedure-time, fluoroscopy-time and dose-area-product (DAP). Analysis of the difference between the method and experience was performed.

Results:

Mean accuracy using CBCT-guidance (2.61 mm) was significantly better compared to fluoroscopy (5.86 mm) ($p < 0.0001$). Procedure-time was in favor of fluoroscopy (7.39 vs 10.13 min $p = 0.001$). Fluoroscopy-time during CBCT-guidance procedures was lower, but this difference is not significant (71.3 vs 95.8 sec; $p = 0.056$). The DAP-values for CBCT-guidance and fluoroscopy were 514 and 174 mGy·cm², respectively ($p < 0.0001$). There was a significant difference in favor of the experienced CBCT-guidance users in accuracy in both methods, procedure-time of the CBCT guidance and of the added DAP-values of the fluoroscopy.

Conclusions:

CBCT-guidance allows users to perform PVP procedure more accurately at the cost of higher patient-dose and longer procedure time. As procedural complications are directly related to the accuracy of the needle placement, improvements of accuracy are clinically relevant. Training in CBCT-guidance is essential to achieve higher accurate and decrease procedure time / dose values.

Introduction

To stabilize and reduce pain of a fractured vertebra, the technique of percutaneous Vertebroplasty (PVP) has been developed. During the PVP procedure medical grade cement is injected via a large bore needle into a fractured vertebra body. It is increasingly used as treatment for patients with symptomatic vertebral compression fractures caused by osteoporosis (270,000 fractures yearly in the USA), but may also provide pain relief for patients with vertebral hemangiomas and pathological fractures from vertebral body tumors or bone metastases. It has been shown that immediate pain relief and improvement of mobility, function and stature after PVP is significantly better in the short term compared with optimal pain medication treatment [1-3].

Although, the success rate for this procedure in treating osteoporotic fractures is 73 to 90 percent, complications occur in about 1-10% of the cases, and they can be severe [4]. Complications include postoperative mortality (rare), pulmonary embolism and spinal cord lesions. They are often related to leakage of cement outside the target vertebral body into adjacent anatomic structures and cause problems such as nerve root irritation or cement embolization to the lungs via the paravertebral venous plexus [5]. Accurate needle placement is crucial for the procedures success and is conventionally performed using fluoroscopy. More accurate and reliable needle placement technique can possibly reduce complications and increase the success rate of PVP.

Recently, a sophisticated technique to guide the needle placement has been developed. In the interventional radiology suite this is achieved by using Cone-beam CT (CBCT), navigation software and real-time fluoroscopy guidance.

The aim of this study is to investigate the accuracy of CBCT with guidance software (CBCT-guidance) in PVP compared to the use of only fluoroscopy guidance. Besides the accuracy we focused on parameters like procedure time, dose (dose area product (DAP)) and the effect of experience in using CBCT-guidance.

Methods and materials

On four separate spine phantoms (Sawbones Europe AB, Sweden) with 11 vertebrae each (Th7-L5), four interventional radiologists punctured all

vertebra with a bipedicular approach at different moments. All radiologists had experience with PVP using fluoroscopy. Two were experienced users of CBCT-guidance (each >200 procedures in clinical setting). In every vertebra two needles (Osteo-site® Vertebroplasty Needle 13 G, Cook Medical Inc, Bloomington, USA), were placed, on one side with the use of only fluoroscopy, and on the other side with CBCT guidance. The level of the vertebra and the method of use were at random selected (*Figure 1*).

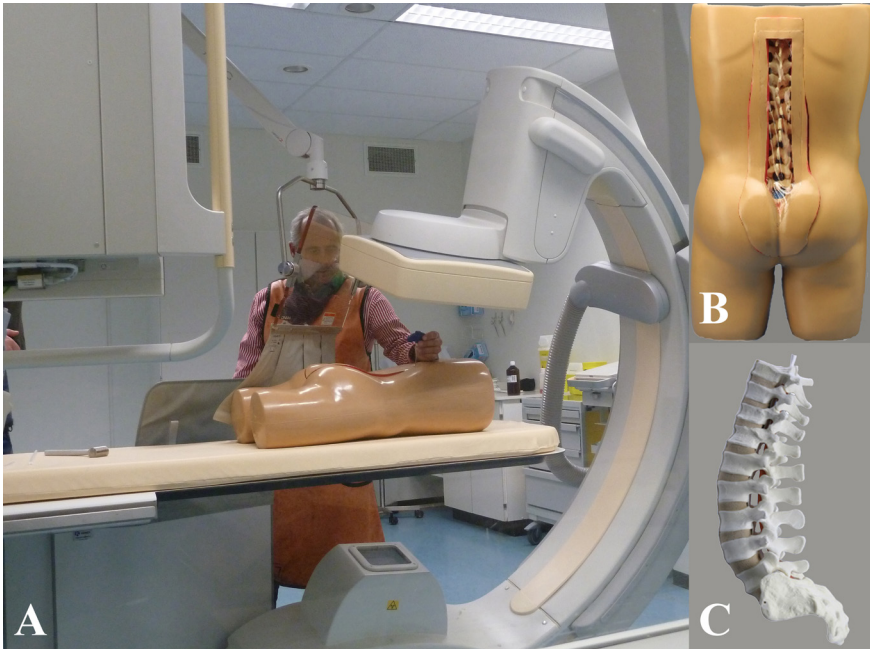


Figure 1. A) Set-up of the procedure. B) Body phantom with a see-thru coverage of the spine phantom. During the procedure the spine phantom was not visible because of a closed coverage. C) Lateral view of the spine phantom (Sawbones Europe AB, Sweden).

Due to the development of flat panel detector in C-arm fluoroscopy systems it is possible to make a Cone-beam CT. Merging the CBCT with dedicated guidance software and real-time fluoroscopy the system is suitable for needle interventions [6,7]. We used the Allura FD20 C-arm interventional system with CBCT-guidance (XperGuide, Philips Healthcare, The Netherlands). In CBCT-guidance a CBCT is made and within the reconstructed volume, the user draws a needle path from the target to the skin, avoiding vital anatomic structures. Once the virtual trajectory is determined, the optimal imaging angulation is calculated and programmed instantly with automated coupling with the

C-arm. The 3D data set and virtual trajectory are co-registered with the real-time fluoroscopy image. The needle path (with a 5 mm safety margin) is projected on to the fluoroscopy image, producing a highly accurate real-time image of needle positioning and progression toward the target. The needle is fixed in the proper angulation at 'entry point view' and with the 'progress view' the progress of the needle to the target is visualized (Figure 2).

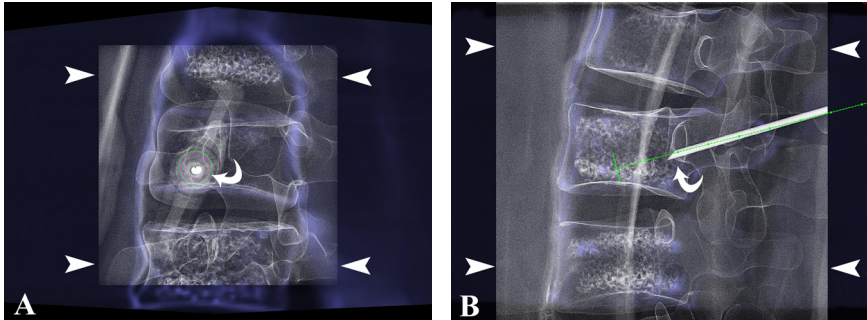


Figure 2. Procedural images; overlay images of the CBCT slice (blue background) and the fluoroscopy image (gray box, marked with arrowheads). The needle is indicated with a curved arrow. A) Shows the entrypoint view and B) shows the progress view.

The defined target point is at the anterior 1/3 border of the vertebral body and on 1/3 of the lateral sides of the vertebral body. The height of the tip is at the lower 1/3 of the vertebral body (Figure 3). To measure this distance [in mm] a control CBCT was performed after the placement of the needle, with the needle still in place. The distances were measured in three dimensions using the measurement tool. A failure was defined as placement of the needle (-tip) outside of the vertebral body, checked during the control CBCT or when

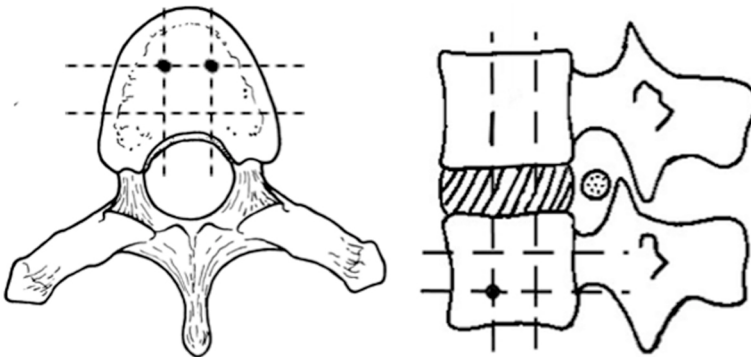


Figure 3. The designated target point in the vertebra (axial and sagittal view), marked as a black dot.

an iatrogenic fracture occurred due to the placement of the needle. The dose values from this control CBCT were not included in the total dose measured with the dose area product (DAP) value [mGy.cm²], since this extra scan is not necessary in a regular percutaneous vertebroplasty procedure.

The following parameters were recorded for each needle placement and are presented with mean and standard deviation (SD) for the two different navigational techniques:

- The accuracy of the needle placement [mm]
- Procedure time: defined as the time from the start of the fluoroscopy until the decision of the interventional radiologist that the needle is in place [min]
- The DAP value (the DAP is split up in the contribution of fluoroscopy and total DAP including the planning CBCT) [mGy.cm²]
- Fluoroscopy time [seconds]

Data analysis was performed using Excel 2007 (Microsoft, Redmond, Washington) and Minitab software (version 15.1.1.0). To measure statistical significance the Two-sample T-test was used to compare the average difference between the two techniques. Differences were considered significant when the p-value was <0.05. Differences were also measured between the two interventional radiologists with experience in using CBCT-guidance as a navigation tool (both done >200 procedures in clinical practice) and the two interventional radiologists that did not have any experience with CBCT-guidance.

Results

All four interventional radiologists punctured each their own spine phantom with 11 vertebrae on both sides. So in total 88 PVP procedures were performed, half with CBCT-guidance and the other half with conventional fluoroscopy. Two of the interventional radiologists placed all the needles successfully; one interventional radiologist had one failure under fluoroscopic guidance. One interventional radiologist had 5 failures in placing the needles. Three of these were done using CBCT-guidance, and two with fluoroscopic guidance. All failures were excluded in the statistical analysis except for the success rate. Overall success rate in needle placement is 86.4 %, with no difference between the two navigation methods.

Guidance by CBCT-guidance compared to guidance by fluoroscopy

A summary of the data is presented in *Table 1*. The mean (SD) accuracy when placing the needle under CBCT-guidance was 2.61 (1.72) mm. This gives a significant difference (p -value < 0.0001) to fluoroscopy guidance with a mean of 5.17 (3.35) mm (*Figure 4*).

Table 1. Detailed information for needle placement in percutaneous vertebroplasty using CBCT-guidance or Fluoroscopy and the difference between experienced CBCT-guidance users versus inexperienced users in needle placement.

	Method	Mean (SD)	p-value	Experienced	Inexperienced	p-value
				Mean (SD)	Mean (SD)	
Accuracy [mm]	CBCT-guidance	2.61 (1.72)	0.000	1.95 (1.18)	3.41 (0.46)	0.010
	Fluoroscopy	5.17 (3.35)		3.41 (1.96)	6.93 (3.56)	0.001
Procedure time [min]	CBCT-guidance	10.23 (3.99)	0.003	7.73 (2.25)	12.73 (3.81)	0.000
	Fluoroscopy	7.66 (3.77)		6.73 (3.64)	8.59 (3.75)	0.102
DAP total [mGy·cm ²]	CBCT-guidance	514 (134)	0.000	468.1 (91.3)	562 (156)	0.019
	Fluoroscopy	174 (113)		134 (114)	215 (100)	0.014
DAP fluoroscopy [mGy·cm ²]	CBCT-guidance	101.4 (94.6)	0.097	64.2 (29)	144 (124)	0.009
	Fluoroscopy	134.1 (91)		98.1 (88.3)	170.1 (80.2)	0.006
Fluoroscopy time [sec]	CBCT-guidance	71.3 (59.2)	0.056	44.2 (22.7)	100.0 (72.3)	0.002
	Fluoroscopy	95.8 (61.9)		68.3 (35.0)	123.4 (70.8)	0.002

The mean (SD) procedure time of the CBCT-guidance navigation had an average procedure time of 10.13 (4.00) minutes, that was significantly longer compared to fluoroscopy guidance with an average procedure time of 7.39 (3.67) minutes (p -value = 0.001); see *Figure 5*.

The mean total DAP value of placing a needle with the CBCT-guidance technique was 514 (134) mGy·cm² compared to 174 (113) mGy·cm² when using only fluoroscopy to place the needles (p -value < 0.0001). Difference in DAP added to the procedure due to fluoroscopy is not significant (p -value = 0.097) when comparing the two navigation techniques. The fluoroscopy time did not show a significant difference (p -value = 0.056) between the two techniques with a mean (SD) for the CBCT-guidance navigation of 71.3 (59.2) seconds compared to 95.8 (61.9) seconds in using fluoroscopy for placing the needles.

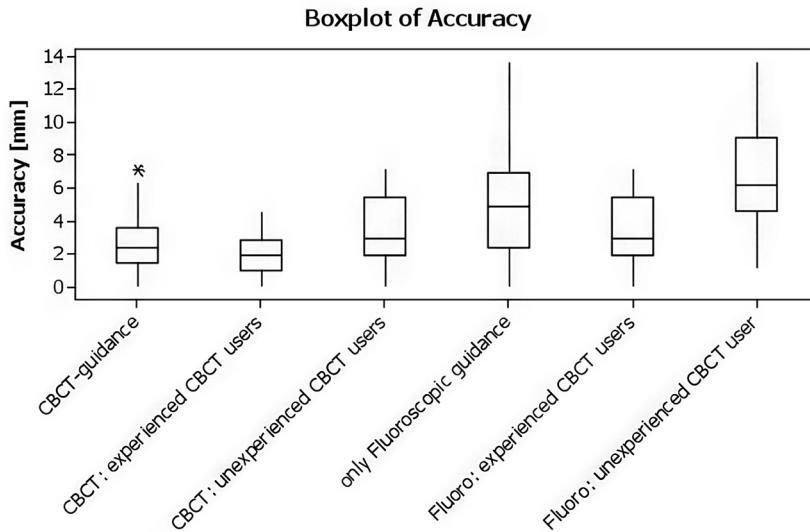


Figure 4. Boxplot of the accuracy of the needle placement. Horizontal line is the mean value; the box is an interquartile range box; the vertical line extends to the maximum data point within 1.5 box heights from the top of the box, the asterisk is an observation that is beyond the upper or lower whisker

Experienced CBCT-guidance users compared to inexperienced CBCT-guidance users

Data is presented in *Table 1*. When comparing the accuracy using only fluoroscopy guidance there was a significant difference (p -value = 0.001) for experienced CBCT-guidance users with a mean (SD) of 3.41 (1.96) mm compared to inexperienced users with a mean (SD) of 6.93 (3.56) mm. When using CBCT guidance as a navigational tool, a significant difference (p -value = 0.010) in accuracy was found for experienced users, 1.95 (1.18) mm, compared to inexperienced CBCT-guidance users, 3.41 (1.96) mm (*Figure 4*).

The mean procedure time using the CBCT-guidance tool for navigation between experienced users (mean (SD) 7.73 (2.25) min) and inexperienced users (mean (SD) 12.73 (3.81) min) of CBCT-guidance was significant different (p -value < 0.001). This difference was not significant (p -value = 0.102) when using fluoroscopy guidance (*Figure 5*). When comparing the dose added to the procedure by fluoroscopy there was a significant difference between experienced and inexperienced users of CBCT-guidance in both methods. (CBCT-guidance (p = 0.009) and conventional fluoroscopy (p = 0.006)) (*Table 1*). The difference of DAP coming from fluoroscopy for both the experienced and inexperienced users between the two techniques was not significant (p -value = 0.092 and 0.409 respectively).

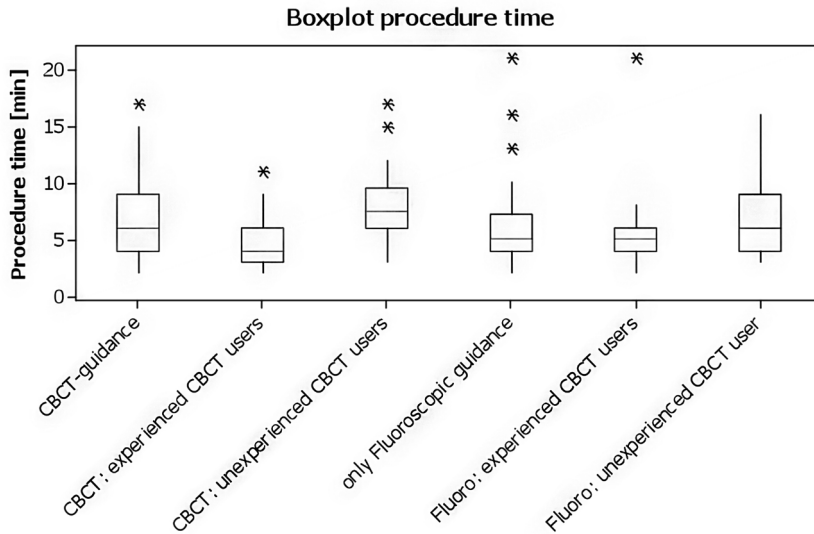


Figure 5. Boxplot of the procedure time of the needle placement. Horizontal line is the mean value; the box is an interquartile range box; the vertical line extends to the maximum data point within 1.5 box heights from the top of the box, the asterisk is an observation that is beyond the upper or lower whisker

Discussion

This study shows that needle placement for PVP with CBCT-guidance is significantly more accurate than placement of the needle with the use of fluoroscopy only. Under fluoroscopy the average distance of the needle tip to the target is over the 5 mm safety margin, while the average needle-tip-to-target distance when using CBCT-guidance was 2.61 (1.72) mm. Furthermore the differences in observations and results between the experienced CBCT-guidance users versus inexperienced CBCT-guidance users suggest that training with CBCT-guidance improves the outcome.

The use of CBCT without guidance software in PVP has been reported in literature. Cone-beam CT aids correct evaluation of vertebral fractures and vacuum phenomena in adjacent disks before PVP and can detect cement leakage after PVP [8]. Compared to conventional CT and biplane fluoroscopy, CBCT offers improved anatomic visualization allowing high accuracy instrumentation placement, improving procedure results and minimizing risk of complications [9]. The results suggest that high-quality CBCT is reliable and safe as a single technique for PVP guidance, control and post-procedure assessment.

It permits fast and cost-effective procedures avoiding multi-modality imaging [10]. Another case reported on the use of CBCT where the most suitable point for needle insertion was determined by using a pilot needle during a second rotational run [11].

However these studies only use the CBCT for start and outcome imaging. Our study uses the additional needle planning's software that shows an additional value.

Maeda et al. [12] presented their experience with experimental phantoms using the CBCT-guidance system. They reported technical success of 93.8% (15/16) for reaching the desired target successfully on the first needle pass. The mean distance from the final needle tip to the target was 3.83 +/- 1.92 mm in the successful passes, which are comparable result to our study.

Clinical experience using CBCT-guidance with needle planning guidance was reported in the following two studies. Tam et al. [13] used needle path overlay to puncture 12 vertebral levels in 10 patients. Technical success rates were 92% for both distance from planned path and distance from midline to final needle tip. The success rate was 100% when distance from needle tip to anterior 1/3 border of the vertebral body was measured, and 75% when distance from target to needle tip was measured. We previously reported on 145 needle interventions performed using CBCT-guidance guidance on 139 patients with a 100% technical success (within 5 mm safety margin) of which 18 procedures were spinal interventions [7].

Our result shows that CBCT-guidance causes a longer procedure time for a PVP procedure, which is a potential disadvantage. Since there is no statistical significant difference in procedure time between the experienced and inexperienced CBCT-guidance users when using only fluoroscopy guidance, the extra procedure time is due to acquisition and planning of the needle trajectory. Training in CBCT-guidance can decrease the procedure time as can be suggested by the results of the comparison between the experienced and inexperienced users.

Also CBCT-guidance has a significant higher dose value compared to fluoroscopy, which is a disadvantage too. This is because the CBCT adds extra dose to the procedure. The reduction of the fluoroscopy dose during a CBCT-guidance is lower than the added value of the CBCT. Miller et al. [14] reports that in general the PVP procedures do not have the issue that the total dose of the

procedure is too high, especially compared to vascular procedures in general in interventional radiology. We believe that the additional dose of a CBCT in a PVP procedure is justifiable because of the additional value of the CBCT (e.g. evaluation of the fracture, determine the target position of the needle, evaluation of cement distribution) and the significant higher accuracy.

The dose received by the staff could be something to worry about. As the staff is not exposed during the acquisition of the CBCT, the only contribution for the staff dose is the fluoroscopy. Using CBCT-guidance the fluoroscopy time is shorter than during fluoroscopy guidance so the staff dose will be lower than during the conventional fluoroscopy method [14,15]. The exact dose for the operator was not recorded in our study. There is a significant difference in DAP added to the procedure by fluoroscopy when using CBCT-guidance when comparing experienced CBCT-guidance users with the inexperienced CBCT-guidance users. This indicates again that training on the CBCT-guidance systems also increases the optimal usage of the X-ray equipment.

The use of CBCT in combination with electromagnetic tracking-based navigation systems allows a precise needle positioning in the vertebra [16]. In the future C-arm CT based navigation systems will probably allow simplified and safer complex interventions and simultaneously reduce radiation exposure [17].

The main complications during PVP have to do with cement leakage. Cement leakage can be caused by over augmentation [18]. Such overfilling also renders the system more sensitive to the placement of the cement because asymmetric distributions with large fills can promote single-sided load transfer. These results suggest that large fill volumes may not be the most biomechanically optimal configuration, and an improvement might be achieved by use of lower cement volume with symmetric placement [19]. This shows that the placement of the needle and distribution of the cement is important. Studies showed that the middle third of the vertebral body is the optimal position regarding cement distribution. It is possible to reliably determine the position of needles in vertebral bodies with the aid of an intraoperative 3D scan. This can lead to a reduction in complications associated with puncture errors in PVP [20]. CBCT-guidance can probably have an additional value for the determination of the target position of the needle and therefore for the distribution of the cement.

There are some limitations to this study; we used a phantom spine in which the vertebra and pedicle structure are standardized. In clinical practice there will be

deformation of the vertebra / pedicles, however to excluded these variability for comparison of the two methods we chose deliberately for this setup. Despite the potentially more difficult to access clinical vertebrae we believe the same results will apply with different target configuration. The next step will be to perform a study in cadaver or in clinical setting to verify our results. Tan et al. [13] described the first clinical results. They report a lower success but they only had PVP performed on 10 patients. The reported DAP values are of no clinical value, but give an estimation of the ratio between CBCT-guidance and fluoroscopy.

Conclusion:

CBCT-guidance allows users to perform PVP procedure more accurately at the cost of more dose and procedure time. As procedural complications are directly related to the accuracy of the needle placement, improvements of accuracy are clinically relevant. Training in CBCT-guidance is essential to achieve higher accuracy and decrease procedure time / dose values.

References

1. Voormolen MH, Mali WP, Lohle PN, et al. Percutaneous vertebroplasty compared with optimal pain medication treatment: short-term clinical outcome of patients with subacute or chronic painful osteoporotic vertebral compression fractures. The VERTOS study. *AJNR Am J Neuroradiol* 2007; 28(3):555-60.
2. Jarvik JG, Hollingworth W. VERTOS: A Step in the Right Direction. *AJNR Am J Neuroradiol* 2007; 28(3):561-2.
3. Klazen CA, Verhaar HJ, Lampmann LE. VERTOS II: percutaneous vertebroplasty versus conservative therapy in patients with painful osteoporotic vertebral compression fractures; rationale, objectives and design of a multicenter randomized controlled trial. *Trials* 2007; 8:33.
4. Predey TA, Sewall LE, Smith SJ. Percutaneous vertebroplasty: new treatment for vertebral compression fractures. *Am Fam Physician* 2002; 66(4):611-5.
5. Venmans A, Lohle PN, van Rooij WJ, et al. Frequency and outcome of pulmonary polymethylmethacrylate embolism during percutaneous vertebroplasty. *AJNR Am J Neuroradiol* 2008; 29(10):1983-5.
6. Racadio JM, Babic R, Homan R, et al. Live 3D Guidance in the Interventional Radiology Suite. *AJR Am J Roentgenol* 2007; 189:W357-W364.
7. Braak SJ, van Strijen MJ, van Leersum M, et al. Real-Time 3D fluoroscopy guidance during needle interventions: technique, accuracy, and feasibility. *AJR Am J Roentgenol* 2010; 194(5):W445-51.
8. Hiwatashi A, Yoshiura T, Noguchi T, et al. Usefulness of cone-beam CT before and after percutaneous vertebroplasty. *AJR Am J Roentgenol* 2008; 191(5):1401-5.
9. Powell MF, DiNobile D, Reddy AS. C-arm fluoroscopic cone beam CT for guidance of minimally invasive spine interventions. *Pain Physician* 2010; 13(1):51-9.
10. Pedicelli A, Rollo M, Piano M, et al. Percutaneous vertebroplasty with a high-quality rotational angiographic unit. *Eur J Radiol* 2009; 69(2):289-95.
11. Tenjin H, Mandai A, Umebayashi D, et al. Percutaneous vertebroplasty under three-dimensional radiography guidance. Technical note. *Neurol Med Chir (Tokyo)* 2009; 49(4):179-83.
12. Maeda N, Osuga K, Higashihara H, et al. Abstract No. 237. A Novel Cone-Beam CT Guided Interventions by XperGuide: Accuracy and Feasibility in a Phantom Model. *J Vasc Interv Radiol* 2008; 19(2):S90.
13. Tam AL, Mohamed A, Pfister M, et al. C-arm cone beam computed tomography needle path overlay for fluoroscopic guided vertebroplasty. *Spine* 2010; 35(10):1095-9.
14. Miller DL, Balter S, Cole PE, et al. Radiation doses in interventional radiology procedures: the RAD-IR study: part I: overall measures of dose. *J Vasc Interv Radiol* 2003; 14(6):711-27.

15. Luchs JS, Rosioreanu A, Gregorius D, et al. Radiation Safety during Spine Interventions. *J Vasc Interv Radiol* 2005; 16:107-11.
16. Hoheisel M, Skalej M, Beuing O, et al. Kyphoplasty Interventions using a Navigation System and C-arm CT data: First Clinical Results. *Medical Imaging 2009: Physics of Medical Imaging*, 2009; 7258:E1-8.
17. Becker HC, Meissner O, Waggershauser T. C-arm CT-guided 3D navigation of percutaneous interventions. *Radiologe* 2009; 49(9):852-5.
18. Limthongkul W, Karaikovic EE, Savage JW, et al. Volumetric analysis of thoracic and lumbar vertebral bodies. *Spine J* 2010; 10(2):153-8.
19. Liebschner MA, Rosenberg WS, Keaveny TM. Effects of bone cement volume and distribution on vertebral stiffness after vertebroplasty. *Spine* 2001; 26(14):1547-54.
20. Beck M, Mittlmeier T, Gierer P, et al. Intraoperative Position Determination of Bone Cement Trocars by 3-dimensional Imaging in Patients With Osteoporotic Vertebral Fractures. *J Spinal Disord Tech* 2010; 23(7):E16-23.



*Wendy MH Busser¹ • Sicco J Braak² • Mark J Arntz¹ • W Klaas Jan Renema¹ • Jurgen J Futterer¹
• Marco JL van Strijen² • Yvonne L Hoogeveen¹ • Frank de Lange¹ • Leo J SchultzeKool¹*

1 Department of Radiology, Radboud University Nijmegen Medical Centre, The Netherlands

2 Department of Radiology, St. Antonius Hospital Nieuwegein, The Netherlands

Submitted AJR Am J of Roentgenol

Chapter 2

Cone-beam CT guidance Provides
Superior Accuracy for Complex Needle
Paths Compared to CT guidance

Abstract

Objective

To determine accuracy of cone-beam CT (CBCT) guidance and CT guidance in reaching small targets in relation to needle path complexity in a phantom.

Materials and Methods

CBCT guidance combines 3-dimensional CBCT imaging with fluoroscopy overlay and needle planning software to provide real-time needle guidance.

The accuracy of needle positioning was assessed for inplane, angulated and double angulated needle paths. Four interventional radiologists reached four targets along the three paths using CBCT and CT guidance.

Accuracies were compared between CBCT and CT for each needle path, and between the three approaches within both modalities. The effect of user experience in CBCT guidance was also assessed.

Results

Accuracies for CBCT are significantly better than CT for the double angulated needle path (2 vs. 7 mm, $p < 0.001$). Angulated and double angulated CT guided needle placements show significantly decreased accuracies compared to inplane placements. CBCT guidance showed no significant differences between the three approaches.

For double angulated needle paths, experienced CBCT users show better accuracy than less experienced users (2 vs. 3 mm, $p = 0.003$).

Conclusion

In terms of accuracy, CBCT is the preferred modality, irrespective of the level of experience, for more difficult guidance procedures requiring double angulated needle paths.

Introduction

Needle guidance for puncture or other minimally invasive procedures is increasing in standard interventional radiology practice. In local therapy procedures, such as percutaneous ablations, accurate placement of one or more needles is important in order to provide effective treatment [1]. Especially in treatment or biopsy procedures of small lesions, the tip of the needle needs to be placed within a range of millimeters of the target point. The role of image guidance therefore becomes more significant as aid in accurate percutaneous needle placement [2].

Currently, most needle placement procedures are performed using computed tomography (CT) guidance, fluoroscopy or ultrasound [3]. CT images provide good visualization of the target and surrounding tissues. For needle guidance, however, CT has limitations mainly because it does not allow real-time feedback on needle progression. For semi-real-time imaging within the CT scanner, CT-fluoroscopy can be used at the expense of higher patient and operator radiation dose [4].

Fluoroscopy in the angio suite, on the other hand, provides optimal patient accessibility and real-time imaging of needle progression but is limited to 2-dimensional visualization. A radiation-free technique that also provides real-time imaging is ultrasound. However, the accuracy is operator dependent and, due to ultrasound's low penetration depth, the area of use is restricted to superficial targets and moderate-sized patients [3].

New techniques combining cone-beam CT (CBCT) and fluoroscopy with dedicated needle guidance software within an angiography C-arm system aim to overcome the disadvantages of CT and allow real-time 3-dimensional needle guidance in the interventional suite [5].

Several authors described the use of this CBCT with navigational tools in various types of procedures [6-15]. Braak et al. [10] describe effective patient dose of CBCT guidance procedures to be 13-42% compared to CT guidance for abdominal and thoracic procedures. However, up until now the accuracy of CBCT guidance for reaching small (millimeter-sized) targets has not been addressed specifically.

The purpose of our phantom study was to determine and compare the accuracy of CBCT and CT guidance in reaching small targets by paths with different levels of complexity under standardized conditions.

Materials and methods

Phantom

To analyze accuracy, a modified model 057 Interventional 3D Abdominal Phantom (CIRS Inc., Norfolk, USA) was used for simulating abdominal needle placements in a standardized setting. The phantom represents a small adult abdomen (range T9/T10-L2/L3) and consists of materials mimicking tissues in CT imaging. Four 2.3 mm spheres (CT spots #119, Beekley, Bristol, USA) acting as targets were placed randomly spread in the phantom.

Needle placement procedure

The procedures were performed using CBCT guidance (XperGuide; Allura Xper FD-20 Angio system, Philips Medical Systems, Best, The Netherlands) and CT guidance (Siemens SOMATOM Sensation 16 CT scanner, Siemens, Erlangen, Germany). Each of the four targets was reached with an 18 G, 20 cm long Trocar needle (COOK Medical, Bloomington, USA) following three paths with different degrees of difficulty (*Figure 1*). First an inplane path in which the skin entry point and the target were in the same axial plane and on a vertical line (direction of A-axis *Figure 1*). The second path followed an angulated line in one axial plane (R/A plane in *Figure 1*). For the third, and most difficult needle path, the skin entry point and target were located on a double angulated line, which means an angulated needle path crossing several axial scanning slices. Four experienced interventional radiologists (JF, SB, MS, LSK) were asked to reach all

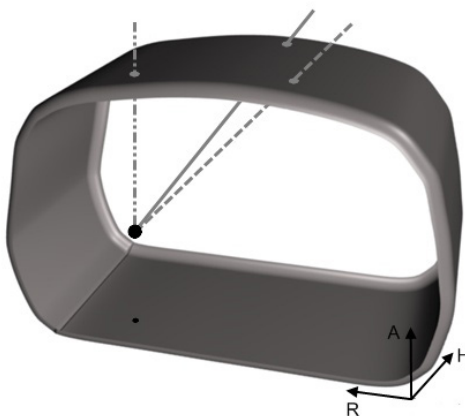


Figure 1. Outline of the Interventional 3D abdominal phantom showing an internal target (black dot) and three corresponding needle trajectories: dotted/dashed line = inplane trajectory, dashed line = angulated trajectory, and solid line = double angulated trajectory. Grey spots represent the corresponding skin entry points. The axes indicate the right (R), head (H) and anterior (A) sides of the phantom.

four targets along the three paths, as if a clinical procedure, on both modalities. All radiologists are experienced users of CT guidance (SB, JF >5 years; MS, LSK >10 years). All four had received training using the CBCT guidance software by a representative of the company and were allowed to practice. However, there were differences in the level of clinical experience with the guidance software. Two radiologists had performed only a few cases (i.e. <10; JF, LSK), the other two (SB, MS) performed over 200 clinical guidance procedures. A slightly different path was chosen for each puncture to avoid placing the needle in a previously followed path possibly still present in the phantom material. The precise angle of the needle path does not necessarily influence or determine the difficulty of the needle placement, however, the direction of the angulation does (inplane angulated vs. angulated through several axial planes).

CBCT

The CBCT guidance procedure started with acquiring an CBCT scan (312 projections over 240°) and reconstruction of a 3D data set. In this 3D data set both target and skin entry point were defined by the interventional radiologist so as to create a safe needle path. The 3D data set with planned needle path was overlaid with the real-time fluoroscopy images and the projection followed the movements of the C-arm [5, 6]. This allowed real-time visualization of needle position and progression towards the target point.

The optimal imaging projections (i.e. rotations and angulations of the C-arm) for needle guidance were automatically calculated after the needle path was determined. The first view was the entry point view in which the skin entry point is superimposed on the target point. This view was used to position the needle at the entry point. Next the progression view, perpendicular to the needle path, was used to monitor needle progression along the planned path allowing real-time guidance of the needle. When the needle had reached the target, an approximately 50% collimated CBCT scan was acquired to check the needle insertion accuracy in 3D. In all CBCT procedures the same imaging protocols were used for CBCT images as well as for fluoroscopy, hence the imaging parameters were equal. A SeeStar needle holder (AprioMed, Uppsala, Sweden) was optionally used to support the needle during insertion by preference of the radiologist.

CT

The CT guidance procedure started with a scan of the entire phantom (45 slices, 120 kV, 110 mAs) to determine the entry point and needle path towards the target. After placing the needle at the entry point repeated axial scans were acquired for progression control (6-24 slices, 120 kV, 54 mAs). For the double angulated needle paths, the complete needle path was scanned to visualize needle progression towards the target.

Analysis

The needle guidance procedures with CBCT guidance were compared to the procedures using CT guidance for each of the needle paths (inplane, angulated and double angulated), based on the accuracies. The accuracy is quantified by measuring the shortest distance from the needle tip to the centre of the target, measured in mm in a reconstructed 3D volume. This deviation from the target was determined on the verification CBCT scan or the last acquired CT scan. As the level of experience in using CBCT guidance differed, accuracy for the experienced users was compared to the trained users. For the CT guided procedures we assessed whether there were differences in accuracies between the four radiologists.

In addition, the needle placement time, from the beginning of the first scan (for needle path planning) to the end of the verification CBCT scan or the last acquired CT scan, was recorded (in minutes) and compared between CBCT and CT procedures.

Statistical analysis

Statistical analysis was performed with use of SPSS version 18.0. The Mann-Whitney test was used to compare the groups. Two-sided p-values ≤ 0.05 were considered statistically significant. All values are represented as median (range).

Results

Accuracy

The accuracies for both CBCT and CT guided procedures are represented in *Figure 2*. The distance between the needle and target centre is smaller using CBCT guidance, i.e. more accurate. The difference between CBCT and CT

guidance is statistically significant for the angulated (3 mm (2-6) vs. 4 mm (3-11), respectively) [$p=0.024$] and double angulated paths (2 mm (1-7) vs. 7 mm (2-11), respectively) [$p<0.001$].

With CT guidance the accuracy decreases with increasing level of difficulty. The accuracies of both the angulated [$p=0.007$] and double angulated [$p<0.001$] paths are significantly worse compared to the inplane path. With the increasing median deviation distance, also the range of the deviation distances increases, from 6 mm for the inplane path to 9 mm for the double angulated path. For CBCT guidance, however, the three needle paths result in the same level of accuracy (about 3 mm) with no significant differences between the three paths (Figure 2).

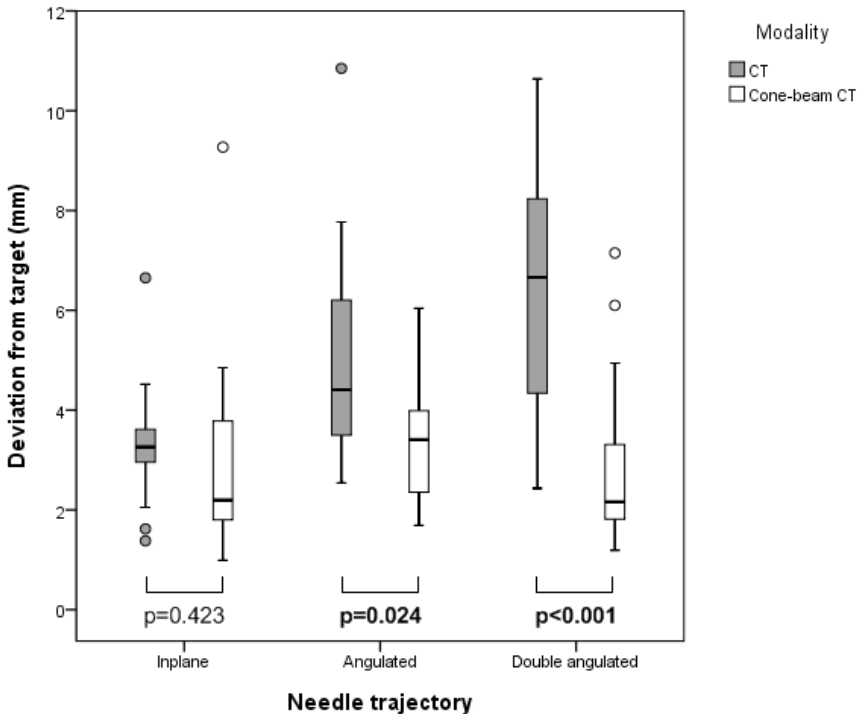


Figure 2. Boxplot showing deviation of the needle tip from target point for both CT (solid) and cone-beam CT guided procedures (white) for the three trajectories separately.

Experience level

The accuracies for the trained and experienced CBCT users are presented in Figure 3. With a median of 2 mm for all three needle paths and all needles placed within 4 mm of the target point, the experienced users are more accurate

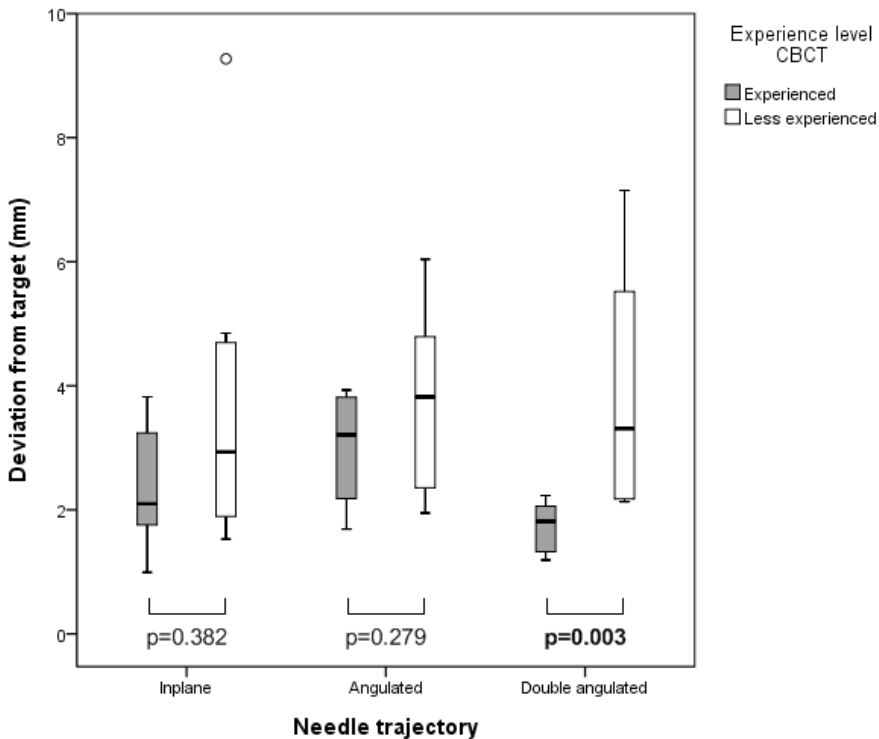


Figure 3. Boxplot showing the deviation from target point for each needle path as was reached by experienced users (solid) and less experienced users (white) of CBCT guidance.

compared to the trained CBCT users (median 4 mm) [$p=0.002$]. The ranges of accuracies achieved by trained users are larger compared to the ranges of experienced users, while the median values are comparable. Comparing the two levels of experience results in statistically significant difference for the double angulated needle paths (3 mm (2-7) vs. 2 mm (1-2) for the trained and experienced CBCT users, respectively) [$p=0.003$]. For this double angulated needle path, both trained and experienced users show statistically significant better accuracies using CBCT guidance compared to CT guidance [p -values are 0.016 and <0.001 , respectively]. For the inplane and angulated needle paths, the differences between trained and experienced users are not statistically significant (3 mm (2-9) vs. 2 mm (1-4) and 4 mm (2-6) vs. 3 mm (2-4) for inplane and angulated needle paths, respectively). Comparing the three needle paths within the group of trained users, there are no significant differences. For the

experienced users, however, the double angulated needle path shows a small but significant increase (1 mm) in accuracy compared to the angulated needle path [$p=0.015$]. The small range and low median value of the double angulated path compared to the other paths might be explained by the limited number of radiologists.

For the CT guided procedures, there are no statistically significant differences between the four radiologists. This indicates that the large spread in accuracy for the double angulated path is not influenced by experience in using CT guidance.

Needle placement time

There were no significant differences between CBCT and CT guidance for any of the used needle paths. A slight increase in placement time was only statistically significant between the inplane and double angulated paths for both CBCT (7 min vs. 10 min [$p=0.015$]) and CT guidance (6 min vs. 8 min [$p=0.018$]).

Discussion

The salient result of the presented phantom study is that effective needle guidance with approximately 3 mm accuracy was found to be feasible using CBCT guidance irrespective of the difficulty of the needle path. This contrasts to CT guidance where the accuracy decreases significantly with increasing level of difficulty, resulting in deviations from target of up to 7 mm for the double angulated path. The level of experience in using CBCT is another factor influencing accuracy, as the results indicate a learning curve for more difficult needle paths. However, even the less experienced users achieved significantly better accuracies compared to CT guided needle placements.

This study shows no differences in needle placement time between CBCT and CT. The measured time is only an indication for the time needed to actually place the needle. Total procedure time in clinical practice comprises more aspects, such as patient preparation and treatment time. Braak et al. have reported median intervention time to be 28.5 minutes, with a range from 3 to 96 minutes [6]. Our phantom study results are in the lower part of the range with 4 to 13 minutes for all needle placements.

This study is, to the best of our knowledge, the first to evaluate accuracy of needle guidance with regard to the level of the complexity of the used needle path. Some authors have reported achieved accuracies using CBCT guidance in small patient groups to be <5 mm in most of their cases [8, 12, 13], however, these groups are small and there is no or little information about the used needle paths. Nonetheless, this suggests that also in clinical practice accuracies of around 3 mm can be reached irrespective of the complexity of the needle path and the user experience level.

Accurate needle placement is essential for effective treatment in local therapy. However, a minimal deviation from the target, in the order of a few millimeters, will not always affect treatment outcome. The 7 mm deviation as observed in the case of the double angulated procedures using CT guidance, on the other hand, can be expected to impact treatment outcome. For instance, the targeted small high contrast nidus in radiofrequency ablations of osteoid osteoma is most often smaller than 10 mm [13]. Here, as the ablation zone is approximately 2 cm around the needle tip, a deviation from the target point of over 5 mm will result in partial treatment, or even worse, missing the nidus completely. Our phantom study results show that needle placement within 5 mm of target point is most commonly achieved using CBCT guidance. Such accuracy was not attained in most CT guidance procedures. We therefore suggest that these procedures are performed using CBCT guidance.

Some limitations in our study have to be addressed. As we used solid targets of 2.3 mm inside the phantom, the maximal experimental accuracy to be achieved was limited to 1-2 mm.

Radiation dose was not addressed in this study, partly because the small abdominal phantom used resulted in dose values that are not representative for patient care. Moreover, a comparison of effective patient doses between CBCT and CT guidance has already been provided by Braak et al. who report 13-42% dose reduction for CBCT guidance compared to CT guidance [10].

As our study was a phantom study, all puncture conditions were optimized. In clinical practice the conditions and the patient could result in increased deviation from the target. A factor influencing accuracy, irrespective of the guiding modality, is movement of either patient or target tissue. In CBCT guided procedures, patient movement such as breathing results in a mismatch

between the fluoroscopy overlay and the planned path on CBCT images. In our phantom study this was not an issue, but in clinical practice this is likely to influence procedure accuracy. For this reason we are currently looking into methods to account for breathing motions to improve accuracy of CBCT guided needle placement in tissues affected by breathing.

We have quantified accuracies of needle guidance using a model for high contrast lesions. Clearly, the success of needle placement depends on the visibility of the target and surrounding tissues. Low contrast targets are not always well visible in CBCT images. Therefore, other methods of visualization of the target tissue should be used. One method is contrast enhancement by administering a contrast agent. Another method is to bring images of other modalities into the angio suite by image registration with prior acquired CT or MR images that do visualize the target and surrounding tissues.

In conclusion, CBCT shows significantly higher accuracy than CT in reaching small targets with double angulated needle paths. Here, notwithstanding the apparent learning curve, CBCT allows more accurate needle placement.

References

1. Racadio JM, Babic D, Homan R, et al. (2007) Live 3D guidance in the interventional radiology suite. *AJR Am J Roentgenol* 189:W357-W364
2. Braak SJ, van Strijen MJL, van LM, van Es HW, van Heesewijk JPM (2010) Real-time 3D fluoroscopy guidance during needle interventions: technique, accuracy, and feasibility. *AJR Am J Roentgenol* 194:W445-W451
3. Mohlenbruch M, Nelles M, Thomas D, et al. (2010) Cone-beam computed tomography-guided percutaneous radiologic gastrostomy. *Cardiovasc Intervent Radiol* 33:315-320
4. Tam A, Mohamed A, Pfister M, Rohm E, Wallace MJ (2009) C-arm cone beam computed tomographic needle path overlay for fluoroscopic-guided placement of translumbar central venous catheters. *Cardiovasc Intervent Radiol* 32:820-824
5. Morimoto M, Numata K, Kondo M, et al. (2010) C-arm cone beam CT for hepatic tumor ablation under real-time 3D imaging. *AJR Am J Roentgenol* 194:W452-W454
6. Braak SJ, van Strijen MJL, van Es HW, Nievelstein RAJ, van Heesewijk JPM (2011) Effective dose during needle interventions: cone-beam CT guidance compared with conventional CT guidance. *J Vasc Interv Radiol* 22:455-461
7. Jin KN, Park CM, Goo JM, et al. (2010) Initial experience of percutaneous transthoracic needle biopsy of lung nodules using C-arm cone-beam CT systems. *Eur Radiol* 20:2108-2115
8. Leschka SC, Babic D, El Shikh S., Wossmann C, Schumacher M, Taschner CA (2012) C-arm cone beam computed tomography needle path overlay for image-guided procedures of the spine and pelvis. *Neuroradiology* 54:215-223
9. Busser WMH, Hoogeveen YL, Veth RPH, et al. (2011) Percutaneous radiofrequency ablation of osteoid osteomas with use of real-time needle guidance for accurate needle placement: a pilot study. *Cardiovasc Intervent Radiol* 34:180-183
10. Kroeze SGC, Huisman M, Verkooijen HM, van Diest PJ, Bosch JLR, van den Bosch MAAJ (2012) Real-time 3D fluoroscopy-guided large core needle biopsy of renal masses: a critical early evaluation according to the IDEAL recommendations. *Cardiovasc Intervent Radiol* 35:680-685
11. Higashihara H, Osuga K, Onishi H, et al. (2012) Diagnostic accuracy of C-arm CT during selective transcatheter angiography for hepatocellular carcinoma: comparison with intravenous contrast-enhanced, biphasic, dynamic MDCT. *Eur Radiol* 22:872-879

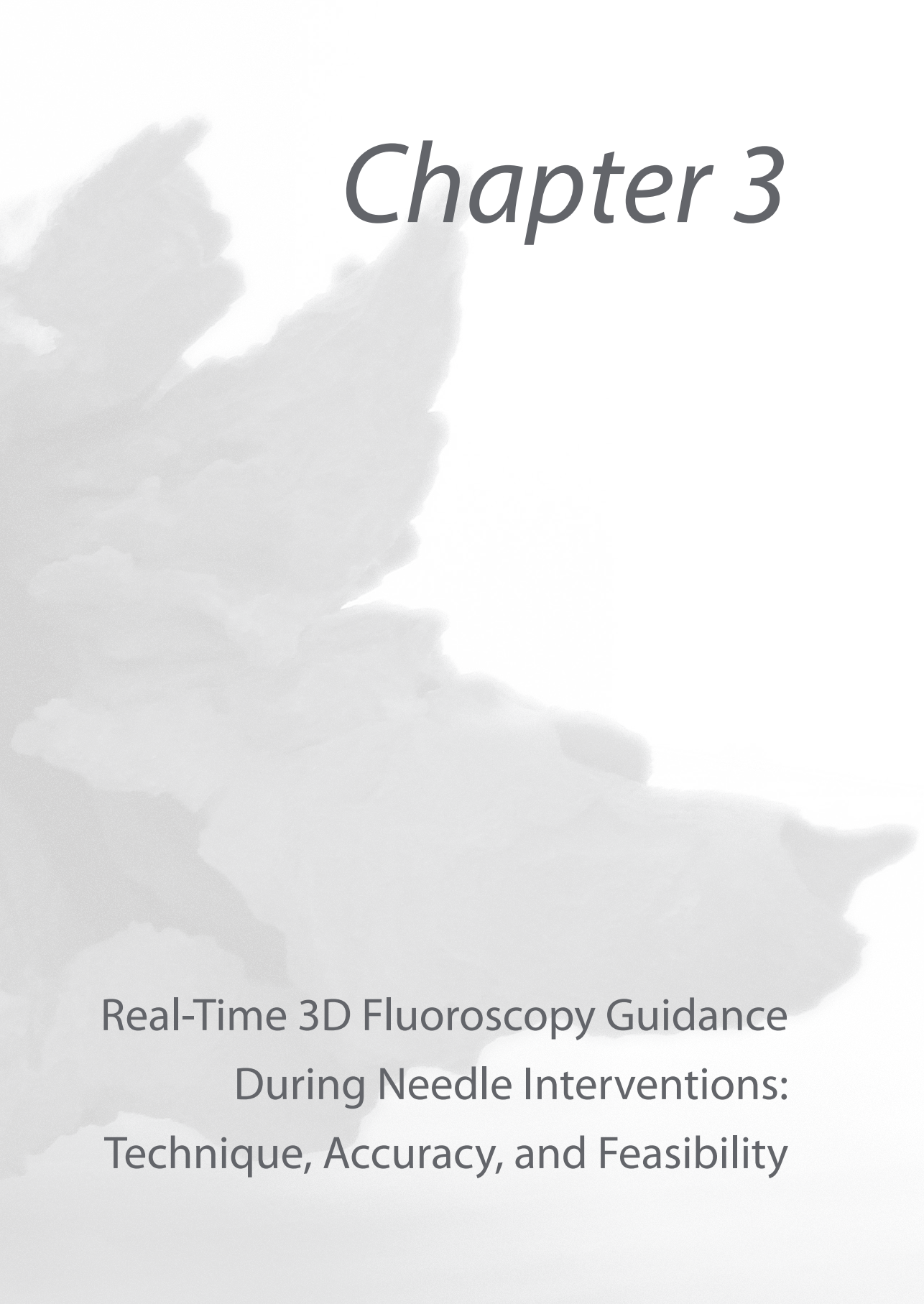


S. J. Braak • M. J. L. van Strijen • M. van Leersum • H. W. van Es • J. P. M. van Heeswijk

Department of Radiology, St. Antonius Hospital, Nieuwegein, The Netherlands

AJR 2010; 194:W445–W451

Received September 18, 2009; accepted after revision November 12, 2009.



Chapter 3

Real-Time 3D Fluoroscopy Guidance
During Needle Interventions:
Technique, Accuracy, and Feasibility

Abstract

Objective

Real-time 3D fluoroscopy guidance using cone beam CT with dedicated needle path planning software is a promising new interventional technique. The objective of this study was to evaluate the procedure and to assess the accuracy and feasibility of this technique for use in needle interventions.

Subjects and methods

All procedures were performed using a flat panel-based fluoroscopy system capable of acquiring cone beam CT images and dedicated needle path-planning software. This new technology allows the use of fluoroscopy coregistered with a 3D data set reconstructed from the acquired attenuation information. The needle trajectory is planned in the 3D data set using the needle path-planning software. The calculated trajectory is then projected on to the real-time fluoroscopy image. Fluoroscopy time, accuracy, technical success of the procedures, median procedure time, and complications were recorded in 145 interventions.

Results

One hundred forty-five needle interventions were performed in 139 patients using real-time 3D fluoroscopy guidance. Procedures were divided into five groups according to anatomic region: upper thoracic (n = 19; 13.1%), lower thoracic (n = 18; 12.4%), upper abdominal (n = 65; 44.8%), lower abdominal (n = 13; 9.0%), and musculoskeletal (n = 30; 20.7%). Thirty needle interventions were therapeutic, and 115 were diagnostic biopsies. All interventions were within the predefined 5-mm safety margin and achieved 100% technical success. A histopathologic diagnosis could be made in 91.4% of the diagnostic biopsies. The median interventional procedure time was 28.5 minutes, and the median fluoroscopy time was 2 minutes 58 seconds. There were minor complications in six patients (4.3%) and one major complication (0.7%).

Conclusion

Real-time 3D fluoroscopy guidance is a new, promising, and feasible technique providing high accuracy in needle interventions.

Introduction

Several different techniques are available for performing imaging guided needle interventions, all with their own specific advantages and disadvantages. Ultrasound and CT are most commonly used. Cone beam CT is a new emerging technology that allows 3D image acquisition via a C-arm fluoroscopy system. It has been reported as a valuable imaging tool for preoperative planning in (invasive) head and neck surgery because of its good bone and soft-tissue resolution [1, 2]. Until recently, cone beam CT was not used with real-time tracking and navigation. A newly developed real-time 3D fluoroscopy guidance system for needle interventions merges cone beam CT with dedicated planning software and real-time fluoroscopy (XperCT, XperGuide, and Allura FD20 angiography interventional system, all from Philips Healthcare) [3]. This prospective article explains the technique and describes the accuracy and feasibility of real-time 3D fluoroscopy guidance during needle interventions in a wide clinical setting.

Subjects and Methods

Patients

Patients were included from October 2006 to November 2008. All patients with an indication for CT-guided needle intervention were included in the evaluation and were referred for this new technique. Eligible patients included those who needed percutaneous intervention for a target lesion that was not accessible by ultrasound. In addition, patients had to be able to lie reasonably still for ≤ 45 minutes and, preferably, to comply with breath-hold commands if needed. There was no target lesion size limit. Patients with contraindications for percutaneous intervention (e.g., blood coagulation disorder) were excluded. If a safe needle path was not possible in planning of the needle trajectory (because of interposition of other vital anatomic structures), the patient was excluded. This was never the case in our population. Informed consent was obtained for all patients. One hundred forty-five procedures were performed in 139 patients: 90 (64.7%) were men, and 49 (35.2%) were women. The mean (\pm SD) age at the time of the procedure was 63.7 ± 1.09 years (range, 23.9–91.0 years). The mean (\pm SD) diameter of the target lesion was 32.04 ± 1.8 mm (range, 9–124 mm).

Table 1. Baseline Data Study Population

Characteristic	Value
No. of procedures per patient, mean	1.04
Age (y), mean	63.7
Male (%)	64.7
No. of biopsy passes, mean \pm SD	2.7 \pm 1.2
Diameter of target lesion (mm), mean \pm SD (range)	42.6 \pm 6.3 (14-124)
Upper thorax (n = 19)	39.4 \pm 4.9 (9-77)
Lower thorax (n = 18)	32.7 \pm 2.7 (9-102)
Upper abdomen (n = 65)	36.4 \pm 5.0 (10-66)
Lower abdomen (n = 30)	17.9 \pm 1.1 (10-33)

Note: There were 145 procedures performed for 139 patients.

The baseline data of the study population are shown in *Table 1*. In 21 patients, a second location within the target lesion was biopsied to collect additional tissue samples. To perform the biopsy of the second location, a different (second) needle trajectory was defined within the available 3D data set (details of the interventions are shown in *Table 2*).

Technique, System, and Method

Image acquisition is via a flat-panel detector C-arm system (XperCT, XperGuide, and Allura FD20; Philips Healthcare). During a 180–240° rotation of the C-arm around the patient, 312 (optionally 624) projections are acquired. The rotation time is 4–10 seconds, depending on the scanning protocol used (thoracic, abdominal, or spine and high or low dose). The flat-panel detector system can provide high contrast resolution. The highest spatial resolution is 0.4 mm, depending on the resolution matrix used and the field of view. Contrast resolution of the cone beam CT is approximately 5 HU at a slice thickness of 10 mm (N. J. Noordhoek, white paper, Philips Healthcare). A 3D soft-tissue data set is reconstructed from the calibrated rotational acquisition. Within this 3D data set, a needle path is drawn by the user from the lesion to the skin in the proposed access route, avoiding vital anatomic structures (*Figure 1*). Once the virtual trajectory is determined, the optimal imaging angulation is calculated and programmed instantly with automated coupling with the C-arm. The 3D data set and virtual trajectory are coregistered with the real-time fluoroscopy image, and the calculated (parallax corrected) needle path is projected on to

Table 2. Details of the Performed Needle Interventions

Category		No. of Procedures							
		Aspiration	Biopsy	Drainage	Infiltration	Localization	Nephrostomy	Vertebroplasty	Total
Upper thorax									
Lung	Pleural		11					11	
	Parenchymatous		8					8	
<i>Subtotal</i>			19					19	
Lower thorax									
Lung	Pleural		3	1				4	
	Parenchymatous		8			1		9	
Mediastinal	Anterior	1	3	1				5	
<i>Subtotal</i>		1	14	2		1		18	
Upper abdomen									
Adrenal			1					1	
Liver			4	4				8	
Stomach				1				1	
Kidney upper pole	Endophytic	1	4					5	
	Exophytic		4					4	
Kidney interpolar	Endophytic		9			3		12	
	Exophytic		5					5	
Kidney lower pole	Endophytic		4					4	
	Exophytic		3					3	
Peraaortal mass		1	18		1			20	
Paracolic abscess				1				1	
Spleen			1					1	
<i>Subtotal</i>		2	53	6	1	3		65	
Lower abdomen									
Ovarian mass		2	3					5	
Iliac mass			3					3	
Parasigmoid mass			1	3				4	
Paraurethral mass			1					1	
<i>Subtotal</i>		2	8	3				13	
Musculoskeletal									
Shoulder region			2					2	
Thoracic region			7				4	11	
Lumbar region			5				2	7	
Pelvic region			7	1	2			10	
<i>Subtotal</i>			21	1	2		6	30	
Total		5	115	12	3	1	3	6	145

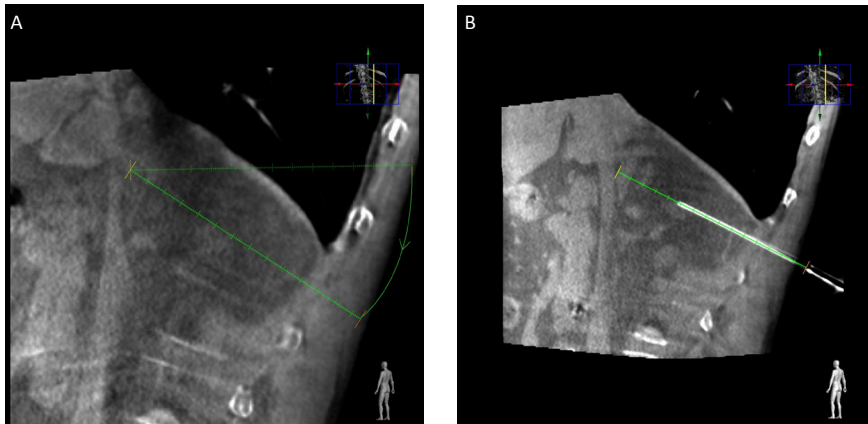


Figure 1. 77-year-old man with history of bladder cancer and adenocarcinoma of lung. Patient was diagnosed with focal mass in left adrenal gland. During examination, mass showed malignant enhancement pattern on CT and increased uptake at FDG PET scan. Histopathologic analysis revealed adrenal adenoma. Insets in top right corner of images show orientation of cone beam CT volume (blue) used with yellow line indicating slice position, x-axis (red), and z-axis (green). A, Adjusted user-defined needle trajectory in acquired cone beam CT 3D data set in sagittal oblique plane avoiding vital anatomic structures (lung and diaphragm) is seen. B, Control cone beam CT image obtained to check for accuracy and possible complications shows oblique sagittal view of coaxial needle and planned needle trajectory.

the fluoroscopy image, producing a highly accurate real-time image of needle progression toward the target (*Figure 2*). The movement of the C-arm is coupled with the fluoroscopy projection of the 3D data set. Consequently, the needle trajectory is always visible in the appropriate projection of the data set.

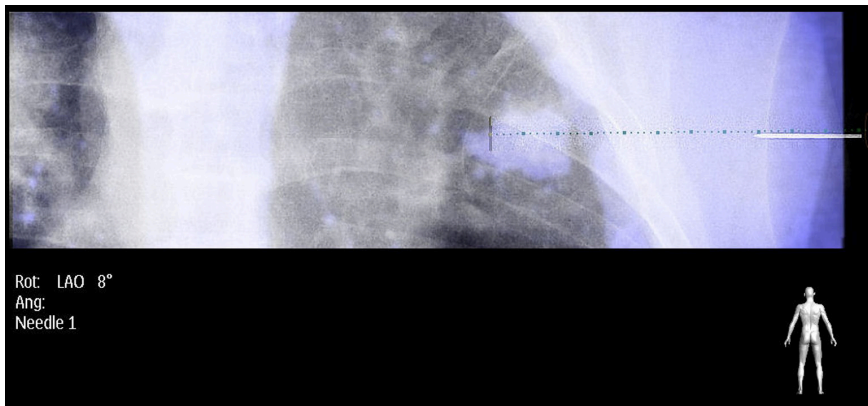


Figure 2. 66-year-old man with suspected mass in right upper lobe. Threedimensional data set and virtual trajectory are coregistered with real-time fluoroscopy, and calculated needle path (blue) is projected on fluoroscopy image (gray) producing real-time image of needle progression to target with high accuracy. Histopathologic analysis revealed non-small cell lung carcinoma. Ang = angulation, LAO = left anterior oblique, and Rot = rotation.

Two main C-arm geometry positions (*Figure 3*) are used for this type of intervention. One view looks on top of the needle path (entry point view), and the second view is perpendicular to the needle path (progression view). Both are easily accessed with a single touch of a button on the tableside controls. Once the C-arm is in the entry point view position, a central dot depicting the needle path is shown encircled by two colored rings with an adjustable diameter marking the beginning and end points of the needle path. This entry point view is used for accurate needle positioning when entering the skin, to administer local anesthetics and to advance the needle by a few centimeters. When the C-arm is moved to the progression view, the angle of the needle is fixed using a needle-guiding device or with the assistance of a

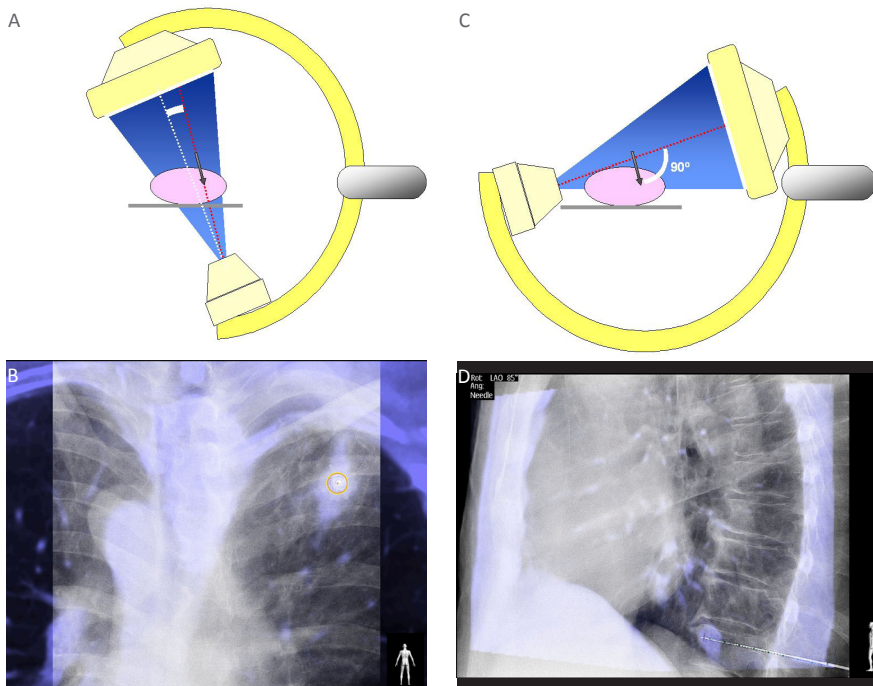


Figure 3. Two main C-arm geometry positions are used.

A, Schematic depiction of entry point view shows top of needle path (parallax corrected).

B, Image shows entry point view (yellow circle) in 67-year-old man with mass in right upper lobe. Histopathologic analysis revealed necrotic granulomatous infectious mass, which proved to be tuberculosis.

C, Progression view is seen in schematic depiction of second view, 90° perpendicular to needle path.

D, Image shows progression view in 73-year-old man with mass in right lower lobe. Histopathologic analysis revealed metastasis of renal cell carcinoma. Ang = angulation, LAO = left anterior oblique, and Rot = rotation.

table-mounted laser. Needle progression along the planned path is visualized on the progression view as a central needle path with centimeter markings, surrounded by a cylinder corresponding to the size of the entry and target point circles, providing a safety margin (standard diameter, 1 cm; *Figure 4*) on the fluoroscopy image. With the use of a needle guide or laser guide, only the progression view is used to advance the needle. During the intervention, a new cone beam CT acquisition can be performed to check the needle position or to check for possible complications. After the needle intervention, a control cone beam CT is always performed, for checking needle accuracy and to check for possible complications [3].

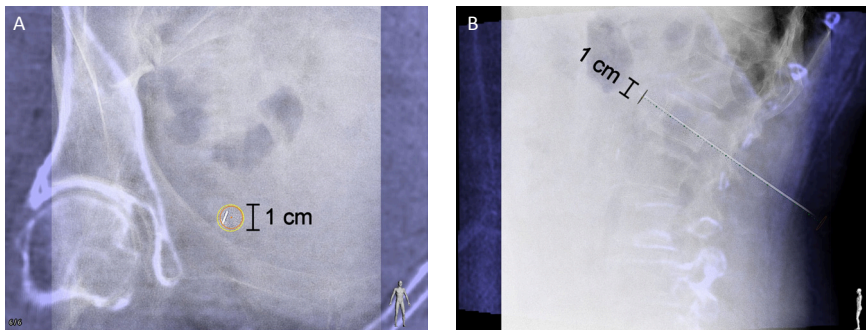


Figure 4. Safety margin during procedure.

A, Safety margin around planned needle path is shown as two circles (yellow and red) around single dot (needle path) with standard diameter of 1 cm.

B, During progression of needle, trajectory is shown on progression view as central needle path with centimeter markings with surrounding cylinder of 1-cm safety margin.

Procedure

Using the method described in the previous section for localizing the entry point, the location is disinfected with either chlorhexidine (0.5%) or iodine (1%). A sterile environment is created by using adhesive drapes. Local anesthetic (lidocaine 1%) is used at the entry point and along the needle path. Depending on the location (i.e., upper abdomen or lower thoracic procedures), patients are given breath-hold commands at different steps of the needle intervention procedure. During the procedure, the patient's ECG and blood pressure are monitored, and a precautionary IV line is inserted. Fluoroscopy time, accuracy of the needle insertion, technical success, median (peri-) procedure time, target size, dose–area product ($\text{Gy}\cdot\text{cm}^2$), and possible complications were registered.

Technical success was defined as a needle intervention in the marked user-defined location with an acceptable safety margin of 5 mm, checked by a control cone beam CT acquisition. The accuracy of the procedure was defined by the result of the histopathologic diagnosis (diagnostic biopsies) and an adequate procedure (correct placement of a drainage tube in the collection with a positive aspiration, correct placement during vertebroplasty, and localization wire for surgery) during therapeutic interventions. The median interventional time was the median occupation time of the interventional room (median procedure time) minus the median preparation time and postinterventional time. The biopsy specimens were defined as being suitable for histopathologic examination if a solid cylinder of tissue of at least 1.0 cm in length was obtained. To obtain the adequate length, the mean (\pm SD) number of passes was 2.7 ± 1.2 (range, 1–7 passes). All biopsies were performed using a coaxial technique. For the guidance needle, we used the TruGuide coaxial needle (C. R. Bard) of 7 or 13 cm length (17 gauge). For the biopsy needle, we used the Bard Magnum core biopsy system (18 gauge) with 16-, 20-, or 25-cm biopsy needles. For drainage procedures, we used a trocar needle (18 gauge, 15 or 20 cm length; Two-Part Trocar Needle, ref 090020, Cook Medical), and a 100-cm (0.035 inch) Schueller Exchange Wire (Angiomed) for eventually placing a 8.5-French Mac Lock drain (Cook Medical) in all cases. The interventions were divided into five different anatomic regions, because of the size of the panel detector (field of view) and because of the expected largest movement of the target associated with breathing movement around the diaphragm level. This could then be separately evaluated using this categorization. The anatomic regions were the upper thoracic category (clavicle to carina), lower thoracic category (carina to lowest diaphragm level), upper abdominal category (upper diaphragm level to umbilical level), lower abdominal category (umbilical level to ischial tuberosity), and a separate musculoskeletal category. The most suitable cone beam CT protocol for the position of the lesion was chosen. Complications were divided into minor and major. A minor complication was defined as a self-limiting complication (e.g., small pneumothorax) requiring no further intervention or additional hospitalization or as easily treatable adverse effects (e.g., minor bleeding) during the procedure. Major complications were defined as complications needing additional therapeutic interventions or prolonged hospitalization.

Statistical Analyses

Microsoft Office Excel 2007 was used for summarizing the results and SPSS software (version 16.0, SPSS) was used for the statistical analysis.

Results

Between October 2006 and November 2008, we performed 145 interventions for 139 patients using the real-time 3D fluoroscopy guidance system. All 145 procedures were performed by the same board-certified interventional radiologist with > 10 years' experience. Of these procedures, 13.1% were in the upper thorax (n = 19), 12.4% were in the lower thorax (n = 18), 44.8% were in the upper abdomen (n = 65), 9.0% were in the lower abdomen (n = 13), and 20.7% were musculoskeletal (n = 30). Thirty procedures were therapeutic interventions, and 115 were diagnostic interventions. Detailed information about the needle interventions is shown in *Table 2*. All target lesions were safely accessible on the basis of the initial cone beam CT. During all interventions, the placement of the needle was within the user-defined acceptable safety margin of 5 mm (*Figure 4*). Technical success was achieved in 100% of the procedures, as verified by control cone beam CT (*Figure 1B*). All therapeutic interventions were successful. Of the 115 diagnostic needle interventions, a histopathologic diagnosis could be made in 91.3% of the biopsy samples. Eight of the 10 non-diagnostic biopsies were in the upper abdomen group, one was in the upper thoracic group, and one was in the lower abdomen group. As a result, the overall accuracy in the total population (including the therapeutic interventions) was 93.1%. The median procedure time was 45 minutes (range, 15–110 minutes). This includes the actual interventional time (28.5 minutes; range, 3–96 minutes) and the peri-interventional management time (13 minutes; range, 5–49 minutes). Separate category data are shown in *Table 3*. The median fluoroscopy time was 2 minutes 58 seconds (range, 54 seconds–13 minutes 55 seconds). The median dose–area product was 44.4 Gy.cm². Using the dose–area product–to–effective dose conversion factor of 0.28–0.29 (mSv x Gy⁻¹ x cm⁻²) reported by Suzuki et al. [4], a median effective dose of 12.7 mSv was calculated using real-time 3D fluoroscopy guidance. No significant difference in fluoroscopy time, procedure time, and interventional time was observed between the subgroup data (*Table 3*). Complications occurred in seven patients (5.0%), of which six were minor.

Table 3. Result of Procedure, Intervention, Periinterventional, and Fluoroscopy Time in the Separate Anatomic Categories

Category	Procedure Time (Min)	Intervention Time (Min)	Fluoroscopy Time (Min)	Dose-Area Product (Gy.cm ²)
Upper Thorax	42 (23-79)	24 (6-60)	2:55 (1:44-9:11)	26.4 (19.6-31.2)
Lower Thorax	46 (15-75)	26.5 (5-65)	2:40 (1:54-6:49)	27.4 (16.9-37.9)
Upper Abdominal	42 (18-98)	26 (3-56)	2:47 (1:14-7:55)	48.9 (42.5-55.5)
Lower Abdominal	54 (26-75)	35 (20-58)	3:03 (1:33-7:10)	63.6 (50.6-76.5)
Musculoskeletal	52 (15-110)	34 (5-96)	4:49 (0:54-13:55)	50.7 (40.0-61.4)
Total	45 (15-110)	28.5 (3-96)	2:58 (0:54-13:55)	44.4 (40.0-48.8)

Note: All data are median (range).

Four patients had a small pneumothorax, which was self-limiting. Two patients had post puncture bleeding, which was easily controlled by simple coagulation therapy (Spongostan, Baxter) during the procedure. One major complication consisted of a pneumothorax requiring chest tube placement (0.7%).

Discussion

Real-time 3D fluoroscopy guidance with cone beam CT is a new, promising, and feasible technique for needle interventions. Because of the integration of the information of cone beam CT and live fluoroscopy, real-time 3D fluoroscopy can be used for real-time needle intervention, with a high degree of accuracy. The purpose of this study was to give a description of the procedure technique and to determine the accuracy and feasibility of this new technique. To our knowledge, there are no data concerning the accuracy and feasibility of comparable techniques using real-time 3D fluoroscopy guidance. The only available data are for CT or ultrasound. All the needle placements were a 100% technical success, meaning that the target defined by the interventional radiologist was correctly reached. Despite this, in 10 patients (7.2%), no histopathologic diagnosis could be made. In three of these patients, the cause, in retrospect, was found to be that the radiologist had inadvertently defined the target just next to the lesion. The defined target had, in fact, been correctly biopsied, as verified by a control cone beam CT scan. In all three cases, the explanation for planning just next to the target was misinterpretation of the position of the lesion in the 3D data set. In the remaining seven cases, the predefined target was biopsied correctly but, according to the pathologist, the

histopathologic material was either too necrotic ($n = 4$) for microscopic analysis, or the pathologic diagnosis did not correlate with the expected diagnosis ($n = 3$), which was expected to be renal cell carcinoma. In the last three cases, the diagnosis was post inflammatory changes ($n = 2$) and a finding of normal kidney tissue ($n = 1$). During 18-month follow-up, no indications for malignancy were found in these three cases. It is therefore debatable whether these cases were not conclusive. The accuracy rate of 93.1% is comparable to that of interventions performed using CT fluoroscopy, with no real difference in accuracy from that reported in the literature (82–100%) [5–10]. The accuracy rate using CT fluoroscopy in thoracic interventions is 88–100% [6–9]. The use of CT fluoroscopy guidance for abdominal interventions has an accuracy rate of 82–98% [6, 9, 10]. For musculoskeletal interventions, an accuracy rate of 85.4–90.5% is reported for CT fluoroscopy guidance [5, 6]. The recorded intervention time of 28.5 minutes is comparable to results reported in the literature (12 minutes 7 seconds–54 minutes) [5–8, 10]. Our median fluoroscopy time (2 minutes 58 seconds), compared with CT fluoroscopy time, is considerably longer [6–11]. The mean CT fluoroscopy time of these authors is 88.1 seconds (20.7–143.9 seconds). A reason for the considerable longer fluoroscopy time is because many needle interventions performed needed a double oblique steep angle approach (Figs. 1 and 4B). Using CT fluoroscopy, the needle interventions were in the same (near) axial plane [6–11]. Ultrasound guided needle interventions, in general, have a shorter procedure time, but is not always possible in difficult to reach lesions. The median effective dose of 12.7 mSv during real-time 3D fluoroscopy guidance is comparable to the effective dose using CT fluoroscopy guidance [12, 13]. Complications are not completely avoidable during needle interventions. We report a total of seven complications (4.9%) in seven patients, all non fatal. In the group of minor complications ($n = 6$), four patients had a small self-limiting pneumothorax after biopsy of the lung. A control radiograph of the thorax showed no progression or clinically significant existing pneumothorax 2 hours later, and the patients were released to go home within the planned period for hospitalization. Two patients had some continued bleeding through the coaxial guiding needle. Thrombotic material (Spongostan) was injected at the end of the procedure. The bleeding stopped, and no prolonged hospitalization or other intervention was necessary. One major

complication occurred, a pneumothorax that did not resolve spontaneously. The patient received a drainage tube and was discharged 3 days later (2 days extra hospitalization). De Mey et al. [6] reported nine (11.1%) patients with complications in their study group—six with minor complications (five small pneumothorax and one parenchymatous bleeding) and three with major complications (two pneumothorax for which the patient needed drainage or prolonged hospitalization and one patient with fatal pulmonary bleeding). There were no complications in the group with abdominal interventions. Kirchner et al. [11] reported 12.5–16% of patients with major complications after needle interventions, all confined to the thoracic interventions. Froelich et al. [7] reported a 15% complication rate (three pneumothorax, two aspiration, and one drainage tube). Compared with these studies, our complication rate is reasonably low. The main limitation of this technique is the necessity for the patient to remain still on the table during the entire procedure. Because of the superposition of the planning trajectory in the acquired 3D data set, any movement of the patient will result in a misplaced target position. Most movement during the intervention is to be expected around the diaphragm and, therefore, this categorization was made to evaluate the accuracy in the case of moving targets (lower thoracic and upper abdomen category). The potential interventional targets subject to breathing movement can be approached accurately by using breath-hold commands during the 3D data set acquisition. After adequate anesthetic preparation, progression of the needle can be done by holding the respiration when a recognizable structure on the fluoroscopy image (mainly the diaphragm) is in the same position as in the overlay image of the 3D data set. In our population, we performed 62 biopsies in lesions subject to respiratory movement. All interventions with movement were a technical success (checked by a control cone beam CT). Because the needle intervention is performed in real time, the radiologist can verify that no movement of the patient has occurred. If movements have occurred and are observed, small adjustments are possible to readjust the fluoroscopy overlay image to match easily identifiable landmarks in the 3D data set. Despite the open structure of the C-arm, the angulation has its limitations, depending on the C-arm position (propeller or roll scan) and the patient size. Particularly in interventions with very steep angulations, the entry point view position cannot

always be completely reached. However, accurate needle placement can still be achieved by switching between the positions close to the entry point view and the progression view positions. All interventional procedures are operator dependent. To eliminate interoperator variability and difference, all procedures were performed specifically by one interventional radiologist. Nevertheless, we think that our findings are applicable to others because this interventional procedure is rather easy to perform and our accuracy and procedure time are comparable to those reported in the literature. A limitation of this study could be the prospective nature of the observations and the possible lack of a (randomized) control group. Needle interventions are most often performed using ultrasound. It is accurate, can be performed in real time, is safe, uses no ionizing radiation, and is widely available. In comparison with CT fluoroscopy, ultrasound is faster. Limitations of ultrasound-guided needle interventions are operator dependence, difficulty in visualization of the needle during needle advancement to the target, and procedure-dependent performance. Ultrasound provides insufficient imaging capability for interventions in bone and in structures surrounded by air because of impermeability for sound waves (e.g., overlying gastrointestinal gas) [14]. Furthermore, ultrasound has limited spatial and contrast resolution, especially in obese patients [15]. The second most often used technique is CT fluoroscopy, which is also widely available. It has high resolution and is usable for needle interventions independently of tissue type, and most radiologists are confident in using this technique. Increasingly, more CT scanners are equipped with a fluoroscopy option that allows real-time visualization of a small section of the relevant anatomy. The disadvantages of CT fluoroscopy are limited patient access due to gantry size and a usually nonsterile working environment. The major advantage of using real-time 3D fluoroscopy for needle intervention over CT fluoroscopy is patient access. The C-arm allows optimal patient accessibility and can be performed in a proper sterile environment. The large range of motion in angulations and rotations of the C-arm is a considerable advantage, compared with the limited angulation of the gantry ($\pm 30^\circ$) in CT fluoroscopy. A potential problem is the respiration motion when not using real-time CT fluoroscopy. The largest disadvantage is the radiation dose to the patient and interventional radiologist [16]. Regular fluoroscopy uses real-time visualization with a wide field of view,

but provides only a 2D image with poor soft-tissue contrast resolution. Our study shows the advantage of this new technique during needle interventions with a high technical success, high accuracy, short fluoroscopy time and procedure time, low complication rate, and easy operability. In addition to biopsies and drainage, other therapeutic interventions can also be considered, such as cryoablation or radiofrequency ablation. In conclusion, real-time 3D fluoroscopy guidance is a new, promising, and feasible technique used for needle interventions, with high technical success, short procedure times and fluoroscopy times, comparable accuracy to CT fluoroscopy, low complication rates, and is easy to perform. The C-arm architecture allows optimal patient access, and it is easy to maintain sterility.

Acknowledgments

We acknowledge the assistance of A. Balguid and E. van Ommen (Philips Healthcare, Clinical Science).

References

1. Siewerdsen JH, Moseley DJ, Burch S, et al. Volume CT with a flat-panel detector on a mobile, isocentric C-arm: pre-clinical investigation in guidance of minimally invasive surgery. *Med Phys* 2005; 32:241–254
2. Ritter D, Orman J, Schmidgunst C, Graumann R. 3D soft tissue imaging with a mobile C-arm. *Comput Med Imaging Graph* 2007; 31:91–102
3. Racadio JM, Babic D, Homan R, et al. Live 3D guidance in the interventional radiology suite. *AJR* 2007; 189:1523 [web]; W357–W364
4. Suzuki S, Furui S, Yamaguchi I, et al. Effective dose during abdominal three-dimensional imaging with a flat-panel detector angiography system. *Radiology* 2009; 250:545–550
5. Huch K, Roderer G, Ulmar B, Reichel H. CT-guided interventions in orthopedics. *Arch Orthop Trauma Surg* 2007; 127:677–683
6. De Mey J, Op de Beeck B, Meysman M, et al. Real time CT-fluoroscopy: diagnostic and therapeutic applications. *Eur J Radiol* 2000; 34:32–40
7. Froelich JJ, Ishaque N, Regn J, Saar B, Walthers EM, Klose KJ. Guidance of percutaneous pulmonary biopsies with real-time CT fluoroscopy. *Eur J Radio*. 2002; 42:74–79
8. White CS, Meyer CA, Templeton PA. CT fluoroscopy for thoracic interventional procedures. *Radiol Clin North Am* 2000; 38:303–322
9. Carlson SK, Bender CE, Classic KL, et al. Benefits and safety of CT fluoroscopy in interventional radiologic procedures. *Radiology* 2001; 219:515–520
10. Silverman SG, Tuncali K, Adams DF, Nawfel RD, Zou KH, Judy PFCT. Fluoroscopy-guided abdominal interventions: techniques, results, and radiation exposure. *Radiology* 1999; 212:673–681
11. Kirchner J, Kickuth R, Laufer U, Schilling EM, Adams S, Liermann D. CT fluoroscopy-assisted puncture of thoracic and abdominal masses: a randomized trial. *Clin Radiol* 2002; 57:188–192
12. Joemai RMS, Zweers D, Obermann WR, Geleijns J. Assessment of patient and occupational dose in established and new applications of MDCT fluoroscopy. *AJR* 2009; 192:881–886
13. Tsalafoutas IA, Tsapaki V, Triantopoulou C, Gorantonaki A, Papailiou J. CT-guided interventional procedures without CT fluoroscopy assistance: patient effective dose and absorbed dose considerations. *AJR* 2007; 188:1479–1484
14. Winters SR, Paulson EK. Ultrasound guided biopsy: what's new? *Ultrasound Q* 2005; 21:19–25
15. Hangiandreou NJ. AAPM/RSNA physics tutorial for residents: topics in US: B-mode US—basic concepts and new technology. *RadioGraphics* 2003; 23:1019–1033
16. Nawfel RD, Judy PF, Silverman SG, Hooton S, Tuncali K, Adams DF. Patient and personnel exposure during CT fluoroscopy-guided interventional procedures. *Radiology* 2000; 216:180–184



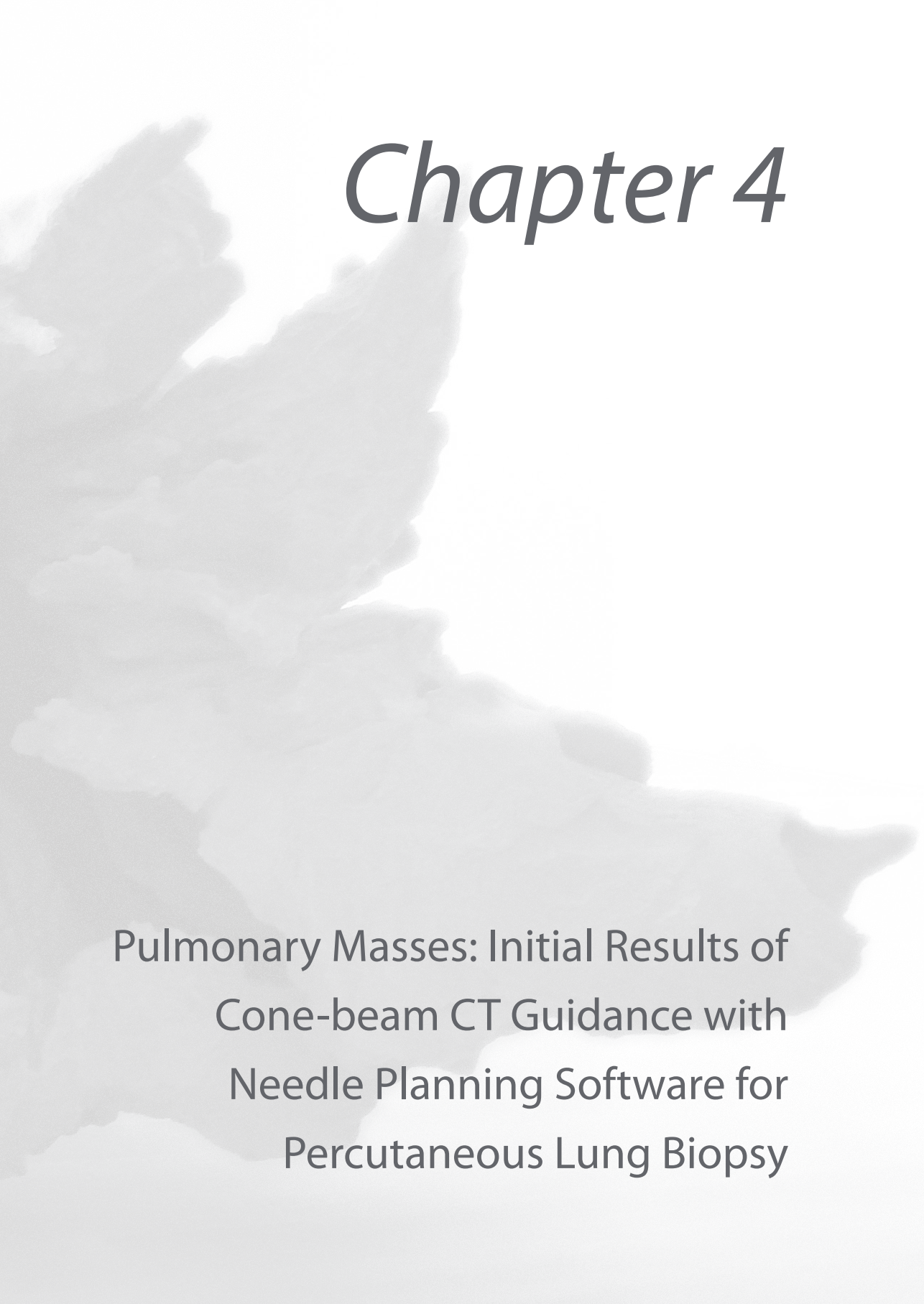
Sicco J. Braak¹ • Gerarda J.M. Herder² • Johannes P.M. van Heesewijk¹ • Marco J.L. van Strijen¹

¹Department of Radiology, St. Antonius Hospital, Nieuwegein, The Netherlands

²Department of Pulmonology St. Antonius Hospital, Nieuwegein, The Netherlands

Cardiovasc Intervent Radiol 2011; 7 December [epub ahead of print]

Received 6 August 2011; accepted after revision 13 October 2011.



Chapter 4

Pulmonary Masses: Initial Results of
Cone-beam CT Guidance with
Needle Planning Software for
Percutaneous Lung Biopsy

Abstract

Objective

To evaluate the outcome of percutaneous lung biopsy (PLB) findings using cone-beam computed tomographic (CT) guidance (CBCT guidance) and compared to conventional biopsy guidance techniques.

Materials and Methods

CBCT guidance is a stereotactic technique for needle interventions, combining 3D soft-tissue cone-beam CT, needle planning software, and real-time fluoroscopy. Between March 2007 and August 2010, we performed 84 Tru-Cut PLBs, where bronchoscopy did not provide histopathologic diagnosis. Mean patient age was 64.6 (range 24–85) years; 57 patients were men, and 25 were women. Records were prospectively collected for calculating sensitivity, specificity, positive predictive value, negative predictive value, and accuracy. We also registered fluoroscopy time, room time, interventional time, dose–area product (DAP), and complications. Procedures were divided into subgroups (e.g., location, size, operator).

Results

Mean lesion diameter was 32.5 (range 3.0–93.0) mm, and the mean number of samples per biopsy procedure was 3.2 (range 1–7). Mean fluoroscopy time was 161 (range 104–551) s, room time was 34 (range 15–79) min, mean DAP value was 25.9 (range 3.9–80.5) Gy.cm², and interventional time was 18 (range 5–65) min. Of 84 lesions, 70 were malignant (83.3%) and 14 were benign (16.7%). Seven (8.3%) of the biopsy samples were non-diagnostic. All non-diagnostic biopsied lesions proved to be malignant during surgical resection. The outcome for sensitivity, specificity, positive predictive value, negative predictive value, and accuracy was 90% (95% confidence interval [CI] 86–96), 100% (95% CI 82–100), 100% (95% CI 96–100), 66.7% (95% CI 55–83), and 91.7% (95% CI 86–96), respectively. Sixteen patients (19%) had minor and 2 (2.4%) had major complications.

Conclusion

CBCT guidance is an effective method for PLB, with results comparable to CT/CT fluoroscopy guidance.

Introduction

The first step in the assessment of a patient with a suspicious lung mass is usually bronchoscopy. Bronchoscopy can evaluate the nature of a lung mass, and it allows for tissue sampling and determining the extent of the lesion. Success rates of bronchoscopy for diagnosing malignancy range 30–80% depending on the method of sampling (e.g., biopsy, fine-needle aspiration, bronchoalveolar lavage), where the highest percentages are found in visible, centrally located masses [1]. In the case of a non-diagnostic bronchoscopy, i.e., where bronchoscopy fails to yield a histopathologic diagnosis of a pulmonary mass, an image-guided percutaneous lung biopsy (PLB) is usually performed. In general, these procedures are performed under ultrasound or computed tomographic (CT) guidance. Ultrasound is quick and safe, and it is the least expensive method. This technique is limited to pleural-based lesions [2]. Nowadays, most PLB's are performed under CT guidance [3]. This technique has good accuracy and is widely used [4,5]. With CT guidance, there is good in-plane resolution, but double-oblique (e.g., an angulated needle trajectory in both the axial and sagittal plane) biopsies are more difficult to perform [6]. Furthermore, workspace is limited by the bore of the CT system, and real-time visualization of needle progression is only available using CT fluoroscopy (CTF). 3D cone-beam CT guidance (CBCT guidance) is a new real-time stereotactic needle guidance technique using a combination of 3D soft tissue cone-beam CT and fluoroscopy. This technique offers advanced needle planning and is performed in a sterile workspace with good angulation/rotation capability as well as real-time fluoroscopy feedback [7]. The aim of our study was to assess the diagnostic outcome of CBCT guidance in a prospective cohort of patients with suspicious lung masses.

Materials and Methods

Between March 2007 and August 2010, we prospectively included our cohort of patients. All patients included were referred for percutaneous biopsy to determine the nature of the suspected pulmonary mass. All patients had a previous non-diagnostic bronchoscopy. There was no target lesion size limit. Patients had to be able to lie reasonably still and comply with breath-hold

commands. Patients with contraindications for percutaneous intervention (e.g., abnormal coagulation indices) were excluded. We performed 84 CBCT-guided procedures in 82 patients. There were 57 men and 25 women, with a mean age of 64.6 (range 23.9–84.7) years. Baseline data are shown in *Table 1*. The procedure and possible complications were discussed with each patient before the procedure. This study was approved by the institutional review board, and informed consent was obtained from all patients.

Table 1 Patient data and tumor characteristics of PLB performed with CBCT guidance

Characteristic	Value
No. of patients/no. of procedures	82/84
Sex (M/F)	59/25
Age, mean (range) (y)	64.6 (23.9–84.7)
Nondiagnostic bronchoscopy	100%
DAP, mean (range) (Gy.cm ²)	25.9 (3.9–80.5)
Location of mass (N)	
Left upper lobe	21
Left lower lobe	13
Lingula	2
Right upper lobe	23
Middle lobe	7
Right lower lobe	18
Lesion size, mean (range) (mm)	32.5 (3-93)
Distance to pleura mean in parenchymatous lesions (range) (cm)	15.8 (2-49)

Note: DAP = dose-area product

Procedure

PLB was performed using CBCT guidance. This new technique is based on a flat-panel-detector C-arm system with dedicated software (XperCT and XperGuide, Allura FD20; Philips Healthcare, Best, The Netherlands). It combines a 3D cone-beam CT volume with needle trajectory planning software and real-time fluoroscopy. For sampling, two interventional radiologists (MvS, 10 years' experience, and SB, 5 years' experience) used a coaxial cutting needle technique. Our local experience in using this CBCT technique was 3.5 years. The sequential steps for CBCT guidance are as follows [7]. Depending on the location of the pulmonary mass (identified on the CT scan of the thorax performed during the diagnostic assessment), the patient is placed in either a prone or supine position. The patient is positioned under fluoroscopy in such a way that the mass will be located centrally in the acquired CBCT volume. During a single breath hold, a cone-beam CT scan is acquired with a 240° rotation in 4.1 s around the region of interest. The radiologist then determines a safe needle trajectory within this data set, taking into account the essential anatomic structures (*Figure 1*).

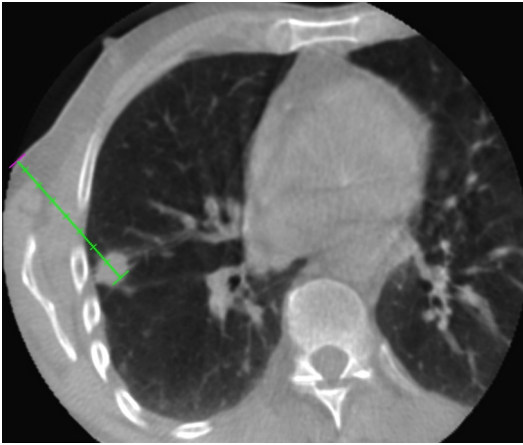


Figure 1 Step 2 of a CBCT guidance procedure. After the acquisition of a soft tissue CBCT data set, a safe needle trajectory (with centimeter markings) is determined from the lesion (12.9.16 mm) to the skin, avoiding essential anatomic structures

Using the information of the planned needle trajectory, a live fusion image of fluoroscopy and a representative slice of the cone-beam CT is created in which the needle can be accurately positioned (*Figure 2*) [7]. The skin entry location is sterilized and a local anesthetic is injected (≤ 10 ml lidocaine 1%). Using real-time fluoroscopy and the CT slice overlay the guiding cannula (C. R. Bard Inc.; Murray Hill, NJ; TruGuide; 17 gauge; 13 or 17 cm length) is positioned at the proper angulation with the tip of the needle just in the subcutis.

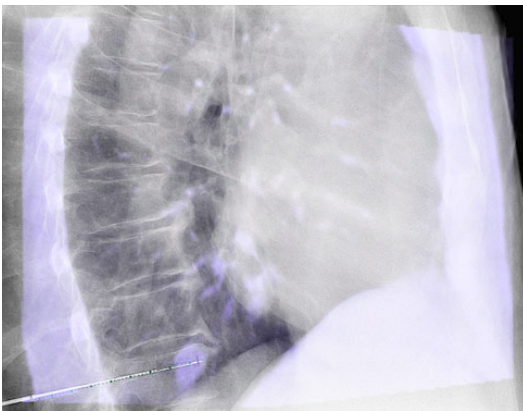


Figure 2 Step 3 of a CBCT guidance procedure. A fusion image is created between the fluoroscopy image (gray) and the CBCT slice (blue) showing the needle trajectory, making accurate needle placement possible

The C arm is then moved to a 90° perpendicular position to allow the needle to be advanced under real-time fluoroscopy over the needle trajectory. A centimeter scale is displayed to mark the proper depth. During the progression of the needle, the patient is asked to stop breathing when the outline of the

diaphragm of the fluoroscopy overlay matches the outline of the diaphragm of the cone-beam CT slice (*Figure 3*). The guiding cannula is positioned just outside of the pleura. For sampling, several 18-gauge Tru-Cut biopsy samples are taken, until approximately 1 cm of tissue length is obtained; using a Tru-Cut needle (Magnum; C. R. Bard Inc., 18 gauge; 16, 20, or 25 cm; side cutting, 22 mm), which is placed into an automated biopsy gun (Bard).

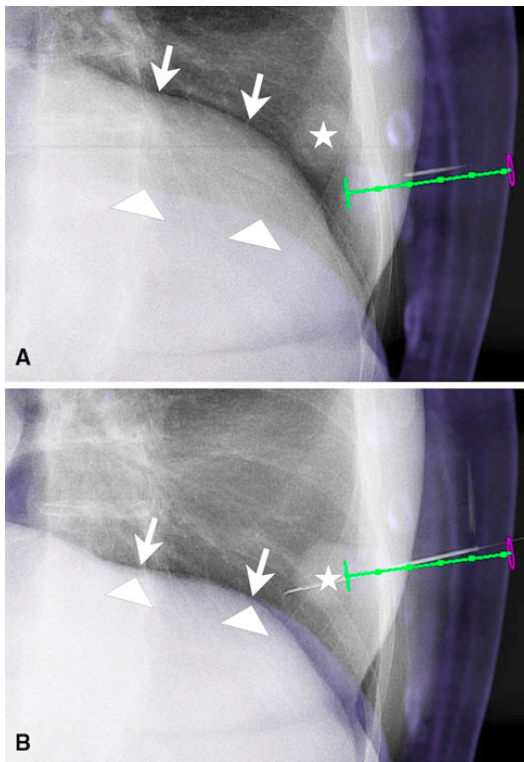


Figure 3 Step 5 of a CBCT guidance procedure. *A*, In expiration. The position of the diaphragm in the live fluoroscopy image (gray, arrows) does not match the CBCT slice with the planned trajectory (blue, arrowheads). Progression of the biopsy needle over the needle trajectory would fail to get a representative tissue sample of the tumor mass (white star). *B*, After the patient has been instructed to breathe in, the fluoroscopy image (gray, arrows) of the diaphragm now matches the CBCT slice (blue, arrowheads). Progressing the needle in this situation will result in an accurate biopsy of the tumor (white star)

After the needle intervention, a collimated control cone-beam CT is always performed to check needle position accuracy and to look for possible complications (*Figure 4*). Patients remained under observation in the hospital until the next morning. An erect chest radiograph was performed 2 h after the procedure to detect any (late) complication. In the case of marked changes in vital signs or clinical status, repeat imaging was indicated.



Figure 4 Step 7 of a CBCT guidance procedure. A (collimated) control CBCT is performed to check the accuracy of the (guiding) needle and to check for possible complications. In this case the guiding needle is in the right direction and a small hematoma (white star) can be seen around and medial to the small tumor (white arrow)

Data Collection and Analysis

For each procedure, radiologic reports, histopathologic data, and medical records were prospectively collected. The result of a PLB was defined as truly positive if the histopathologic examination revealed a malignancy. A falsely positive biopsy finding was defined as a sample showing malignancy, where surgical resection showed no evidence of malignancy (in the absence of preoperative chemotherapy) or the lesion showed regression at follow-up CT examination (>6 months) without any therapy. A truly negative sample was defined as a proven histopathologic benign lesion at biopsy without pathologic change during follow-up imaging or definite proof by histology at surgery. A falsely negative sample was defined as a biopsy sample that showed normal lung parenchyma or a benign histopathologic result, but proved to be a malignant lesion during surgical resection. For the diagnosis of malignancy, the sensitivity, specificity, positive predictive value (PPV), negative predictive value (NPV), and diagnostic accuracy were calculated. We also registered fluoroscopy time, procedure time, dose–area product (DAP), location of the lung mass, and mass aspect and length. Procedure time was split into two parts; room time was defined as the time the patients actually were in the interventional suite, and interventional time was defined as the time from the start of the fluoroscopy (step 1) until extraction of the (guiding) needle after the control cone-beam CT (step 7). The location of the pulmonary mass was categorized into anatomic lobes, where the lingula was defined as a separate lobe. A differentiation was made into masses subjected to breathing movement and masses that were not influenced by breathing movement. A differentiation was also made

between the anatomic location of the lesions: pleural or parenchymatous masses. In the parenchymatous masses group, we measured the shortest distance to the pleura (in millimeters) in addition to the largest diameter (in millimeters) of the lesion. Complications were defined as described by Gupta et al. [8]. Procedures with complications without sequelae were defined as minor complications: hemoptysis with no additional treatment, small or moderate pneumothorax (quantification of pneumothorax is explained below), and prolonged admission for monitoring (<48 h). The complication was considered major if additional treatment was needed (e.g., tube placement for a large pneumothorax; treatment of hemoptysis) or if the patient was admitted longer in the hospital (>48 h). A pneumothorax was graded as small if no additional treatment was necessary, moderate if the pneumothorax could directly be aspirated by the coaxial guiding needle at the end of the procedure with no additional treatment later, or large if a tube placement was necessary [4]. Data analysis was performed by Excel 2007 (Microsoft, Redmond, WA) and SPSS software (version 16.0; SPSS, Chicago, IL). Subgroup analysis was performed by the independent-sample t-test. The differences were considered significant for p-values less than 0.05.

Results

Overall sensitivity was 90% (95% confidence interval [CI] 86–96), specificity 100% (95% CI 82–100), PPV 100% (95% CI 96–100), NPV 66.7% (95% CI 55–83), and diagnostic accuracy for CBCT-guided biopsies of pulmonary masses 91.7% (95% CI 86–96). Of the biopsy samples, 70 (83.3%) of 84 proved to be malignant. Fifty-two (74.3%) of 70 were primary lung malignancies, 14 (20%) of 70 metastases, and 4 (5.7%) of 70 lymphomas. Fourteen (16.7%) of 84 samples were classified as definitely benign (*Figure 5*): 3 (21.5%) of 14 were infectious changes, 9 (64.3%) of 14 chronic infectious changes with fibrosis, 1 (7.1%) of 14 normal lung parenchyma, and 1 (7.1%) of 14 fungus. This definite classification was based on the histopathologic results and the fact that the lesions showed a reduction in diameter or no changes of the diameter during follow-up CT scans (mean 14.9 months, range 6–31 months). The histopathologic results of the seven false-negative samples (7 of 84, 8.3%) (*Table 2*) were initially considered to be necrotic (n = 2), normal lung parenchyma (n = 4), and infectious changes

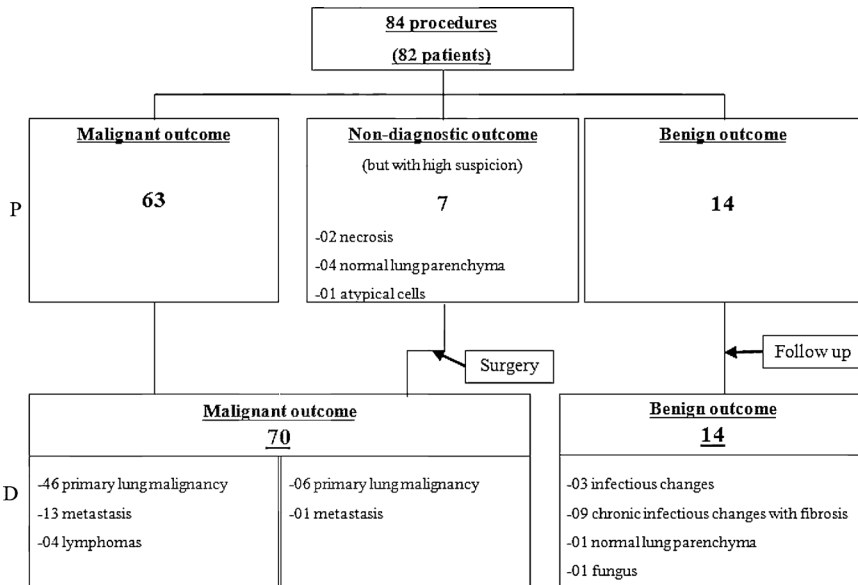


Figure 5 Flowchart of the outcome of the CBCT-guided PLBs. Mean follow-up was 14.9 months. P = primary outcome of biopsy, D = definite outcome of biopsy

but with suspicion of malignancy (n = 1). During surgical resection, these lesions proved to be primary lung cancer (n = 6) and a metastasis of esophageal carcinoma (n = 1). The total mean fluoroscopy time was 161 (range 104–551) s, room time 34 (range 15–79) min, and interventional time 18 (range 5–65) min. Mean DAP was 25.9 (range 3.9–80.5) Gy.cm². Detailed data of the subgroups are provided in Table 2. The overall complication rate of minor complications was 19%. Eight patients (9.5%) had a small pneumothorax and five (5.9%) a moderate pneumothorax. In one patient (1.2%) with a parenchymatous mass in the left upper lobe, a brief period of hemoptysis occurred without need of therapeutic interventions. Two patients (2.4%) were admitted longer (>48 h) for observations without any other intervention to monitor their pneumothorax. Two major complications (2.4%) consisted of a large pneumothorax requiring chest tube placement in one patient, and one patient was admitted for a longer period (7 days) to monitor a moderate pneumothorax. We did not find any significant differences between the subgroups (pleural vs. parenchymatous lesions; movement vs. non-movement; and the combination of these subgroups) concerning the sensitivity, specificity, PPV, NPV, and accuracy (p > 0.05) (Table 2). However, we found a significant difference (p = 0.001)

Table 2 Outcome of PLB using CBCT guidance

Characteristics	Pleural (n = 42)		Parenchymatous (n = 42)	
	+	-	+	-
Movement				
No.	15	27	25	17
Mean diameter ± SD (mm)	33.8 ± 4.9	42.4 ± 4.2	25.8 ± 3.9	25.5 ± 3.4
Mean pleural-lesion diameter ± SD (mm)	-	-	14.6 ± 1.7	17.6 ± 3.6
No. of biopsies, mean ± SD	3.3 ± 0.2	3.3 ± 0.2	3.0 ± 0.2	3.2 ± 0.2
DAP ± SD (Gy.cm ²)	20.5 ± 10.8	24.2 ± 16.6	27.4 ± 15.6	31.4 ± 21.4
Minor complications				
small pneumothorax	-	-	5	3
moderate pneumothorax	2	-	2	1
hemoptysis	-	-	-	1
Prolonged admittance (<48h)	-	1	-	1
Major complications				
large pneumothorax	-	-	1	-
prolonged (>48h) admittance	-	-	1	-
Truly positive	10	21	22	10
Truly negative	4	3	2	5
Falsely negative	1	3	1	2
Fluoroscopy time ± SD (s)	132 ± 6.5	156 ± 14.1	162 ± 15.9	194 ± 28.2
Room time ± SD (min)	27.3 ± 1.8	35.8 ± 3.1	34.5 ± 3.9	37.2 ± 4.0
Interventional time ± SD (min)	13.7 ± 1.3	18.2 ± 2.6	18.0 ± 3.2	21.9 ± 4.0
Sensitivity (%) (95% CI)	90.9 (77-99)	87.5 (81-97)	95.7 (90-99)	83.3(69-98)
Specificity (%) (95% CI)	100.0 (61-100)	100.0 (48-100)	100.0 (39-100)	100.0 (65-100)
Positive Predictive Value (%) (95% CI)	100.0 (72-100)	100.0 (93-100)	100.0 (95-100)	100.0 (93-100)
Negative Predictive Value (%) (95% CI)	80.0 (49-99)	50.0 (24-81)	66.7 (26-94)	71.4 (47-92)
Accuracy (%) (95% CI)	93.3 (72-99)	88.9 (77-98)	96.0 (86-99)	88.2 (68-98)

Note: DAP = dose area product, SD = standard deviation

between the parenchymatous lesions (35.7%) and the pleural lesions (7.1%) regarding total complication rate. There was no significant difference in the total complication rate between the lesions subjected to movement (27.5%) and the lesions without movement (15.9%). No significant difference was found between the outcome of the biopsies performed by the two operators (*Table 3*). The effect of the lesion size showed that the smallest lesions had a lower accuracy but the difference between the lesion size groups was not significant. However, there was a significant difference ($p = 0.027$) in total complication rate between lesions ≤ 30 mm (30%) and lesions > 30 mm (11%) (*Table 3*).

Table 3 Comparison of diagnostic outcome between the operators and between the different lesion sizes

Characteristics	Operator I	Operator II	Lesion ≤ 15 mm	Lesion 16-30 mm	Lesion 31-45 mm	Lesion ≥ 46 mm
Number	39	45	20	26	20	18
Truly positive	34	29	14	20	15	14
Truly negative	3	11	3	5	4	2
Falsely negative	2	5	3	1	1	2
Sensitivity	94.4%	85.3%	82.4%	85.2%	93.8%	87.5%
Specificity	100%	100%	100%	100%	100%	100%
PPV	100%	100%	100%	100%	100%	100%
NPV	60%	68.8%	50%	83.3%	80%	50%
Accuracy	94.9%	88.9%	85%	96.2%	95%	88.9%
Complication rate	25,6%	20%	20%	34.6%	10%	11.1%

Note: PPV = positive predictive value, NPV = negative predictive value

Discussion

In general, evaluation of a pulmonary mass by transthoracic biopsy is considered to be safe and accurate [6, 9]. These reports concern biopsies that use other methods than CBCT guidance. To our knowledge, only Jin et al. [10] recently published data concerning PLB using CBCT guidance, with a sensitivity, specificity, and accuracy of 97, 100, and 98.4%, respectively. There are two major differences between his study and ours. The first is that our CBCT guidance system combines fluoroscopy with an overlay of a CBCT slice with a predefined needle trajectory with a centimeter scale, providing direct feedback of the needle position. In the system used by Jin et al. [10], there is no direct feedback on the needle trajectory and needle depth, especially in targets that are not visible on fluoroscopy. Second, Jin et al. [10] excluded indeterminate nodules, defined as an inconclusive histopathologic outcome after PLB (no definite benign or malignant), resulting in a possible higher accuracy, sensitivity, and specificity. Concerning the recorded procedure time, the reported results on PLB range 13.4–23.8 min, depending on the definition of procedure time and procedure method [11,12]. We divided the procedure time into the room occupation time and actual intervention time. The definition of the procedure time in the literature in general is the same as our defined interventional time. Jin et al. [10] report a procedure time of 17.9 min, which is comparable to our interventional

time of 18.1 min. Compared to CT guidance (mean reported procedure time of 23.1 min), there is a slight difference in the procedure time in favor of CBCT guidance, but compared to CTF guidance (mean reported procedure time 15.3 min), the advantage is more likely to be in favor of CTF [11–14]. The mean DAP value of 25.9 Gy.cm² is comparable to the value reported in the literature using the same system [7]. To compare these dose values to CT/CTF guidance dose values, transformation of DAP values into millisieverts is necessary because both systems use different parameters to evaluate the dose used. The DAP to effective dose conversion factor of 0.183 mSv.Gy⁻¹.cm⁻² determined by Betsou et al. [15] was used to calculate an effective dose of 4.7 mSv using CBCT guidance. The effective dose during CT/CTF guidance reported in the literature ranges 2.7–6.5 mSv, which is comparable [11,13]. Complications are a calculated risk during percutaneous needle interventions. There is great variation in the pneumothorax rate in the literature, 0–61%, with a minority of these requiring additional treatment. The rate of hemoptysis ranges 0–14% [4,6,9,10,12,13]. In our study, a small or moderate pneumothorax was reported in 15.4% and self-limiting hemoptysis in 1.2%, which is within the range reported in the literature [16]. We report a major complication rate of 2.4%, including pneumothoraxes requiring a chest tube (1.2%) and prolonged admission (1.2%). In most studies in the literature, however, prolonged admission to the hospital is not reported as a (major) complication, resulting in a lower reported (major) complication rate (3.3–15%) compared to our study [4,9,10,13,14,16,17]. Movement of the target lesion due to breathing during CT/CTF guidance as well as double oblique approaches (e.g., an angulated needle trajectory in both the axial and sagittal plane) are interventional challenges [6,18]. In our experience, one of the advantages of CBCT guidance is the real-time fluoroscopy feedback of movement due to respiration, which can then be controlled so that the depth of respiration matches the CBCT slice overlay. Furthermore, as a result of the wide range of angulation and rotation of the C arm, double oblique approaches were easier to perform. Other advantages are the 3D soft tissue information include needle planning software and real-time visualization of the needle progression. Another advantage of CBCT guidance is the open sterile workspace, compared to the restrictions of a CT system [7,10,12,18]. There are several limitations to our study. First, no randomized comparison was made between CBCT guidance and CT/CTF guidance. This is because all patients for PLB were routinely referred

to CBCT guidance because of the good local experience and logistic reasons [7]. The results of CBCT guidance are comparable to the results of CT/CTF guidance reported in the literature, but a prospective, randomized study between these two should be performed to definitely determine this. Former studies have shown a sensitivity, specificity, and PPV of CT/CTF guidance of 76.9–97.8%, 93.6–100%, and 95.9–100% respectively, with NPV ranging 61.4–96% and accuracy ranging 80–98.4% [4,5,13,14,19,20]. The wide range of the individual outcomes is due to different methods used, where CTF guidance results in higher percentages than conventional CT guidance. Despite the comparable results, our overall NPV was only 66.7% (which is in line of the reported NPV using CT guidance). This is primarily the result of the combined 8.3% false-negative rate and the predominance of malignant lesions effect [21]. This indicates that a negative outcome for malignancy should be followed up. The bigger the size of the target lesion, the higher the accuracy rate, with masses of 1.0–5.0 cm having the highest accuracy rate [14,19]. The accuracy rate drops in lesions smaller than 1.0 cm because these are more difficult to sample and in lesions sized >5.0 cm because there is substantially more necrosis, altering the possible outcome. Our results reveal the same trend. A second limitation is that we were unable to obtain a histologic confirmation of 10 lesions defined as nonmalignant (truly negative), because all were treated conservatively. However, follow-up (mean 14.9 months) showed no changes indicating malignancy, so these were defined as benign lesions.

In conclusion, CBCT guidance appears to be a safe and accurate method to biopsy lung masses with a sensitivity 90%, specificity 100%, PPV 100%, NPV 66.7%, and accuracy 91.7%, which is comparable to the results of CT/CTF-guided PLB reported in the literature.

References

1. Herth FJF, Eberhardt R, Ernst A (2006) The future of bronchoscopy in diagnosing, staging and treatment of lung cancer. *Respiratory* 73:399–409
2. Sheth S, Harper UH, Stanley DB et al (1999) US guidance for thoracic biopsy: a valuable alternative to CT. *Radiology* 210:721–726
3. Diacon AH, Theron J, Shubert P et al (2007) Ultrasound-assisted transthoracic biopsy: fine needle aspiration or cutting-needle biopsy? *Eur Respir J* 29:357–362
4. Heck SL, Blom P, Berstad A (2006) Accuracy and complications in computed tomography fluoroscopy-guided needle biopsies of lung masses. *Eur Radiol* 16:1387–1392
5. Hiraki T, Mimura H, Gobara H et al (2009) CT fluoroscopy-guided biopsy of 1,000 pulmonary lesions performed with 20-gauge coaxial cutting needles: diagnostic yield and risk factors for diagnostic failure. *Chest* 136:1612–1617
6. Cham MD, Lane ME, Henschke CI et al (2008) Lung biopsy: special techniques. *Semin Respir Crit Care Med* 29:335–349
7. Braak SJ, van Strijen MJL, van Leersum M et al (2010) Real-time 3D fluoroscopy guidance during needle interventions: technique, accuracy, and feasibility. *AJR Am J Roentgenol* 194:W445–W451
8. Gupta S, Wallace MJ, Cardella JF et al (2010) Quality improvement guidelines for percutaneous needle biopsy. *J Vasc Interv Radiol* 21:969–975
9. Duncan M, Wijesekera N, Padley S (2010) Interventional radiology of the thorax. *Respirology* 15:401–412
10. Jin KN, Park CM, Goo JM et al (2010) Initial experience of percutaneous transthoracic needle biopsy of lung nodules using C-arm cone-beam CT systems. *Eur Radiol* 20:2108–2115
11. Carlson SK, Felmlee JP, Bender CE et al (2005) CT fluoroscopy-guided biopsy of the lung or upper abdomen with a breath-hold monitoring and feedback system: a prospective randomized controlled clinical trial. *Radiology* 237:701–708
12. Schaefer PJ, Schaefer FKW, Heller M et al (2007) CT fluoroscopy-guided biopsy of small pulmonary and upper abdominal lesions: efficacy with a modified breathing technique. *J Vasc Interv Radiol* 18:1241–1248
13. Kim GR, Hur J, Lee SM et al (2011) CT fluoroscopy-guided lung biopsy versus conventional CT-guided lung biopsy: a prospective controlled study to assess radiation doses and diagnostic performance. *Eur Radiol* 21:232–239
14. Tsukada H, Satou T, Iwashima A et al (2000) Diagnostic accuracy of CT-guided automated needle biopsy of lung nodules. *AJR Am J Roentgenol* 175:239–243

15. Betsou S, Efsthopoulos EP, Katritsis D et al (1998) Patient radiation doses during cardiac catheterization procedures. *Br J Radiol* 71:634–639
16. Yamagami T, Kato T, Hiroto T et al (2006) Usefulness and limitation of manual aspiration immediately after pneumothorax complication interventional radiological procedures with the transthoracic approach. *Cardiovasc Intervent Radiol* 29:1027–1033
17. Froelich JJ, Ishaque N, Regn J et al (2002) Guidance of percutaneous pulmonary biopsies with real-time CT. *Eur J Radiol* 42:74–79
18. Moore EH (1998) Technical aspects of needle aspiration lung biopsy: a personal perspective. *Radiology* 208:303–318
19. Priola AM, Priola SM, Cataldi A et al (2007) Accuracy of CT-guided transthoracic needle biopsy of lung lesions: factors affecting diagnostic yield. *Radiol Med* 112:1142–1159
20. Laurent F, Latrabe V, Vergier B et al (2000) Percutaneous CT-guided biopsy of the lung: comparison between aspiration and automatic cutting needles using a coaxial technique. *Cardiovasc Intervent Radiol* 23:266–272
21. Moulton JS, Moore PT (1993) Coaxial percutaneous biopsy technique with automated biopsy devices: value in improving accuracy and negative predictive value. *Radiology* 186:515–522



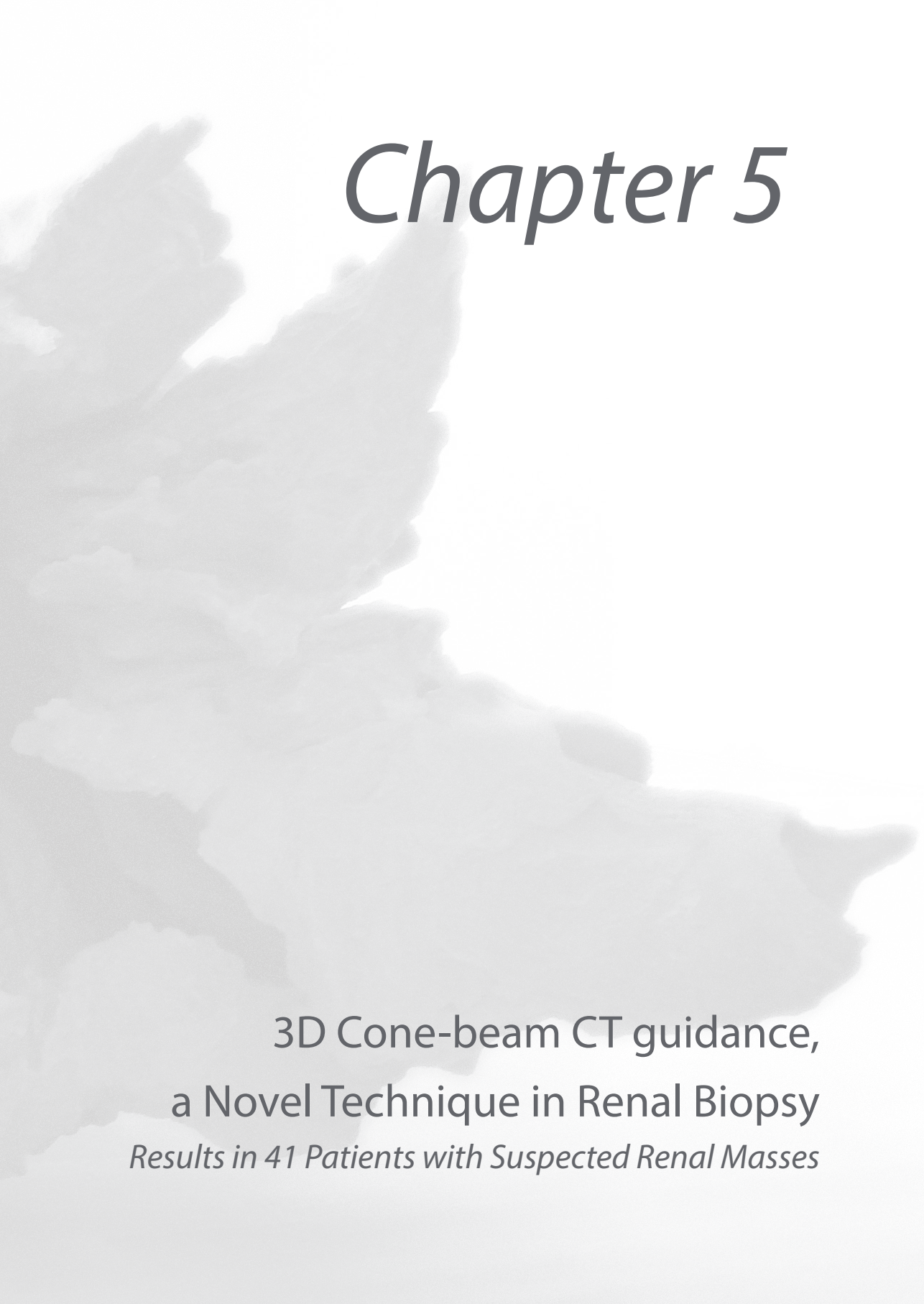
Sicco J. Braak¹ • Harm H.E. van Melick² • Mircea G. Onaca² • Johannes P.M. van Heesewijk¹ • Marco J.L. van Strijen¹

¹Department of Radiology, St. Antonius Hospital, Nieuwegein, The Netherlands

²Department of Urology, St. Antonius Hospital, Nieuwegein, The Netherlands

Eur Radiol 2012; 2 Jun [epub ahead of print]

Received: 22 January 2012 / Revised: 7 April 2012 / Accepted: 10 April 2012



Chapter 5

3D Cone-beam CT guidance,
a Novel Technique in Renal Biopsy
Results in 41 Patients with Suspected Renal Masses

Abstract

Objective

To determine whether 3D cone-beam computed tomography (CBCT) guidance allows safe and accurate biopsy of suspected small renal masses (SRM), especially in hard-to-reach anatomical locations.

Materials and methods

CBCT guidance was used to perform 41 stereotactic biopsy procedures of lesions that were inaccessible for ultrasound guidance or CT guidance. In CBCT guidance, a 3D-volume data set is acquired by rotating a C-arm flat-panel detector angiosystem around the patient. In the data set, a needle trajectory is determined and, after co-registration, a fusion image is created from fluoroscopy and a slice from the data set, enabling the needle to be positioned in real time.

Results

Of the 41 lesions, 22 were malignant, 17 were benign, and 2 were non-diagnostic. The two non-diagnostic lesions proved to be renal cell carcinoma. There was no growth during follow-up imaging of the benign lesions (mean 29 months). This resulted in a sensitivity, specificity, PPV, NPV, and accuracy of 91.7, 100, 100, 89.5, and 95.1%, respectively. Mean dose-area product value was 44.0 Gy·cm² (range 16.5–126.5). There was one minor bleeding complication.

Conclusion

With CBCT guidance, safe and accurate biopsy of a suspected SRM is feasible, especially in hard-to-reach locations of the kidney.

Introduction

The classic but nonspecific symptoms of a renal tumor are loin pain, hematuria, or a palpable mass. In this setting most masses are malignant [1]. This classic triad is rare nowadays. Due to an increase in the use of high-quality abdominal imaging for other, unrelated reasons there is an increasing number of incidentally found renal masses. Many of these masses are asymptomatic and small (<4 cm) renal masses (SRMs). These SRMs tend to behave less aggressively [2, 3]. Thompson et al. [4] found a relationship between tumor size and malignancy. Larger masses have a significantly higher ratio of malignancy. Marinez-Pineiro et al. [5] pointed out the important role in the diagnostic and therapeutic algorithm of biopsying small renal masses for histopathological proof [4] because a substantial percentage of SRMs are benign (13.0–46.3%). Some SRMs can be diagnosed by imaging (e.g., fat in the lesion on CT indicating an angiomyolipoma), but many SRMs cannot be diagnosed based on the imaging alone. This will result in increased indications for performing biopsies. A new real-time stereotactic needle guidance technique, 3D cone-beam computed tomography (CBCT) guidance, uses a combination of cone-beam CT and real-time fluoroscopy in the angiography suite [6, 7]. Lesions that cannot be clearly identified on ultrasound (US) can be rendered visible. Compared with conventional computed tomography (CT)-guided biopsy, CBCT guidance offers more sterile workspace and better angulation/rotation ability because of the C-arm configuration, making it easier to biopsy hard-to-reach SRMs, especially in the upper pole and/or on the anterior side of the kidney [7]. The objective of this study is to determine the outcome of biopsying SRMs, especially hard-to-reach lesions, in a prospective cohort of patients.

Materials and methods

This study was approved by the institutional review board. Informed consent was obtained from all patients. Between October 2006 and November 2009 we performed 43 procedures in 43 patients using CBCT guidance. There were 28 men and 15 women, with a mean age of 61.9 years (range 35–81). The baseline data of the study population are shown in *Table 1*. These patients had undergone abdominal imaging for nonurogenital issues, during which a suspicious

Table 1. The baseline data of the study population

Characteristic	Value
Age (years), mean \pm SD	62.0 \pm 11.3
Male/female (N)	26/15
Body mass index (kg/m ²), mean \pm SD	27.1 \pm 3.5
Diameter of lesion (mm), mean \pm SD	25.0 \pm 7.6
Number of biopsies per procedure, mean \pm SD	3.4 \pm 0.7
Lesion solid/cystic/both (N)	38/1/2
Procedure time (min), mean \pm SD	29.2 \pm 10.7
Dose area product (Gy·cm ²), mean \pm SD	44.0 \pm 21.0

Note: SD = standard deviation

renal mass was discovered as an incidental finding. Based on the abdominal imaging, the lesions were not (easily) accessible under CT guidance because of the anatomical position of the lesion. Before referring these patients for CBCT guidance, the patients were evaluated by ultrasound. Only patients with lesions inaccessible under ultrasound guidance (due to body habitus, mass location, invisibility due to gas or bone, or interposition of other organs) were included in this study. There was no target lesion size limit. During CBCT guidance, patients had to be able to lie reasonably still for a short period of time (approximately 30 min) and comply with breath-hold commands if needed. Furthermore, patients with contraindications for percutaneous intervention (e.g., blood coagulation disorders) were excluded.

Procedure

CBCT guidance uses a flat panel detector C-arm system (XperCT[®] and XperGuide[®], Allura FD20, Philips Healthcare, the Netherlands). A 3D volume data set is acquired during a 240° rotation of the C-arm around the upper abdomen of the patient in 4–10 s. In six patients, intravenous contrast (50 mL with 4 mL/s Xenetix[®] 300 mg/mL, Guerbet, the Netherlands; delay before data acquisition of 40 s) was administered during the examination to discriminate the mass from surrounding structures/parenchyma (*Figure 1*). For all other masses, no contrast administration was needed because they were exophytic or had other discriminating factors. The radiologist determines a safe needle trajectory within the reconstructed data set, taking account of critical anatomical structures (*Figure 2a, b*). Using the information of the planned needle trajectory, a fusion image of fluoroscopy and the relevant double oblique slice of the cone-beam CT

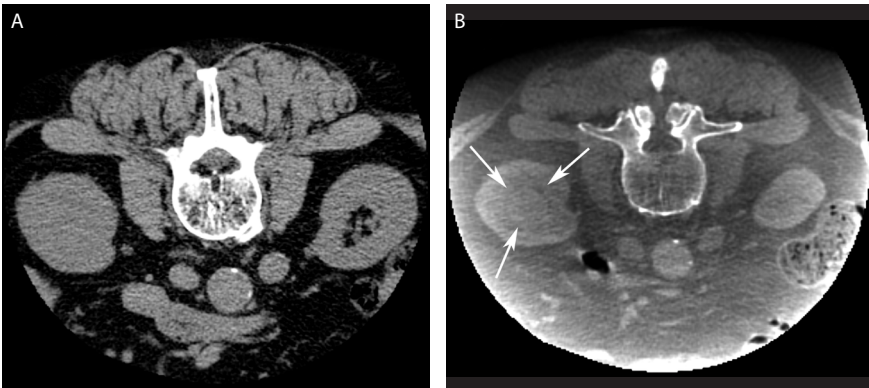


Figure 1. An 81-year-old man with a suspected endophytic kidney mass during abdominal CT imaging. After biopsy, histopathological analysis revealed a clear cell renal cell carcinoma. Difference in cone-beam CT (CBCT) without contrast medium (A) and contrast-enhanced CBCT (B). The endophytic renal mass (white arrows) is only visible on the contrast-enhanced CBCT

is created in which the needle can be accurately positioned. The patient is asked to breathe in until the diaphragm is in the same position as the double oblique slice of the CBCT. When the diaphragm on the fluoroscopy image matches the CBCT slice during inspiration, the patient was given a breath-hold command, and under real-time fluoroscopy the needle is advanced over the predefined needle path to the right depth (*Figure 2c*) [6, 7]. The procedure is performed with local anaesthesia. Sampling was done using a coaxial technique with a guiding cannula [Bard® TruGuide®; 17 G; 13 or 17 cm (Bard Biopsy Systems, Tempe, AZ, USA)] positioned just proximal to the renal mass. Three to six 18 G biopsies were then taken through the guiding needle to obtain at least 1 cm of biopsy length. The Tru-Cut needle (Bard® Magnum®; 18 G; 16, 20 or 25 cm; side cutting, 15 or 22 mm) is loaded in an automated biopsy gun (Bard®). After the needle intervention, a (collimated) control cone-beam CT was always performed for checking needle position accuracy and to check for possible complications (*Figure 2d*). The procedures were performed by an interventional radiologist (M.S., >10 years of experience) and a radiology resident (S.B., 5 years of experience), both with equal experience in CBCT guidance. Local experience in using this CBCT technique is now 3 years. After the procedure, patients remained under observation in the hospital for 4 h. In case of significant changes in vital signs or clinical status, repeat abdominal imaging was indicated (e.g., ultrasound or CT depending on the clinical condition of the patient).

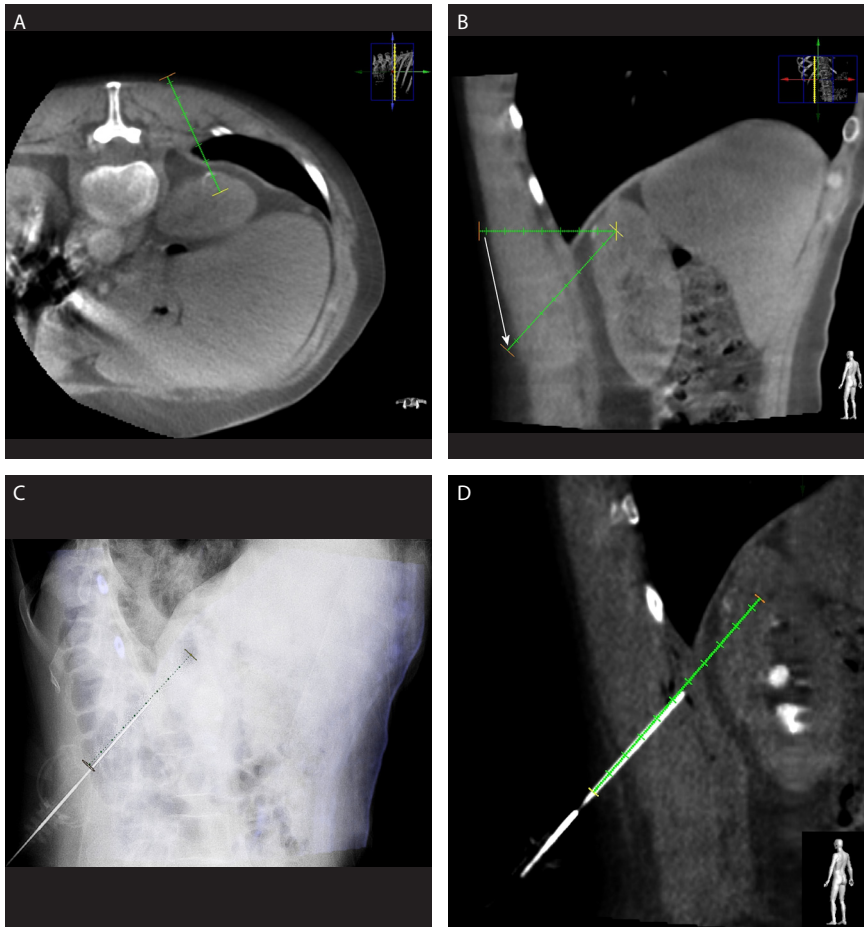


Figure 2. A 73-year-old man with a suspected lesion at the dorsal side of the upper pole of the left kidney. Histopathological analysis revealed a clear cell renal cell carcinoma. Cone-beam computed-tomography (CBCT) guidance sequences during a procedure. A, After obtaining a CBCT the radiologist determines in the axial CBCT the desired needle trajectory in the axial view (avoiding the costae). B, The needle trajectory is adjusted by the radiologist (white arrow) to avoid essential organs (the diaphragm/lung). C, Fusion image of fluoroscopy and the double oblique cone-beam CT slice with the predefined needle trajectory, making real-time accurate needle placement possible. D, Control cone-beam CT image (double oblique) with the guiding cannula in place over the predefined needle trajectory, checking needle position and possible complications

Data collection and analysis

All the radiological reports, histopathological data, and medical records were collected for each procedure. The result of a percutaneous renal mass biopsy was defined as true positive (TP) if the histopathological examination revealed a renal cell carcinoma or a metastasis. A false positive (FP) biopsy was defined as a biopsy showing malignancy, where there was no evidence of a

malignancy during surgery (in the absence of preoperative chemotherapy of other (ablative) therapy). If the histopathology showed a benign result (e.g., normal renal parenchyma, infection, infarction, or oncocytoma), the biopsy was considered true negative (TN) if the renal mass proved to be benign during surgical resection or if there was no suspicion of a malignancy during follow-up imaging for at least 12 months [8]. If the final diagnosis during surgery showed malignancy and the diagnosis based on the results of the biopsy procedure was benign or non-diagnostic, the biopsy result was defined as false negative (FN). Sensitivity, specificity, positive predictive value (PPV), negative predictive value (NPV), and diagnostic accuracy were calculated. The dose-area product (DAP) (Gy·cm²), which was obtained from the system, was also registered for an indication of the radiation dose involved. Data registration was performed using Excel (Microsoft® Office Excel, Redmond, WA, USA). The outcome was determined by using a 2 x 2 table.

Results

The sensitivity, specificity, PPV, NPV, and accuracy of CBCT guidance in renal masses were 91.7, 100, 100, 89.5, and 95.1%, respectively (Table 2). In 41 biopsies, 22 (53.7%) malignancies were found: 10 clear cell renal cell carcinomas (RCCs), two papillary RCCs, one chromophobe RCC, one eosinophilic RCC, one sarcomatoid type RCC, four transitional cell carcinomas, two metastases of non-small-cell lung cancer, and one B-cell lymphoma. All of these except the metastases and lymphoma were also surgically proven. During follow-up imaging of these patients, no evidence of tumor seeding on the needle track was seen. Seventeen (41.5%) biopsies, without rebiopsying, were classified as benign: four post-infectious changes, three oncocytomas, six biopsies showing normal renal parenchyma, one organizing hematoma, one angiomyolipoma,

Table 2. Outcome of percutaneous biopsy of small renal masses using 3D cone-beam computed tomography (CBCT) guidance

CBCT guidance	Renal mass		Total
	Malignant	Benign	
Malignant	22	0	22
Benign	2	17	19
Total	24	17	41

one inflammatory pseudotumor, and one infarction. The mean follow-up of the benign lesions was 29 months (range 18–45), without evidence of malignancy (e.g., lesion size growth). Two (4.9%) were non-diagnostic biopsies. The two patients with non-diagnostic lesions of 23.3 and 31 mm underwent (partial) nephrectomy because of suspicious cells found during histopathological examination. These masses proved to be RCC after surgical resection. Twenty-two (53.7%) lesions were endophytic. Contrast was used to visualize the lesion on CBCT in six patients (14.6%). Detailed information on tumor location is shown in *Table 3*. Mean diameter was 25.0 mm (range 10–40 mm), and the mean number of biopsies per procedure was 3.4 (range 3–6). Mean DAP value was 44.0 Gy·cm² (standard deviation (SD) 21.0; range 16.5–126.5). There were no serious adverse events. In one patient (2.4%) a continuing minor bleeding through the co-axial needle was present. This was treated directly by injecting hemostatic material (Spongostan®; Baxter, Deerfield IL, USA)]. No additional intervention or prolonged hospital admission was required.

Table 3. Anatomical details of tumor location

	Lower half	Upper half	Total
Dorsal	2	11	13
Lateral	-	8	8
Medial	-	5	5
Ventral	7	8	15
Total	9	32	41

Discussion

CBCT guidance has a sensitivity of 91.7%, an NPV of 89.5%, and an accuracy of 95.1% for histopathological biopsies of renal masses. To the authors' knowledge, only Kroeze et al. [9] has so far described CBCT guidance for biopsy of renal masses. They reported a technical feasibility of 77% in a small patient population (N=13) [9]. We report a better outcome, probably because of our larger population and longer experience with CBCT guidance. Volpe et al. [10] reviewed the technique, safety, and accuracy of sampling of renal tumors by core biopsy using CT or US and reported a sensitivity of 70–100%. In the study performed by Rybicki et al. [11], a sensitivity of 90% was reported. Several other

studies have also evaluated the sensitivity of renal biopsies, resulting in an overall sensitivity for diagnosis of malignancy of 80–95%. However the studies show considerable variation in population and method of guidance (US or CT) [1, 12–14]. Vasudevan et al. [1] report 47 malignant biopsies, 23 benign biopsies, and 4 false negative biopsies resulting in an NPV of 85.2%. Rybicki et al. [11] had an NPV of 64% in their population. In our study population, the NPV was 89.5%. Nadal et al. [12] described an accuracy of 87% on the initial biopsy improving to 97% after a second biopsy. Biopsies were performed using an 18 G core biopsy needle, and an overall accuracy of 89% was achieved [15, 16]. Shannon et al. [17] reported a diagnostic biopsy rate of 78%, with 22% non-diagnostic biopsies due to insufficient material or nonmalignant renal material. Our accuracy is in the same range (95.1%). Our results of the percutaneous renal biopsies using CBCT guidance are comparable with those in the literature. However in most of our procedures the needle trajectory had to be at a (steep) double oblique angle, which is more difficult to perform using CT (fluoroscopy) guidance. To perform angulated procedures with CT guidance, there are a couple of techniques available. One possibility is the gantry tilting method, whereby the gantry of the CT system is tilted between 0 and 30° depending on the vendor, making an angulated biopsy possible. The tilting method proved to be accurate (90–96%) in biopsy of hard-to-reach upper abdominal masses [18]. The operator can, during the tilting method, also use CT fluoroscopy, visualizing the slices of interest in real time. A drawback of tilting is the negative influence on the sterile workspace, which is already reduced during conventional CT (fluoroscopy) guidance compared to the C-arm configuration [19]. Another technique, which has a histopathological accuracy of 76%, is the triangulation technique as described by vanSonnenberg et al. [20]. It requires calculation of the angle and trigonometric tables. During the procedure a large number of slices need to be scanned to visualise the whole needle trajectory, resulting in longer procedure times and more radiation exposure to the patient. Because of the long needle trajectory, the needle passes different soft tissues with different resistance; this, in combination with respiratory movement, adds more complexity to the procedure [21]. For angulated procedures, MRI also offers a good alternative to a needle intervention, especially for lesions invisible on CT and US. Stattaus et al. [22] reported a sensitivity of 95.5%, specificity of 100%, and an accuracy of 96% using a short, wide-bore 1.5 T MR system. Kühn et al. [23] reported an

accuracy of 94%. Both groups agree that MR-guided procedures are also feasible for lesions with quite a steep angulation due to MRI's capacity for multiplanar viewing. However, they acknowledge that the gantry size in regular MR systems is limited. Other possible disadvantages of MR-guided procedures include that they are considered expensive because of dedicated materials and biopsy systems, the reported mean procedure time is 42–48 min (compared to our 29 min), and needle artifacts may be present. In our experience steep, double-angulation procedures are easier with CBCT guidance because of the C-arm geometry with an angulation range up to 50°. In addition to this, there is real-time feedback of the fluoroscopy with a large field-of-view compared to CT fluoroscopy. Breathing can be halted at a point where the diaphragm on the fluoroscopy image exactly matches the diaphragm in the (double oblique) overlay slice of the cone-beam CT. This enables real-time compensation of breathing movements during the progression of the needle, compensating for the respiratory movement and deviation due to different tissue resistance. Therefore, in our experience, CBCT guidance is better for biopsying hard-to-reach lesions than CT or MRI. The two non-diagnostic lesions presented normal kidney parenchyma with atypical cells, but the biopsies were found to be insufficient for diagnosis in the histopathological report. Because of this report and the malignant features on abdominal imaging with CT, the decision was made to perform a (partial) nephrectomy. Both of these lesions were exophytic. The definite diagnosis in both patients was a renal cell carcinoma. Checking with the control CBCT, it appears that the biopsies were most likely planned slightly peripheral to the lesions. That is a possible reason for the presence of at least some atypical cells in the specimen suggesting a malignancy, but there was not enough material to make a definitive conclusion. The comparable results of CBCT guidance and the literature suggest that this new technique can be performed easily and accurately, but it is not as widely available as CT, ultrasound, or MRI. Using the reported conversion factor from DAP to effective dose of 0.28–0.29 (mSv·Gy⁻¹·cm⁻²) by Suzuki et al. [24] during abdominal cone-beam CT, our mean effective dose was 12.5 (± 5.9 SD) mSv. This conversion was done to compare the dose of CBCT guidance to CT guidance in the literature. Tsalafoutas et al. [25] report an effective dose of 23 mSv during conventional CT-guided biopsies in which unenhanced, intervention, and control post-procedure CT data acquisitions were performed. Other studies report a lower

effective dose (7.1–12 mSv) during CT-guided biopsies; however in these procedures no final post-procedure CT data acquisition was performed to check for possible complications [26, 27]. No serious complications occurred during our procedures. The literature on renal mass biopsy shows complications of pain, hematuria, bleeding, and tumor seeding. The percentage of complications depends on the size of the needle [28, 29]. Vaseduvan et al. [1] used a 16 G needle and reported a complication rate in 100 biopsies of 1%, for which the patient needed a blood transfusion. Nadal et al. [12] reported a complication rate of 12% in biopsy of renal masses using an 18 G biopsy needle. In this report 3% of the procedures needed a blood transfusion. In the report of Whittier et al. [30], a 13% overall complication rate was reported using a 14 G biopsy needle. Fifty percent of these were major complications (e.g., gross hematuria, death). In our population we had one patient (2.4%) with some persistent bleeding out of the co-axial needle (17 G), which could be directly treated. No other complications or tumor seeding along the needle track was noticed during the follow-up. A limitation of this study is the inability to obtain a definitive confirmation of the lesions defined as nonmalignant (except the two non-diagnostic lesions with suspicious cells which were operated), e.g., organising hematoma, pseudotumor, and the three non-diagnostic results, because all were treated conservatively. However, no changes on subsequent CT indicating malignancy (e.g., increasing size) were noted during follow-up, and therefore the definitive diagnosis was assumed to be benign. A second possible limitation is our relatively short follow-up period of 2 years. A new image-merging feature has recently been introduced into the planning system (XperGuide®, Philips Healthcare, the Netherlands). This tool allows recent cross-sectional DICOM data (CT or MRI) to be used to plan the needle trajectory. After importing these data into the system, a match is made manually between the recent DICOM data and the (low-dose) cone-beam CT data. Preliminary experimental results of this merging feature for accurate planning are promising, possibly leading to even higher accuracy, especially in endophytic masses.

In conclusion, our results demonstrate acceptable sensitivity and accuracy of renal mass needle biopsy using 3D CBCT guidance. CBCT guidance appears to be a safe and accurate procedure for biopsy of small (<4 cm) renal masses, especially those in difficult-to-reach anatomical regions.

References

1. Vasudevan A, Davies RJ, Shannon BA, Cohen RJ (2006) Incidental renal tumours: the frequency of benign lesions and the role of preoperative core biopsy. *BJU Int* 97:946–949
2. Patard JJ, Rodriguez A, Rioux-Leclercq N, Guillé F, Lobel B (2002) Prognostic significance of the mode of detection in renal tumours. *BJU Int* 90:358–363
3. Luciani LG, Cestari R, Tallarigo C (2000) Incidental renal cell carcinoma—age and stage characterization and clinical implications: study of 1092 patients (1982–1997). *Urology* 56:58–62
4. Thompson RH, Kurta JM, Kaag M et al (2009) Tumor size is associated with malignant potential in renal cell carcinoma cases. *J Urol* 181:2033–2036
5. Marinez-Pineiro L, Maestro MA (2010) Challenging the EAU guidelines: role of biopsy and management of small renal tumours. *Eur Urol* 9:450–453
6. Racadio JM, Babic D, Homan R et al (2007) Live 3D guidance in the interventional radiology suite. *AJR Am J Roentgenol* 189:W357–W364
7. Braak SJ, van Strijen MJL, van Leersum M, van Es HW, van Heesewijk JPM (2010) Real-time 3D fluoroscopy guidance during needle interventions: technique, accuracy and feasibility. *AJR Am J Roentgenol* 194:W445–W451
8. Chawla SN, Crispen PL, Hanlon AL, Greenberg RE, Chen DYT, Uzzo RG (2006) The natural history of observed enhancing renal masses: meta-analysis and review of the world literature. *J Urol* 175:425–431
9. Kroeze SGC, Huisman M, Verkooijen HM, van Diest PJ, Bosch JLHR, van den Bosch MAAJ (2012) Real-time 3D fluoroscopy guided large core needle biopsy of renal masses: a critical early evaluation according to the IDEAL recommendations. *Cardiovasc Intervent Radiol* 35:680–685. doi:10.1007/s00270-011-0237-4
10. Volpe A, Kachura JR, Geddie WR et al (2007) Techniques, safety and accuracy of sampling of renal tumors by fine needle aspiration and core biopsy. *J Urol* 178:379–386
11. Rybicki FJ, Shu KM, Cibas ES, Fielding JR, vanSonnenberg E, Silverman SG (2003) Percutaneous biopsy of renal masses: sensitivity and negative predictive value stratified by clinical setting and size of masses. *AJR Am J Roentgenol* 180:1281–1287
12. Nadal L, Baumgartner BR, Bernardino ME (1986) Percutaneous renal biopsies: accuracy, safety, and indications. *Urol Radiol* 8:67–71
13. Schmidbauer J, Remzi M, Memarsadeghi M et al (2008) Diagnostic accuracy of computed tomography-guided percutaneous biopsy of renal masses. *Eur Urol* 53:1003–1012

14. Silverman SG, Unn Gan Y, Morteale KJ, Tuncali K, Cibas ES (2006) Renal masses in the adult patient: the role of percutaneous biopsy. *Radiology* 240:6–22
15. Lechevalier E, André M, Barriol D et al (2000) Fine needle percutaneous biopsy with computerized tomography guidance. *Radiology* 216:506–510
16. Lechevalier E (2007) Core biopsy of solid renal masses under CT guidance. *Eur Urol* 6:540–543
17. Shannon BA, Cohen RJ, de Bruto H, Davis RJ (2008) The value of preoperative needle core biopsy for diagnosing benign lesions among small, incidentally detected renal masses. *J Urol* 180:1257–1261
18. Sharma KV, Venkatesan AM, Swerdlow D et al (2010) Image guided adrenal and renal biopsy. *Tech Vasc Interv Radiol* 13:100–109
19. Hussain S (1996) Gantry angulation in CT-guided percutaneous adrenal biopsy. *AJR Am J Roentgenol* 166:537–539
20. vanSonnenberg E, Wittenberg J, Ferruci JT, Mueller PR, Simeone JF (1981) Triangulation method for percutaneous needle guidance: the angled approach to upper abdominal masses. *AJR Am J Roentgenol* 137:757–761
21. Odisio BC, Tam AL, Avritscher R, Gupta S, Wallace MJ (2012) CT-guided adrenal biopsy: comparison of ipsilateral decubitus versus prone patient positioning for biopsy approach. *Eur Radiol*. doi:10.1007/s00330-011-2363-4
22. Stattaus J, Maderwald S, Baba HA et al (2008) MR-guided liver biopsy within a short, wide-bore 1.5 Tesla MR system. *Eur Radiol* 18:2865–2873
23. Kühn JP, Langner S, Hegenscheid K et al (2010) Magnetic resonance-guided upper abdominal biopsies in a high-field widebore 3-T MRI system: feasibility, handling, and needle artifacts. *Eur Radiol* 20:2414–2421
24. Suzuki S, Furui S, Yamaguchi I et al (2009) Effective dose during abdominal three-dimensional imaging with a flat-panel detector angiography system. *Radiology* 250:545–550
25. Tsalafoutas IA, Tsapaki V, Triantopoulou C, Gorantonaki A, Papailiou J (2007) CT-guided interventional procedures without CT fluoroscopy assistance: patient effective dose and absorbed dose considerations. *AJR Am J Roentgenol* 188:1479–1484
26. Teeuwisse WM, Geleijns J, Broerse JJ, Obermann WR, van Meerten EL Van Persijn (2001) Patient and staff dose during CT guided biopsy, drainage and coagulation. *Br J Radiol* 74:720–726
27. Joemai RMS, Zweers D, Obermann WR, Geleijns J (2009) Assessment of patient and occupational dose in established and new applications of MDCT fluoroscopy. *AJR Am J Roentgenol* 192:881–886

28. Nicholson ML, Wheatley TJ, Doughman TM et al (2000) A prospective randomized trial of three different sizes of core cutting needle for renal transplant biopsy. *Kidney Int* 58:390–395
29. Kolb LG, Velosa JA, Bergstralh EJ, Offord KP (1994) Percutaneous renal allograft biopsy a comparison of two needle types and analysis of risk factors. *Transplantation* 57:1742–1746
30. Whittier WL, Korbet SM (2004) Renal biopsy: update. *Curr Opin Nephrol Hypertens* 13:661–665 *Eur Radiol*



Sicco J. Braak¹ • Lars van Bindsbergen² • Marco J.L. van Strijen¹ • Jean-Paul P.M. de Vries²

¹Department of Radiology, St. Antonius Hospital, Nieuwegein, The Netherlands

²Department of Vascular Surgery St. Antonius Hospital, Nieuwegein, The Netherlands

J Vasc Interv Radiol 2010; 21:1443–1447

Received November 21, 2009; final revision received March 31, 2010; accepted May 21, 2010.

L.v.B. and S.J.B. contributed equally to this article.

Chapter 6

Type II Endoleak Embolization after
Endovascular Abdominal Aortic
Aneurysm Repair with Use of
Real-time Three-dimensional
Fluoroscopic Needle Guidance

Abstract

Current treatment for type II endoleak includes transarterial embolization and translumbar puncture, but each method has its drawbacks. With real-time three-dimensional fluoroscopy guidance, a cone-beam computed tomography (CT) image is created in which the needle trajectory is determined. The trajectory is superimposed on the fluoroscopy image, allowing real-time needle placement for precise embolization. We have used this method to treat five patients with complex type II endoleaks. All interventions were successful and uncomplicated. At 6-month follow-up, CT scan showed no recurrences. Direct puncture and injection with real-time three-dimensional fluoroscopy guidance shows encouraging results as treatment for complex type II endoleaks after endovascular abdominal aortic aneurysm repair (EVAR).

Introduction

During the last decade, endovascular abdominal aortic aneurysm repair (EVAR) has emerged as the preferred treatment in patients with suitable vascular anatomy. Short-term results of EVAR are significantly better compared with open repair (1–4). With the introduction of EVAR, new, treatment-specific complications have also emerged, including endoprosthesis migration and endoleaks. Type II endoleak, defined as retrograde aneurysm sac filling by backbleeding of patent aortic side branches, such as the lumbar arteries or inferior mesenteric artery, has an incidence of 10%–25% at 3 months of follow-up (5,6). Type II endoleaks can be categorized as simple (IIA, to-and-from endoleak from one patent branch) and complex (IIB, two or more patent branches) (5,7,8). Most simple type II endoleaks that are detected early are self-limiting; however, complex type II endoleaks may persist and may cause aneurysm enlargement. Aneurysm rupture after EVAR because of a persistent type II endoleak has been reported (8). Most centers, including our own, abandon a conservative approach and treat a type II endoleak if the native aneurysm becomes symptomatic or if persistent aneurysm volume growth is documented (9,10). There are several options for treatment of persistent, mainly complex type II endoleaks. One option is catheter-derived transarterial embolization through a transfemoral or transbrachial access. This technique is often labor-intensive, and even with the use of microcatheters, some side branches are too small to catheterize. Another treatment option is direct translumbar puncture guided by CT (11). An alternative, invasive approach is laparoscopic clipping and division of all patent side branches, sometimes with fenestration of the native aneurysm wall to remove the thrombus. The search for a minimally invasive, reliable technique for embolization of type IIB endoleaks without the limitations of catheter size has led to the use of a real-time three-dimensional fluoroscopic technique that can be used for optimal needle guidance (XperCT and XperGuide, Allura FD20 angiography interventional system; Philips Healthcare, Best, The Netherlands). We describe this technique for the treatment of post-EVAR type IIB endoleaks in five patients.

Materials and methods

Between March 2008 and March 2009, we treated five men with complex post-EVAR type II endoleaks using real-time three-dimensional fluoroscopy needle guidance in the angiography suite of the Interventional Radiology Department. Patients had an average age of 78.2 years (range 74–82 years). The indication for treatment was growth of the aneurysm with a type 2 endoleak visible on CT scan. Average aneurysm size measured on the last CT scan before treatment was 66.2 mm (range 51–87 mm). Baseline characteristics are listed in the *Table*. The patients were treated in the prone position under local anesthesia. No antibiotic prophylaxis was given. Real-time three-dimensional fluoroscopy guidance uses a flat panel detector system (XperCT and XperGuide, Allura FD20; Philips Healthcare, Best, The Netherlands) capable of creating a three-dimensional soft tissue cone-beam CT scan after rotating 180–240 degrees around the patient in 4–10 seconds. Within the three-dimensional soft tissue data set, the optimal needle trajectory is determined by the interventional radiologist, taking care to avoid vital anatomic structures. In our series, visualization of the type II endoleak was obtained by administering 50 mL (4 mL/sec) of contrast agent (Xenetix 300, Guerbet SA, Villepinte, France) 20 seconds before acquiring the cone-beam CT volume. In the three-dimensional volume, the center of the contrast flush within the aneurysm sac (endoleak nidus) is marked as the target, and the ideal needle trajectory is drawn (*Figure 1*). The optimal C-arm geometry is calculated after the virtual trajectory within the three-dimensional cone-beam CT volume is determined. The three-dimensional cone-beam volume and needle trajectory are coregistered with the movement of the C-arm. The fluoroscopy image is superimposed over the three-dimensional volume slice, producing a guiding path within the coupled images (*Figure 2*). This needle path can be used to advance the 15- or 20-cm trocar needle (Cook Medical, Bloomington, Indiana) accurately (within a safety margin of 5 mm) into the endoleak nidus in real time. Digital subtracted angiography (DSA) is performed after direct puncture of the endoleak to visualize the complex feeding vessels (*Figure 3 and 4*). The contrast agent is injected through the needle; no separate catheter is placed. This is followed by direct pressure measurement within the endoleak. Embolization of the endoleak is performed using Tissucol (Baxter Healthcare, Deerfield Illinois) in most patients or 1.0 mL of Lipiodol (Guerbet SA, Villepinte, France)

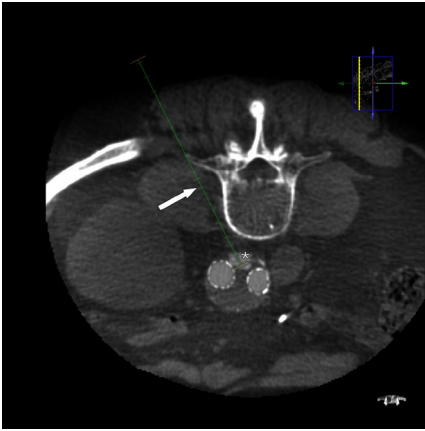


Figure 1. Axial three-dimensional soft tissue cone-beam CT after intravenous contrast agent administration with the planned needle trajectory (arrow) from the nidus of the endoleak (asterisk) to the skin.

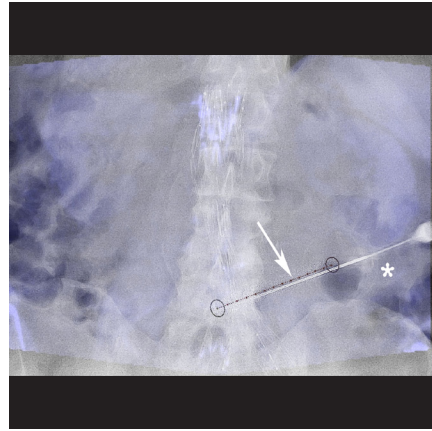


Figure 2. Fusion image of patient 4 shows a transection image of three-dimensional volume and fluoroscopy image, with planned needle trajectory (arrow) and placed needle (asterisk).



Figure 3. Fluoroscopic image of patient 4 shows the needle in the type IIB endoleak (asterisk), with multiple arterial feeding vessels (arrows).

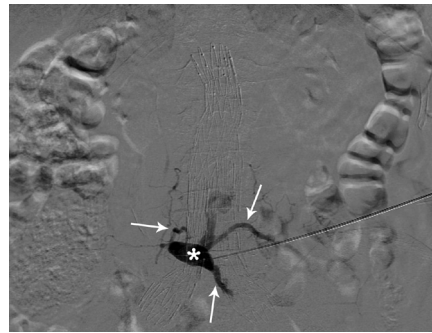


Figure 4. DSA from patient 1 confirms the complexity of the endoleak (asterisk) with multiple feeding vessels (arrows).

mixed with 1.0 mL of Histoacryl (B. Braun AG, Melsingen, Germany) (Figure 5). Directly after the embolization, the needle is gently flushed with a mixture of saline and contrast agent so that the needle is not obstructed by the glue. A second DSA is then possible to check the effect of the embolization. Depending on the result, the embolization is considered completed, or more embolic agent is added into the nidus. A control CT angiogram of the abdominal aorta is performed 1 month and 6 months after the embolization for evaluation of short-term results (Figure 6). Procedure time is defined as the room occupation time. This study was approved by our institutional review board.

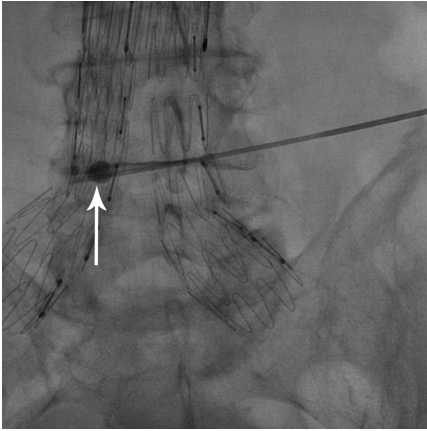


Figure 5. Fluoroscopic real-time embolization (arrow) of the endoleak, using Histoacryl and Lipiodol, is shown in patient 1.

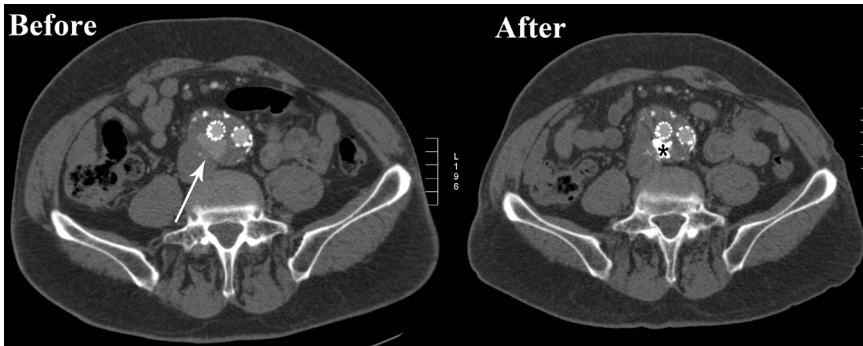


Figure 6. CT angiogram of patient 1, before and after real-time three-dimensional fluoroscopic needle guidance embolization, shows contrast material outside the endoprosthesis (arrow) and embolization material in situ after the embolization procedure (asterisk).

Results

All patients were successfully treated for type IIB endoleaks without initial complications. Patient 1 was treated with a mixture of 1.0 mL of Histoacryl and 1.0 mL of Lipiodol, and patients 2 through 5 were treated with Tissucol. The median (\pm SD) procedure time of the treatment was 35.5 minutes (range 34.0–37.0 minutes), and the median amount of contrast agent was 65.0 mL (range 60.0–70.0 mL). Median radiation dose (dose area product) was 120,837 mGy.cm² (range 107,123–150,060 mGy.cm²). The measured pressure in the aneurysm sac was lower after treatment in all patients. All patients returned for the 6-month follow-up CT scan, which showed no recurrence of treated endoleaks and no occurrence of new endoleaks (*Table*).

Patient data												
Patient	Age (y)	Initial Aneurysm Size (mm)	Aneurysm Size on Treatment (mm)	EVAR	Endoleak	Treatment Indication	Embolization Material	Radiation Dose (DAP; mGy·cm ²)	Aneurysm Sac Pressure		Follow-up (months)	
									Before treatment	After treatment		
1	74	58	64	Zenith bifurcation	Type II b	Aneurysm growth	Histoacryl/lipiodol	142090	66	149 / 100 (119)	64 / 61 (60)	15
2	82	60*	64	Talent Mono ileal †	Type II b	Aneurysm growth	Tissuocol	42013	72	109 / 87 (97)	12 / 10 (10)	8
3	82	57	65	Zenith bifurcation	Type II b	Aneurysm growth	Tissuocol	150060	68	97 / 54 (74)	2 / 0 (1)	7
4	77	83	87	Talent bifurcation	Type II b	Aneurysm growth	Tissuocol	120837	64	125 / 62 (88)	99 / 58 (76)	7
5	76	36 ‡	51	Excluder bifurcation	Type II b + Type II a	Aneurysm growth	Tissuocol	80616	63	120 / 90 (100)	2 / 2 (2)	6

All patient were men. The treatment was successful in all patients, and there were no complications.

* Ruptured aortic aneurysm.

† Uniliac endoprosthesis with contralateral occluder in the common iliac artery and a femorofemoral crossover bypass.

‡ AAA 39 mm and aneurysm of common iliac artery of 36 mm.

Discussion

We have described our results of real-time three-dimensional fluoroscopic needle guidance for translumbar treatment of type IIB endoleaks after EVAR. Within the three-dimensional data volume of the cone-beam CT, the endoleak and the needle path can be visualized in relation to the surrounding anatomic structures. This allows the interventional radiologist to choose the exact trajectory and avoid damage to the soft tissues without the risk of graft puncture. The coregistration of the fluoroscopy image and the three-dimensional cone-beam CT volume provide visual real-time feedback on needle position during the puncture in relation to the intestinal organs and the endoprosthesis. A comparable technique was described previously, but that technique does not benefit from direct superimposition of the fluoroscopy images on the three-dimensional volume and the added real-time periprocedural feedback it gives (12). Real-time three-dimensional fluoroscopic needle-guided treatment of complex type II endoleaks has several advantages compared with standard transarterial microcatheter embolization. In transarterial microcatheter embolization, coils are placed in the endoleak nidus or in the feeding arteries to the endoleak nidus. This transarterial route is often labor-intensive and time-consuming. Owing to direct puncture with real-time three-dimensional fluoroscopic needle guidance, treatment time is likely to be shorter, and less contrast agent is likely to be needed. The real-time three-dimensional fluoroscopic guidance technique allows successful treatment of endoleaks that cannot be reached through transarterial access because of the small caliber of most of the feeding arteries. Another treatment option is direct translumbar puncture after identifying the endoleak on CT and localizing it during the fluoroscopic needle-guided procedure through fluoroscopically identifiable landmarks and radiopaque markers on the stent (11,13). Embolization of the endoleak itself prevents flow between different feeding vessels. This method has been described to have good results in case series (11,13,14). A recent larger retrospective study has shown no benefit of translumbar embolization over transarterial embolization; however, both methods had a primary success rate of less than 80% (15). In our series and in the series of Binkert et al. (12), all patients have been successfully treated. Real-time three-dimensional fluoroscopic needle guidance in essence works through the same mechanism as

translumbal embolization but has advantages. In our opinion, more endoleaks can be reached with cone-beam CT guidance compared with fluoroscopic advancement of a needle based on the anatomy of a pretreatment CT scan. Vulnerable structures can be spared because of real-time feedback in the three-dimensional volume while still following the predetermined trajectory. Endoleaks with a small nidus can be accurately reached. This problem has been reported in previous descriptions of direct puncture methods (16). Puncturing in steep angles in all planes is more easily visualized and executed under real-time three-dimensional fluoroscopic needle guidance. To our knowledge, there are no reports concerning the dose during similar percutaneous type II embolization procedures. Our median radiation dose compared with interventional radiology procedures generally is low (17). Limitations of our study are that only five patients have been treated, with a relatively short average follow-up of about 8 months (range 6–15 months). Another shortcoming is that the embolization is visible only using a Histoacryl and Lipiodol mixture, which was done in our first patient. Histoacryl is known to be a good thrombotic agent, and Lipiodol works well as a contrast agent. The combination of these two agents makes the embolization itself visible; however, preparation of this mixture is labor-intensive, compared with use of Tissucol. The mixture of Histoacryl and Lipiodol creates a radiopaque scattering artifact during the follow-up CT scan, making small repeat endoleaks difficult to see. To see any changes during the follow-up examination, a noncontrast-enhanced CT should be performed just before the CT angiogram, which is not necessary when using Tissucol. The advantage of Tissucol is that it is ready to use after thawing. A disadvantage of Tissucol is that it cannot be mixed with a contrast medium. The amount of Tissucol and the speed of injection using the embolization should be titrated using test contrast agent injections before injection of the thrombotic agent itself to prevent thromboembolization distally to the mesenteric arteries in case of type II endoleaks from the inferior mesenteric artery. After the Tissucol is injected, the embolization must be checked by a control DSA. Because of surrounding essential anatomy, the planned trajectory of the needle to enter the nidus of the endoleak can be limited. Selective catheterization of the feeding vessel for embolization with coils is an option but is more labor intensive or sometimes impossible (because of the small size of the nidus and the incoming angle of the needle). In conclusion, direct puncture with real-time three-dimensional

fluoroscopic needle guidance is a minimally invasive treatment for complex type II endoleaks after EVAR, with limited procedural time and limited contrast agent use. All complex endoleaks in this case series of five patients were successfully treated, but long-term follow-up data are lacking.

References

1. Greenhalgh RM, Brown LC, Kwong GP, Powell JT, Thompson SG; EVAR trial participants. Comparison of endovascular aneurysm repair with open repair in patients with abdominal aortic aneurysm (EVAR trial 1), 30-day operative mortality results: randomised controlled trial. *Lancet* 2004; 364: 843–848.
2. Lovegrove RE, Javid M, Magee TR, Galland RB. A meta-analysis of 21,178 patients undergoing open or endovascular repair of abdominal aortic aneurysm. *Br J Surg* 2008; 95:677–684.
3. Prinssen M, Verhoeven EL, Buth J, et al. Dutch Randomized Endovascular Aneurysm Management (DREAM) Trial Group. A randomized trial comparing conventional and endovascular repair of abdominal aortic aneurysms. *N Engl J Med* 2004; 351:1607–1618.
4. Giles KA, Schermerhorn ML, O'Malley AJ, et al. Risk prediction for perioperative mortality of endovascular vs open repair of abdominal aortic aneurysms using the Medicare population. *J Vasc Surg* 2009; 50:256–262.
5. Veith FJ, Baum RA, Ohki T, et al. Nature and significance of endoleaks and endotension: summary of opinions expressed at an international conference. *J Vasc Surg* 2002; 35:1029–1035.
6. Waasdorp E, van Herwaarden JA, van de Mortel RH, Moll FL, de Vries JP. Early computed tomographic angiography after endovascular aneurysm repair: worthwhile or worthless? *Vascular* 2008; 16:253–257.
7. Chaikof EL, Blankensteijn JD, Harris PL, et al. Ad Hoc Committee for Standardized Reporting Practices in Vascular Surgery of the Society for Vascular Surgery/American Association for Vascular Surgery. Reporting standards for endovascular aortic aneurysm repair. *J Vasc Surg* 2002; 35: 1048–1060.
8. Schlösser FJ, Gusberg RJ, Dardik A, et al. Aneurysm rupture after EVAR: can the ultimate failure be predicted? *Eur J Vasc Endovasc Surg* 2009; 37: 15–22.
9. Gelfand DV, White GH, Wilson SE. Clinical significance of type II endoleak after endovascular repair of abdominal aortic aneurysm. *Ann Vasc Surg* 2006; 20:69–74.
10. van Marrewijk CJ, Fransen G, Laheij RJ, Harris PL, Buth J; EUROSTAR Collaborators. Is a type II endoleak after EVAR a harbinger of risk? Causes and outcome of open conversion and aneurysm rupture during follow-up. *Eur J Vasc Endovasc Surg* 2004; 27: 128–137.
11. Baum RA, Carpenter JP, Golden MA, et al. Treatment of type 2 endoleaks after endovascular repair of abdominal aortic aneurysms: comparison of transarterial and translumbar techniques. *J Vasc Surg* 2002; 35:23–29.
12. Binkert CA, Alencar H, Singh J, Baum RA. Translumbar type II endoleak repair using angiographic CT. *J Vasc Interv Radiol* 2006; 17:1349–1353.

13. Stavropoulos SW, Kim H, Clark TW, Fairman RM, Velazquez O, Carpenter JP. Embolization of type 2 endoleaks after endovascular repair of abdominal aortic aneurysms with use of cyanoacrylate with or without coils. *J Vasc Interv Radiol* 2005; 16:857–861.
14. Rial R, Serrano Fj F, Vega M, et al. Treatment of type II endoleaks after endovascular repair of abdominal aortic aneurysms: translumbar puncture and injection of thrombin into the aneurysm sac. *Eur J Vasc Endovasc Surg* 2004; 27:333–335.
15. Stavropoulos SW, Park J, Fairman R, Carpenter J. Type 2 endoleak embolization comparison: translumbar embolization versus modified transarterial embolization *J Vasc Interv Radiol* 2009; 20:1299–1302.
16. Rhee SJ, Ohki T, Veith FJ, Kurvers H. Current status of management of type II endoleaks after endovascular repair of abdominal aortic aneurysms. *Ann Vasc Surg* 2003; 17:335–344.
17. Miller DL, Balter S, Cole PE, et al. Radiation doses in interventional radiology procedures: the RAD-IR study; part I: overall measures of dose. *J Vasc Interv Radiol* 2003; 14:711–727.



Sicco J. Braak¹ • Marco J.L. van Strijen¹ • Hendrik W. van Es¹ • Rutger A.J. Nievelstein² • Johannes P.M. van Heeswijk¹

¹Department of Radiology, St. Antonius Hospital, Nieuwegein, The Netherlands

²Department of Radiology, University Medical Center Utrecht, Utrecht, The Netherlands

J Vasc Interv Radiol 2011; 22:455-461

Received November 6, 2010; final revision received February 5, 2011; accepted February 7, 2011.

Chapter 7

Effective Dose during Needle Interventions:

*Cone-beam CT Guidance Compared
with Conventional CT Guidance*

Abstract

Objective

To determine effective radiation dose to patients during needle interventions with cone-beam computed tomography (CT) guidance and compare it with the dose during conventional CT-guided interventions.

Materials and Methods

Cone-beam CT guidance is a recently developed technique with image acquisition on a flat-panel detector digital angiography system. It is based on a combination of acquired three-dimensional soft-tissue cone-beam CT, dedicated needle trajectory software, and fluoroscopy, providing stereotactic needle guidance. To analyze effective dose, we prospectively recorded all contributing parameters necessary to calculate it in 92 needle interventions (in 88 patients [60 men]; mean age, 63.9 y) using a Monte Carlo program. For CT guidance, we retrospectively scored the necessary parameters during 137 needle interventions (118 patients [81 men]; mean age, 59.5 y) to calculate effective dose with a CT patient dosimetry calculator. The needle interventions were categorized in four regions.

Results

Total mean effective doses with cone-beam CT guidance were 7.6 mSv in the upper thorax, 12.3 mSv in the lower thorax, 16.1 mSv in the upper abdomen, and 13.4 mSv in the lower abdomen. Effective doses with uncollimated cone-beam CT alone were 2.0, 2.9, 4.2, and 3.5 mSv in the respective regions. Effective doses with CT-guided interventions were 13.0, 15.1, 20.4, and 15.4 mSv in the respective regions. Cone-beam CT guidance results in a reduction of 13%–42% of total effective dose compared with conventional CT guidance. The dose reduction is mainly attributable to cone-beam CT, not to fluoroscopy.

Conclusions

A new needle intervention technique with cone-beam CT guidance results in a considerable effective dose reduction for patients compared with conventional CT guidance.

Purpose

In the past decade, there has been an increase in radiation dose to patients that is attributable to an increase in the use of computed tomography (CT) examinations and CT-guided interventions (1,2). For interventional radiologists, needle interventions are part of daily practice for therapeutic drainage, aspiration, or the performance of biopsies. During these interventions, precise positioning of the needle is essential, specifically in small lesions. Ideally, the imaging equipment used for needle interventions should image in real time, with the availability of volumetric images such as CT or magnetic resonance (MR) imaging. Needle interventions with conventional CT guidance are accurate (3), but the gantry of a CT scanner can limit the workspace available, and advancing a needle through an out-of-plane path can be difficult (4). With multiple vendors offering cone-beam CT fluoroscopy as part of flat-panel angiography systems, it has become possible to track the needle in real time, and to have volumetric imaging available at the tableside. This approach and the associated technology are relatively new, so there is a need for reports that define comparative radiation dose values in cone-beam CT guidance. To this end, we prospectively measured and calculated effective patient doses and compared them with those of previously performed conventional CT-guided interventions.

Materials and methods

Cone-beam CT Guidance

Cone-beam CT guidance uses a flat-panel detector system mounted on a C-arm (XperCT/Allura FD20 angiography system; Philips, Best, The Netherlands) capable of acquiring cone-beam CT images (5). A three-dimensional soft-tissue dataset is reconstructed from the cone-beam CT acquisition. The user can then apply dedicated software (XperGuide; Philips) to determine a safe and preferred needle path from the skin to the target lesion through the reconstructed three-dimensional dataset, avoiding vulnerable structures (ie, vessels, organs) (6,7). When the virtual trajectory has been determined, the three-dimensional data and virtual trajectory are coregistered with real-time fluoroscopy. The calculated needle path is projected in the fluoroscopy image, producing a real-

time (fluoroscopic) image of the needle advancing to the target with a high degree of accuracy, compared with CT guidance with comparable procedure times (7).

Patients

Cone-beam CT guidance.

From October 2007 to December 2008, all patients with an indication for a CT guided needle intervention (i.e., in lesions not amenable or visible by ultrasound) were included in the study and underwent a percutaneous needle intervention with cone-beam CT guidance. There was no target lesion size limit. A total of 88 patients who underwent 92 cone-beam CT-guided interventions were included. All the cone-beam CT guidance procedures were performed by two radiologists with 5 and 11 years of experience, respectively. The baseline data in this population are shown in *Table 1*. Written informed consent was obtained from all patients, and the study was approved by the institutional review board.

Conventional CT guidance.

We retrospectively analyzed the data for needle interventions with CT guidance in the period from November 2004 until August 2008. In total, 223 CT-guided needle interventions were performed, of which 137 interventions (in 118 patients) were suitable for analysis. In 86 patients (90 interventions), the recorded data were insufficient because of incomplete or missing scans. The procedures were performed by five radiologists with 4–12 years of experience. The baseline data of this patient population are shown in *Table 1*.

Dose Calculation Method

Cone-beam CT guidance

To perform the intervention with cone-beam CT guidance, at least two cone-beam CT acquisitions were performed during a complete procedure (*Table 2*). The first cone-beam CT acquisition was used to plan the optimal needle path. After needle placement, cone-beam CT images were obtained to assess needle position and potential complications. Initial cone-beam CT runs were performed with a maximum field diameter of 48 cm, without collimation, covering a z-axis of approximately 30 cm. The field diameter at the axis of rotation was 32.5 cm.

Table 1. Baseline Data in Patients Treated with Cone-beam CT-guided and Conventional CT-guided Needle Interventions

Variable	Cone-beam (n = 88)	Conventional (n = 118)
No. of procedures	92	137
Age (y)	63.9 ± 1.4	59.5 ± 1.3
Range	24-85	29-83
Sex (M/F)	60/29	81/37
Weighth (kg)	79.7 ± 1.7	81.2 ± 1.5
Length (m)	1.75 ± 0.01	1.74 ± 0.02
Anatomic category		
1: Upper thorax	17 procedures	11 procedures
Target diameter (mm)		
Mean	29.2 ± 3.6	23.1 ± 2.8
Range	9-66	10-75
2: Lower thorax	16 procedures	20 procedures
Target diameter (mm)		
Mean	36.0 ± 5.5	35.3 ± 7.5
Range	14-85	12-90
3: Upper abdomen	45 procedures	58 procedures
Target diameter (mm)		
Mean	29.8 ± 3.3	31.4 ± 2.9
Range	9-124	12-115
4: Lower abdomen	14 procedures	48 procedures
Target diameter (mm)		
Mean	39.6 ± 4.7	68.3 ± 2.4
Range	20-78	35-140

Note: Values presented as means ± SD where applicable.

The total filtration used was 1.0 mm aluminum and 0.9 mm copper. The distance between the x-ray tube focal spot and the image receptor was 119.5 cm. The distance from the focal spot to the center of rotation was 81 cm. Collimation was frequently used for the cone-beam CT check scans to image only the necessary field of view. Fluoroscopy was used to position the needle and follow its progress. If necessary, fluoroscopy used a smaller field diameter (48 cm) for increased visibility, with all other settings (filtration and distances from focus to skin and focus to center of rotation) kept the same. Needle interventions were divided into four categories depending on anatomic location: upper thoracic (category 1,

lower neck to the level of the carina), lower thoracic (category 2, level of the carina to lower diaphragm level during inspiration), upper abdomen (category 3, from the level of the upper diaphragm on inspiration to the umbilical level), and lower abdomen (category 4, umbilical level to lower level of the ischial tuberosity). With a standard record form, we prospectively recorded the dose–area product value (in mGy.cm²) of all individual procedure steps (eg, cone-beam CT and fluoroscopy runs). A dedicated PC-based Monte Carlo program (PCXMC, version 2.0; Radiation and Nuclear Safety Authority, Helsinki, Finland) was used to calculate effective doses during these procedures (8). PCXMC 2.0 calculates the effective doses with the present tissue-weighting factors of International Commission on Radiation Protection Publication 103 (9) and the old tissue-weighting factors of Publication 60 (10,11). To calculate the effective dose, we mimicked the calculation method as described by Suzuki et al (12). The cone-beam CT imaging was acquired in a 240° rotation. To simplify the calculation, the rotation of the tube was reduced to nine separate projections at 30° intervals (330°, 0°, 30°, 60°, 90°, 120°, 150°, 180°, and 210°), and doses were calculated in these nine projections. To calculate the effective dose of each projection, the projection data (projection angle, position, field size, tube voltage, filtration, and dose–area product [ie, total product divided by nine]) and patient parameters were entered in the PCXMC program. The sum of the reported dose of all nine projections provide nearly the total effective dose of a cone-beam CT study. Positioning and advancing the needle was done

Table 2. Scan Protocol Parameters of Cone-beam CT–guided and CT-guided Needle Interventions
Parameter

Parameter	Low-dose Cone-beam CT			Conventional CT		
	Thoracic	Abdominal	T/A Very Fast	Thoracic	Abdominal	Axial, Sequential Shots
Voltage (kV)	95	119	116	120	120	120
Charge (mAs)	267	252	171	140	165	50
Increment (mm)	NA	NA	NA	1.6	6.5	NA
Pitch	NA	NA	NA	1.5	1.5	NA
Slice Thickness (mm)	NA	NA	NA	3.2	3.0	5
Collimation (mm)	NA	NA	NA	4 x 3	4 x 5	4 x 5
Scan time (s)	10	10	4	20	25	1
Z-axis coverage (cm)	30	30	30	30	30	2

Note: NA = not applicable; T/A = thoracic/abdominal.

under real-time fluoroscopy. The total effective dose of the intervention was the summed dose of the separate cone-beam CT runs performed during the intervention added to the fluoroscopy dose. Effective dose was expressed in mSv.

Conventional CT guidance.

All interventions were performed with a four-slice helical CT scanner (MX8000; Philips). Scan protocol parameters are shown in *Table 2*. To analyze these CT intervention data, the same anatomic categorization was used as for the patients who underwent cone-beam CT. During the procedure, a planning and final check scan was performed without contrast enhancement. During advancement of the needle, sequential axial shots were used. Procedures were routinely stored in the department's picture archiving and communication system, from which they could be retrieved for viewing. To determine the effective dose, we used the dedicated ImpACT CT Patient Dosimetry Calculator (version 1.0.2) (13). The total effective dose during the intervention was calculated as the sum of doses from the CT scans performed and the separate axial shots for monitoring the progression of the needle.

Statistical Analyses

Excel 2007 (Microsoft, Redmond, Washington) was used to summarize results, and SPSS software (version 17.0; SPSS, Chicago, Illinois) was used for statistical analysis. The magnitudes of the differences of the mean total effective doses between cone-beam CT guidance and conventional CT guidance per category were analyzed by the independent-samples t test. The differences were considered significant at P values lower than .05.

Results

Cone-beam CT Guidance

Between October 2007 and December 2008, we performed 92 needle interventions in 88 patients with cone beam CT guidance. After the procedure, four patients returned for an additional needle intervention. In two patients, the biopsy material of the lesion was insufficient: one patient returned for a second, new lesion, and one patient returned because of a recurring abscess (all in the upper abdomen group). In total, we performed 253 cone-beam CT

studies, with an average of 2.8 per guidance procedure. The mean effective doses of uncollimated cone-beam CT runs were 2.0 mSv (95% CI, 1.5–2.4 mSv) for category 1, 2.9 mSv (95% CI 2.3–3.5 mSv) for category 2, 4.2 mSv (95% CI 3.8 – 4.6 mSv) for category 3, and 3.5 mSv (95% CI 3.0 –3.9 mSv) for category 4. Horizontal collimation of the cone-beam CT scan shows a linear decrease in the effective dose of the scan (*Figure 1*). The total mean effective doses during cone-beam CT guidance procedures were 7.6 mSv (95% CI, 5.1–10.0 mSv) for category 1, 12.3 mSv (95% CI, 9.1–14.6 mSv) for category 2, 16.1 mSv (95% CI 13.8 –18.4 mSv) for category 3, and 13.4 mSv (95% CI 9.4 –17.4 mSv) for category 4. Total effective dose was divided into effective dose of the cone-beam CT studies and effective dose of fluoroscopy (*Table 3*). Fluoroscopy used for positioning and advancing of the needle was responsible for 35%–43% of the total cone-beam CT guidance dose (*Table 3*).

Conventional CT-guided Needle Interventions

Between November 2004 and August 2008, we performed 137 needle interventions in 118 patients with conventional CT guidance. Nine patients underwent 22 drainages in total. Three patients underwent three procedures

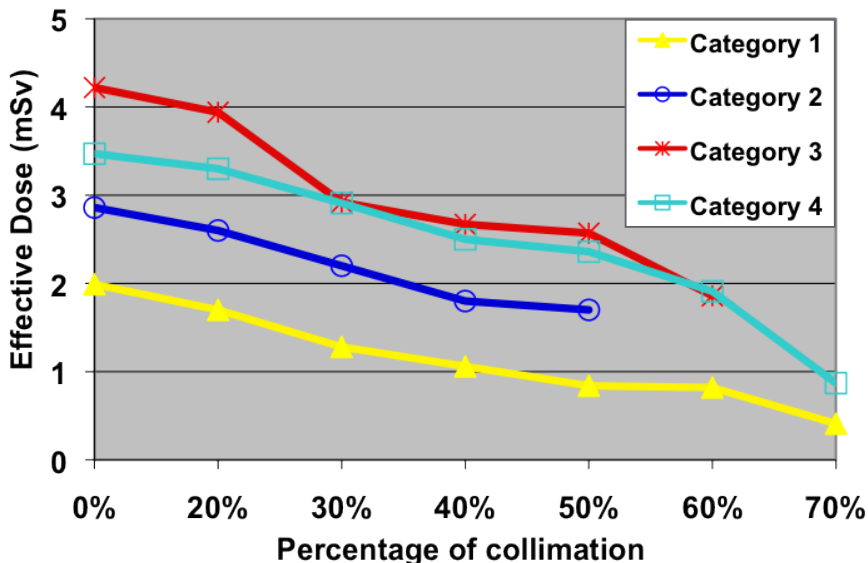


Figure 1. The effect of horizontal collimation for the effective dose of cone-beam CT scans of the upper thorax (category 1), lower thorax (category 2), upper abdomen (category 3), and lower abdomen (category 4).

Table 3. Effective Dose with Cone-beam CT Guidance

Category	Dose (mSv)		
	Cone-beam CT	Fluoroscopy	Total
1: Upper thorax (17 procedures)	4.3 (2.7–5.8)	3.3 (2.0–4.6)	7.6 (5.1–10.0)
2: Lower thorax (16 procedures)	7.8 (4.5–11.2)	4.5 (2.5–6.5)	12.3 (9.1–14.6)
3: Upper abdomen (45 procedures)	10.4 (8.8–11.9)	5.7 (4.6–6.8)	16.1 (13.8–18.4)
4: Lower abdomen (14 procedures)	7.6 (5.8–9.3)	5.8 (2.9–8.8)	13.4 (9.4–17.4)

Note: Values in parentheses are 95% CIs.

each. Two patients had one biopsy and two abscess drainages each, and one patient underwent two biopsies and one abscess drainage. The total mean effective doses during CT-guided interventions were 13.0 mSv (95% CI, 12.4–13.6 mSv) for category 1, 15.1 mSv (95% CI, 14.7–15.5 mSv) for category 2, 20.4 mSv (95% CI, 20.1–20.6 mSv) for category 3, and 15.4 mSv (95% CI, 14.9–15.5 mSv) for category 4. The individual data of planning CT, fluoroscopy shots, and control CT are shown in *Table 4*. Advancing the needle using sequential CT shots was responsible for 6%–22% of the total effective dose of the procedure.

Table 4. Effective Dose of CT-guided Needle Interventions

Category	Dose (mSv)			Dose (mSv)	
	Planning CT	Axial, Sequential Shots	Mean No. of Fluoroscopy Shots	Control CT	Total
1: Upper thorax (11 procedures)	6.9 (6.7–7.1)	2.8 (2.4–3.1)	21.9	3.3 (2.9–3.7)	13.0 (12.4–13.6)
2: Lower thorax (20 procedures)	7.5 (7.4–7.6)	2.4 (2.1–2.6)	9.7	5.2 (4.9–5.5)	15.1 (14.7–15.5)
3: Upper abdomen (58 procedures)	10.1 (10.0–10.2)	3.3 (3.1–3.4)	17.5	7.0 (6.8–7.2)	20.4 (20.1–20.6)
4: Lower abdomen (48 procedures)	8.6 (8.4–8.8)	1.8 (1.7–2.0)	9.8	4.8 (4.6–5.0)	15.4 (14.9–15.5)

Note: Values in parentheses are 95% CIs.

Cone-beam CT Guidance versus Conventional CT Guidance

Comparison of the total mean effective dose between cone-beam and conventional CT guidance shows a dose reduction of 13%–42% depending on the anatomic category (*Figure 2*). The differences in mean effective doses between cone-beam CT guidance and conventional CT guidance are significant

for the upper and lower thorax and upper abdomen ($P = .001$, $P = .012$, and $P < .0001$, respectively). There was no significant difference in mean effective dose between cone-beam CT guidance and conventional CT guidance in the lower abdomen ($P = .075$). The difference between cone-beam CT guidance and conventional CT guidance in the relative dose contribution of planning/control CT and fluoroscopy/single CT shots is shown in *Figure 2*. The dose reduction is mainly attributable to cone-beam CT, not to fluoroscopy (*Figure 2*).

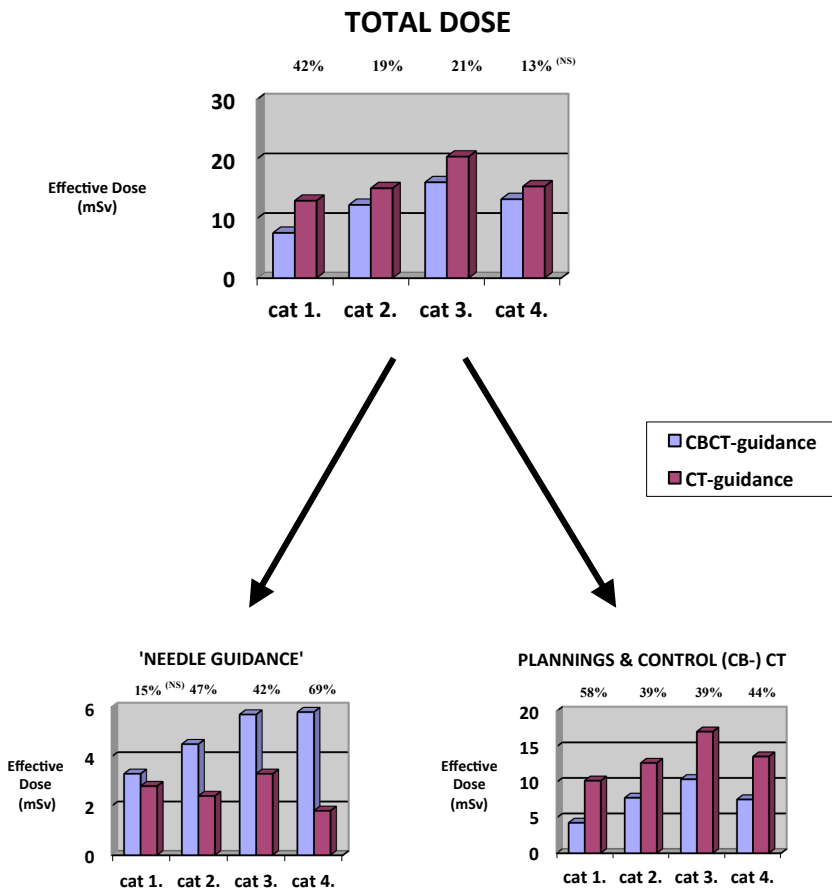


Figure 2. Effective dose of cone-beam CT guidance compared with conventional CT guidance in the upper thorax (category 1), lower thorax (category 2), upper abdomen (category 3), and lower abdomen (category 4). Values above the bars represent the difference between cone-beam and conventional CT guidance. NS = not significant. (*Needle guidance gives the effective dose during needle positioning using fluoroscopy in cone-beam CT guidance and using axial, sequential CT shots during conventional CT guidance).

Discussion

Previous studies have been performed to determine the effective dose of cone-beam CT (12,14). Suzuki et al. (12) reported an effective cone-beam CT dose of 4.2 mSv in the abdomen. The results for the effective dose of a cone-beam CT scan presented in the present study are similar to those reported by Suzuki et al. (12) even though we calculated the dose in nine separate projections (to simplify the calculation) instead of the 13 used by Suzuki et al. (12). The highest effective dose during cone-beam CT guidance was found in the upper abdomen category. The main reason for this is that these procedures are more difficult to perform because of smaller target size and organ movement caused by breathing (7). In general, CT-guided needle interventions can be performed in two ways: the sequential approach and the CT fluoroscopy method. In the present study, the first approach was used for the CT-guided interventions. Our effective dose value result with CT guidance with the sequential “quick-check” method is comparable to those in the literature, with reported effective dose ranges between 6.1 and 23 mSv (13,15,16). With the sequential approach, the effective dose is lower than that with real-time CT fluoroscopy, but the intervention time with the sequential approach is prolonged compared with real-time CT fluoroscopy (17). The results of the present study show a 13%–42% reduction of effective dose in the different anatomic categories with cone-beam CT guidance during a complete procedure compared with CT-guided needle interventions. Hirota et al. (14) found a dose reduction of 45.7 % in cone-beam CT compared with helical CT. They did not examine the effective dose during a complete interventional procedure. By comparing only the effective doses of uncollimated cone-beam CT and conventional CT, we showed a reduction of 58%–71%, which is comparable to previous data reported by Hirota et al. (14). Anatomic category 4 (lower abdomen) showed the lowest dose reduction (13%). This could be related to the difference in the number of patients in this category between cone-beam CT guidance ($n=14$) and CT guidance ($n=48$), the difference in target size (39.6 mm vs 68.3 mm), and the types of needle interventions performed between the two modalities. In the lower abdomen category in the conventional CT group, most interventions were abscess drainages, and these were generally larger collections, making needle placement easier. In the cone-

beam CT guidance group in this category, most interventions were biopsies, which required more accurate needle positioning because of the smaller size of the target lesions. There are several limitations to the present study. Data collection was prospective for cone-beam CT guidance but retrospective for CT-guided needle interventions. This was inevitable because logistic reasons in clinical practice dictated that all CT-guided procedures at our institution now use the cone-beam technique. Despite the difference in data collection, the calculated effective dose is believed to be accurate, and therefore comparison is possible. The effective dose of the scanogram cannot be calculated on the ImPACT CT Patient Dosimetry Calculator. Tsalafoutas et al. (13) reported that the contribution of the scanogram is 2.2%–2.4% of the total effective dose in biopsy and drainage procedures. Because we did not include the contribution of a scanogram in our analysis, our reported effective dose during CT-guided procedures is slightly lower than the actual effective dose. The calculations of effective dose during needle procedures are based on different programs and calculation methods. Despite these different programs, we assume the calculated doses are representative, especially because both programs are widely accepted for calculating effective dose (8,11,12,13,16) and our doses are comparable to the reported doses in the literature. In our experience so far, we expect that a greater dose reduction will be possible with cone-beam CT guidance in the near future. By default, all planning cone-beam CT scans could be performed with collimation. In addition, during advancement of the needle, the contribution of the fluoroscopy is relatively high (35%–43% of the total effective dose). By adjusting the fluoroscopy protocol (e.g., lowering the frame rate), further reduction of the effective dose of fluoroscopy, as described by Vetter et al. (18), should be possible, resulting in a lower overall effective dose. Reducing the charge (mAs) during fluoroscopy would also lower the dose but would have a negative influence on image quality. The relationship between fluoroscopy with lower mAs and acceptable image quality has to be investigated. In the current system, asymmetric collimation during fluoroscopy is not possible. When asymmetric collimation becomes possible for eccentric puncture sites, an even lower effective dose will be the result. In addition, in the procedures described here, a control scan was always performed to rule out any complications, but with relatively limited collimation (most with \leq

50% collimation). Based on the “as low as reasonably achievable” principle, there would be an argument for waiving the standard control scan in specific procedures. Finally, with the recently introduced option to coregister CT or MR data within the cone-beam CT guidance modality, it is possible to perform needle guidance based on previously acquired datasets. In this case, only very low dose protocols would be needed to register both volumes. The effect on dose reduction of this option should be investigated. The use of angular beam modulation for CT or other experimental navigation and guiding systems (e.g., electromagnetic tracking system) for cone-beam CT guidance can also lower the effective dose during percutaneous needle interventions in the future (19,20). Despite the dose reduction for the patient during cone-beam CT guidance compared with CT guidance, the scatter radiation dose for the interventional radiologist might actually increase, especially compared with sequential CT guidance procedures. The amount of scatter radiation during cone-beam CT-guidance is still under investigation. The effective radiation dose to the patient with cone-beam CT guidance is in the range of 7.6–16.1 mSv, depending on anatomic category. Compared with the effective radiation doses of 13.0–20.4 mSv with CT guidance, there is a considerable dose reduction across the different anatomic categories (13%–42%). This reduction is mainly a result of the considerably lower effective dose of cone-beam CT compared with the conventional CT equivalents.

References

1. Brenner DJ, Hall EJ. Computed tomography – an increasing source of radiation exposure. *N Engl J Med* 2007; 357:2277–2284.
2. Stoker J, Kipp JBA, Geleijns K, van der Molen AJ, Venema HW. Radiation exposure in computed tomography in The Netherlands: riskbenefit analysis. *Ned Tijdschr Geneesk* 2009; 153:348–352.
3. Schaefer PJ, Schaefer FKW, Heller M, Jahnke T. CT fluoroscopyguided biopsy of small pulmonary and upper abdominal lesions: efficacy with a modified breathing technique. *J Vasc Interv Radiol* 2007; 18:1241–1248.
4. Daly B, Krebs TL, Wong-You-Cheong JJ, Wang SS. Percutaneous abdominal and pelvic interventional procedures using CT fluoroscopy guidance. *AJR Am J Roentgenol* 1999; 173:637–644.
5. Orth RC, Wallace MJ, Kuo MD. C-arm cone-beam CT: general principles and technical considerations for use in interventional radiology. *J Vasc Interv Radiol* 2009; 20(Suppl):S538–S544.
6. Racadio JM, Babic D, Homan R, et al. Live 3D guidance in the interventional radiology suite. *AJR Am J Roentgenol* 2007; 189:W357–W364.
7. Braak SJ, van Strijen MJL, van Leersum M, van Es HW, van Heesewijk JPM. Real-time 3D fluoroscopy guidance during needle interventions: technique, accuracy, and feasibility. *AJR Am J Roentgenol* 2010; 194:W445–W451.
8. Khelassi-Toutaoui N, Berkani Y, Tsapaki V, et al. Experimental evaluation of PCXMC and prepare codes used in conventional radiology. *Radiat Prot Dosimetry* 2008; 131:374–378.
9. International Commission on Radiological Protection. The 2007 Recommendations of the International Commission on Radiological Protection. ICRP Publication 103. *Ann ICRP* 2007; 37:1–331.
10. International Commission on Radiological Protection. 1990 Recommendations of the International Commission on Radiological Protection. ICRP Publication 60. *Ann ICRP* 1991; 21:1–201.
11. Servomaa A, Tapiovaara M. Organ dose calculation in medical x ray examinations by the program PCXMC. *Radiat Prot Dosimetry* 1998; 80:213–219.
12. Suzuki S, Furui S, Yamaguchi I, et al. Effective dose during abdominal three-dimensional imaging with a flat-panel detector angiography system. *Radiology* 2009; 250:545–550.
13. Tsalafoutas IA, Tsapaki V, Triantopoulou C, Gorantonaki A, Papailiou J. CT-guided interventional procedures without CT fluoroscopy assistance: patient effective dose and absorbed dose considerations. *AJR Am J Roentgenol* 2007; 188:1479–1484.
14. Hirota S, Nakao N, Yamamoto S, et al. Cone-beam CT with flatpanel-detector digital angiography system: early experience in abdominal interventional procedures. *Cardiovasc Intervent Radiol* 2006; 29:1034–1038.

15. Teeuwisse WM, Geleijns J, Broerse JJ, Obermann WR, van Persijn van Meerten EL. Patient and staff dose during CT guided biopsy, drainage and coagulation. *Br J Radiol* 2001; 74:720–726.
16. Joemai RMS, Zweers D, Obermann WR, Geleijns J. Assessment of patient and occupational dose in established and new applications of MDCT fluoroscopy. *AJR Am J Roentgenol* 2009; 192:881–886.
17. Kirchner J, Kickuth R, Laufer U, Schilling EM, Adams S, Liebermann D. CT fluoroscopy-assisted puncture of thoracic and abdominal masses: a randomized trial. *Clin Radiol* 2002; 57:188–192.
18. Vetter S, Faulkner K, Strecker EP, Busch HP. Dose reduction and image quality in pulsed fluoroscopy. *Radiat Prot Dosimetry* 1998; 80:299–301.
19. Hohl C, Suess C, Wildberger JE, et al. Dose reduction during CT fluoroscopy: Phantom study of angular beam modulation. *Radiology* 2008; 246:519–525.
20. Penzkofer T, Isfort P, Bruners P, et al. Robot arm based flat panel CT-guided electromagnetic tracked spine interventions: phantom and animal model experiments. *Eur Radiol* 2010; 20:2656–2662.



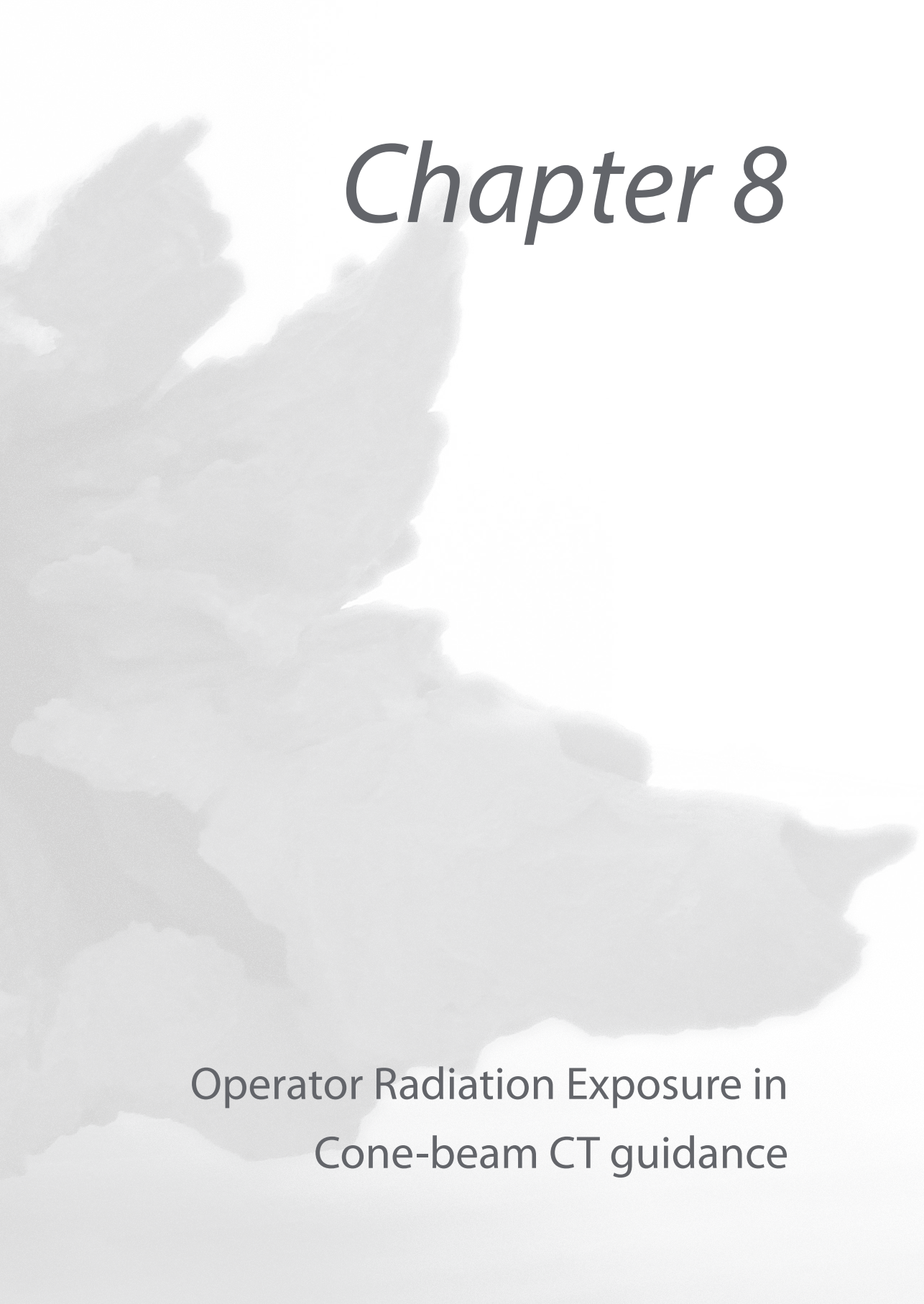
Sicco J. Braak¹ • Marco J.L. van Strijen¹ • Erica Meijer² • Johannes P.M. van Heesewijk¹ • Willem P.Th.M. Mali³

¹Department of Radiology, St. Antonius Hospital, Nieuwegein, The Netherlands

²Department of Clinical Physics, St. Antonius Hospital, Nieuwegein, The Netherlands

³Department of Radiology, University Medical Center Utrecht, Utrecht, The Netherlands

Submitted J Vasc Interv Radiol



Chapter 8

Operator Radiation Exposure in
Cone-beam CT guidance

Abstract

Objective

Quantitative analysis of operator dose in cone-beam CT-guidance (CBCT-guidance) and the effect of protective shielding.

Materials and Methods

Using a Rando-phantom® a model was set-up to measure radiation dose for the operator hand, thyroid and gonad region. The effect of sterile lead drapes and ceiling/couch shielding was measured. Using this model we calculated the dose, based on relevant clinical parameters. The procedures were divided in thoracic and abdominal group. Furthermore dosimetry measurements were performed during clinical cases to correlate with our calculations.

Results

113 procedures were included between December 2007 and January 2010 (47 thoracic, 66 abdominal). The mean hand doses were 34.2 and 54.6 μSv (thoracic/abdominal respectively). The thyroid and gonad regions doses were 83.2 and 34.3 μSv in the thoracic, and 66.2 and 47.2 μSv in the abdominal group. Lead drapes reduced the dose for the hand, but increased for the thyroid/gonad significantly. Combined shielding reduced dose by 98.2-98.9% ($p < 0.05$). The radiation dose in clinical setting in the thoracic group ($n=17$) was 32.9 μSv for the hand, 11.4 μSv for the thyroid and 16.0 μSv for the gonad region. In the abdominal group ($n=20$) the doses were 43.4, 21.7 and 18.8 μSv respectively.

Conclusion

The operator dose in CBCT-guidance without shielding is quite low, compared to the literature. Compared to clinical cases, the model overestimated the radiation dose. Based on the model approximately 240 cases can be performed staying below the yearly limit. Best significant dose reduction is achieved by a combination of different types of shielding.

Introduction

Scatter radiation of fluoroscopy is the major source of radiation dose for the interventional radiologist during procedures. There is an increase in X-ray fluoroscopy use in the angiosuite, because of increasing complexity of procedures performed. There are many reports concerning the radiation dose for the staff in the angiosuite. Only a small part of the described performed procedures concerned percutaneous needle interventions [1,2].

For biopsies and drainages the interventional radiologist can use ultrasound, CT (-fluoroscopy) (CT-F), MRI and fluoroscopy or a combination. In most cases ultrasound or CT(-F) is used. By using ultrasound there is obviously no radiation exposure but many lesions are inaccessible by ultrasound due to the superposition of gas or bone. In these instances CT(-F) is then commonly used. The X-ray exposure for radiologists during CT(-F) guided interventions has been investigated by many authors. A mean dose outside the lead aprons of 71 μSv is reported [3-6].

Since the introduction of flat panel detectors in the angiosuite, the capability of performing a soft tissue cone-beam CT (CBCT) is available, combined with needle planning software and overlay imaging with fluoroscopy allowing to perform real-time guided needle interventions [7,8]. During a CBCT-guided intervention the interventional radiologist potentially stands relatively close to the X-ray beam to position the needle (that is: compared to most common vascular interventional procedures). During CBCT-guidance the C-arm also takes an oblique and possibly lateral position resulting in a possible higher scatter radiation dose. There is currently no literature available on studies investigating the amount of radiation exposure for the operator during these CBCT-guidance interventions. In order to determine the radiation dose for the interventional radiologist during a CBCT-guidance we performed a prospective study to quantify scatter radiation dose. The standardly equipped couch & ceiling shielding of the C-arm is used to determine the effect on the scatter dose. However this shielding will protect mainly the gonad and thyroid region and not the hand region. We used commercially available disposable lead drapes to determine the effect of this shielding especially for the hand. Also a combination of different types of shielding will be evaluated. Also we performed a prospective real-time measurement study on a cohort of clinical patients.

Materials and methods

Cone-beam CT-guidance procedure

CBCT-guidance is based on a flat panel detector C-arm angiosuite system (XperCT® and XperGuide®, Allura FD20, Philips Healthcare, The Netherlands). A soft tissue 3D volume is created during a 4-10 seconds rotation (240 degrees) around the patient. Within this calibrated 3D soft tissue data set the operator determines a needle access route from the skin to the target lesion, avoiding critical structures. This needle path determines the angulation and rotation of the C-arm for visualizing entry point and progression views. The fluoroscopy image is co-registered with the relevant needle path slice of the CBCT, making it possible to position and advance the needle in real-time. There are two main C-arm positions; one looking right on top of the trajectory (entrypoint view; EP) (*Figure 1 a & b*) and the second view is perpendicular to the planned needle path with parallax correction (progress view; PV) (*figure 1 c & d*).

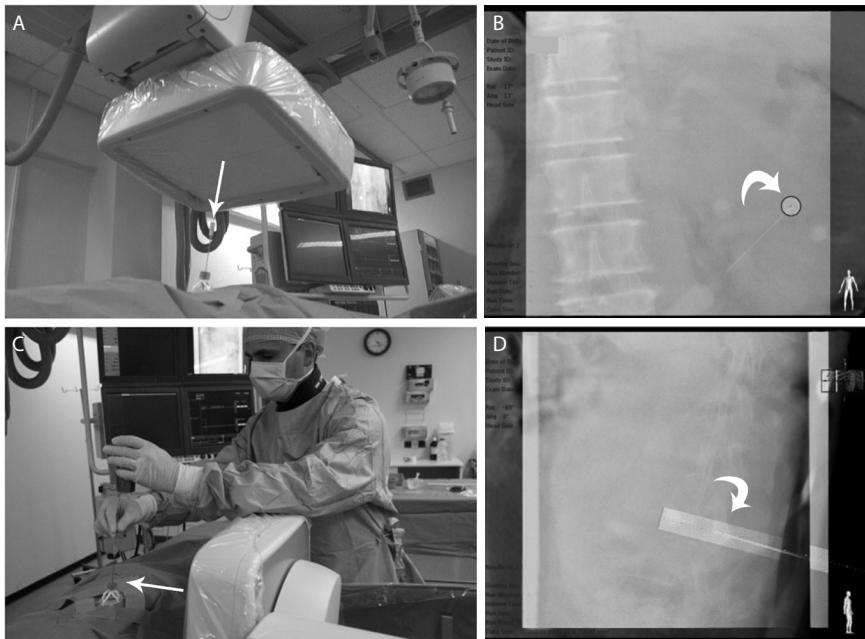


Figure 1. Cone-beam CT-guidance procedure on a 59-years-old male with a suspected mass in the hilum of the right kidney. Histopathological result revealed a small cell neuroendocrine carcinoma for which this patient underwent a nephrectomy. A, Entrypoint (EP) geometric configuration of the C-arm, looking 'down-the-barrel' (with arrow). This view is shown in B with a merged image of the CBCT-slice and the fluoroscopy with the target circles (curved arrow) making accurate needle placement possible. C, shows the common geometric configuration of the C-arm in the Progress view (PV). This clearly shows the close position of the operator to the radiation beam. D, shows the progress view during a CBCT-guidance procedure with merged images of the CBCT-slice and fluoroscopy with the needle trajectory (curved arrow) with centimeter markings.

During the acquisition of the CBCT the operator steps outside of the angiosuite. For positioning and progressing the needle the radiologist uses fluoroscopy and has to stand close to the patient/needle/X-ray beam. After selecting the first view the needle can be placed within a safety margin of 5 mm, however the depth of the needle cannot be monitored real-time in this view. After securing the right EP position of the needle the second position (PV) is selected to progress the needle until the right depth is reached.

The total filtration during fluoroscopy was 1.0 mm Al and 0.9 mm Cu. The X-ray focal spot – image detector distance (FSD) was 119.5 cm. The distance from the focal spot to the center of rotation was 81 cm. The operator could choose the field diameter (FD) and the amount of collimation. The position of the interventional radiologist depends on the C-arm geometry.

Scatter Radiation Model:

To set up a scatter-radiation model during CBCT-guidance we used a human-shaped phantom (Rando® phantom; Phantom Laboratories, Salem, NY). This phantom represents a 175 cm tall and 73.5 kg (body mass index (BMI): 24 kg.m⁻²) hermaphrodite phantom. We measured the scatter radiation dose of the interventional radiologist to the thyroid region (150 cm above ground), gonad region (90 cm above ground) and hand region (next to the needle, right outside the direct X-ray beam) of the operator by using electronic personal dosimeters (EPD) (Mk2, Thermo Fischer Scientific). This dosimeter measures the penetrating dose (Hp(10), µSv), i.e. the individual dose at a depth of 10 mm tissue. Cumulative dose value is displayed on the LCD display of the EPD [5]. The distance of the operator to the radiation source depends on the angulation and rotation of the C-arm. For every geometric position of the C-arm a representative position was chosen to measure the operator dose based on the position during equal clinical procedures (50cm from center point of C-arm outside of the rotational arc). Also we measured the scatter dose behind ceiling and couch attached shielding (0.5 mm Pb equivalent), as well as using sterile disposable lead drapes (Drape Armour®; 0.25 mm Pb equivalent, 41 x 25 cm; Microtek Medical BV, Zutphen, The Netherlands) which are placed on top of the patient around the needle (*Figure 2*) and a combination of lead drapes and shielding. We measured the dose in every combination of rotation projections of the detector between -120 degrees to +120 degrees at an interval of 30

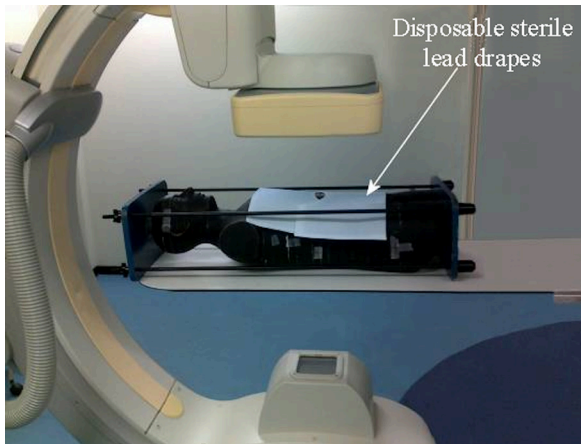


Figure 2. The disposable lead drape armor (Pb equivalent of 0.25 mm) as positioned during the model measurement with a Rando® phantom.

degrees, to simplify the measurements. In every angulation projection the dose was measured with an interval of 20 degrees in a range of -40 degrees to +40 degrees (figure 3). In every geometric setting the backscatter was measured during 15 seconds of fluoroscopy. After every 15 seconds of fluoroscopy the EPD's display was read and recorded. The effect of changing the FD and collimation (0% or 50% collimation) in every combination of geometry and shielding was also determined. The above measurements were performed in the abdominal region and thoracic region of the phantom. This resulted in a scatter dose rate ($\mu\text{Sv/s}$) for every combination of geometric setting, FD, collimation, ceiling/couch shielding and sterile disposable lead drapes.

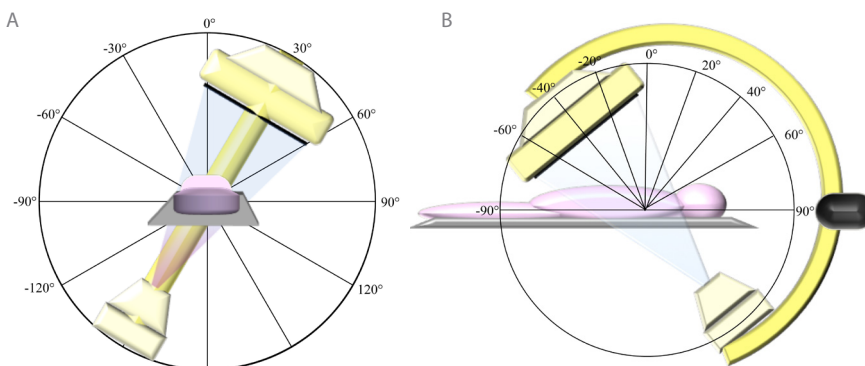


Figure 3. The rotation (A) and angulation (B) of the C-arm used during the model measurements of scatter radiation for the operator. Dose measurement was performed in every combination of rotation projections between -120 degrees to +120 degrees at an interval of 30 degrees and in every angulation projection with an interval of 20 degrees in a range between -40 degrees to +40 degrees.

Patients

Written informed consent was obtained from all patients and the institutional review board approved the study design. Patients were included from December 2007 and January 2010. All patients (N= 186) included in this study had an indication for a CT-guided needle intervention (lesions not accessible by ultrasound due to overlaying gastro-intestinal gas, bony structures or lesions in the lung parenchyma) and underwent a percutaneous needle intervention using CBCT-guidance. There was no target size limit. The phantom used in our model had a BMI (body mass index) of 24 kg.m⁻². Therefore we excluded 73 patients with a BMI outside of the normal range of 22 -26 kg.m⁻². In total 113 patients were included. The baseline data of this population is shown in *Table 1*. The CBCT-guidance procedures were performed by two radiologists (SB & MvS) with 5 and 11 years experience and equal experience in CBCT-guidance. The procedures were divided in 2 groups: thoracic (n = 47) and abdominal procedures (n = 66). During the procedures relevant parameters were prospectively recorded (C-arm position, fluoroscopy time, FD and collimation).

Table 1. Overview of patient characteristics used for the model and during the clinical cases

	Thorax	Abdomen	total
Scatter radiation model	N =47	N =66	N =113
Sex	19 women / 19 men	28 women / 47 men	47 women / 66 men
Mean age (y)	62.1 ± 11.8 SD	63.9 ± 12.3 SD	63.3 ± 12.1 SD
Mean length of target (mm)	31.0 ± 22.1 SD	25.1 ± 18.3 SD	27.8 ± 20.2 SD
Mean BMI (kg/m ²)	23.9 ± 1.42 SD	23.9 ± 1.50 SD	23.9 ± 1.46 SD
Clinical cases	N =17	N =20	N =37
Sex	5 women / 12 men	8 women / 12 men	13 women / 24 men
Mean age (y)	67.3 ± 10.9 SD	62.6 ± 11.3 SD	64.7 ± 11.2 SD
Mean length of target (mm)	23.7 ± 8.5 SD	22.9 ± 7.2 SD	23.3 ± 7.8 SD
Mean BMI (kg/m ²)	24.4 ± 1.9 SD	24.0 ± 1.7 SD	24.2 ± 1.8 SD

Note: SD = standard deviation

Scatter radiation dose calculation:

Based on the scatter radiation model we extrapolated the dose for the radiologist at the thyroid region, gonad region and hand region during procedures performed in a routine clinical setting. We multiplied the fluoroscopy time (sec) of the detailed obtained data during CBCT-guidance procedures with the scatter radiation dose rate (μSv/s) measured in the model, resulting in a scatter radiation dose in μSv per procedure.

Real-time dose measurement

In June 2010 a Dose Aware System (DAS) (Philips Healthcare, The Netherlands) was introduced in our radiological department. In the period between June and November 2010 we performed 37 CBCT-guidance procedures in which we used this system. Baseline data of these patients are shown in table 1. The dosimeter measures the scatter dose rate ($\mu\text{Sv/h}$) and cumulative scatter dose Hp(10) (μSv) and sends this information every second wirelessly to a base station. The dosimetry data from the base station was downloaded to a laptop for further analysis. The dosimeters were placed in the same position as in the scatter radiation phantom measurement (thyroid region (150 cm), gonad region (90 cm) and hand that placed and progressed the needle (closest to the beam). During these clinical procedures we routinely worked with ceiling and couch mounted protective lead shielding.

Analyses

Microsoft Office Excel 2007 was used for registering and summarizing the results and SPSS software (version 16.0, SPSS) was used for the statistical analysis. The magnitudes of the differences between the mean of the different groups of shielding were analyzed with a paired-sample T-test. The differences were considered significant for 'p' values less than 0.05.

Results

The mean fluoroscopy time, kV, mAs, FD, angulation and rotation for the EP position, PV position in the thorax and abdomen group are summarized in *table 2*.

Scatter radiation dose calculation

Thorax group

Radiation dose rates without radiation protection of the operator's hand, thyroid and gonad region ranged from 0.14 to 0.18 $\mu\text{Sv/sec}$; 0.06 to 0.67 $\mu\text{Sv/sec}$ and 0.13 to 0.18 $\mu\text{Sv/sec}$ respectively. The mean calculated dose per procedure was 34.2 μSv (95% Confidence Interval (95% CI) 26.9-41.5 μSv), 83.2 μSv (95% CI 11.1 –155.3 μSv) and 34.4 μSv (95% CI 26.0-42.7) for the hand, thyroid region and gonad region respectively without the use of ceiling/couch mounted protective shielding or lead drape coverage.

The use of ceiling/couch shielding resulted in a significant dose reduction, compared to the dose without any shielding. No difference on the hand dose due to the use of ceiling/couch shielding was found. Using only the lead drape reduced the hand dose significantly but increased the dose to the thyroid and gonad region. The highest reduction was achieved by using both the ceiling/couch shielding and the lead drapes. In this setting the hand dose did not change compared to the use of only the lead. Detailed information of the dose differences is shown in *Table 3*.

abdominal group

In this group the radiation dose rates of the operator's hand, thyroid region and gonad region ranged from 0.28 to 0.33 $\mu\text{Sv}/\text{sec}$; 0.19 to 0.53 $\mu\text{Sv}/\text{sec}$ and 0.24 to 0.29 $\mu\text{Sv}/\text{sec}$ respectively. The mean calculated dose per procedure was 54.6 μSv (95% CI 46.9-62.4 μSv), 66.2 μSv (95% CI 31.4-100.9 μSv) and 47.2 μSv (95% CI 39.9-54.5 μSv) for respectively the hand, thyroid region and gonad region without the use of ceiling/couch shielding or lead drape coverage.

Table 4 shows the detailed information of the dose differences. The use of ceiling/couch shielding resulted in a significant dose reduction, compared to the dose without any shielding. No difference was found on the hand dose due to the use of ceiling/couch shielding. Using only the lead drape reduced the hand dose significantly, but increased the dose to the thyroid and gonad region. Just like in the thoracic group in the abdominal group the highest reduction was achieved by using both the ceiling/couch shielding and the lead drapes. The hand dose did not change compared to the use of only the lead drapes.

Real-time dose measurement

The mean total scatter radiation dose during 17 thoracic procedures was 32.9 μSv (95% CI 16.5-49.4 μSv) for the hand, 11.4 μSv (95% CI 6.5-16.3 μSv) for the thyroid and 16.0 μSv (95% CI 6.7-25.4 μSv) for the gonad region. For the abdominal procedures (N=20) the mean scatter radiation dose was 43.4 μSv (95% CI 30.3-56.5 μSv), 21.7 μSv (95% CI 11.8-31.7 μSv), 18.8 μSv (95% CI 7.1-30.5 μSv) for the hand, thyroid and gonad region respectively. Compared to the mean dose results of the scatter radiation model, the dose measured during the live cases were 11.9%, 417.5% and 132.8% lower for respectively the hand, thyroid and gonad region compared to calculated dose without any

Table 2. Overview of the data in entrypoint view, progress view and in total.

Characteristics	Entrypoint		Progress View		Total	
	Thorax	Abdomen	Thorax	Abdomen	Thorax	Abdomen
Time (s); mean	74.4 (64.6 – 84.3)	68.3 (62.4-74.1)	137.9 (124.8-150.9)	111.4 (103.9-118.8)	212.3 (192.7-231.9)	179.7 (168.7-190.6)
kV; mean	91.9 (90.4-93.3)	98.6 (97.2-100.1)	103.3 (101.2-105.3)	117.7 (117.0-118.4)		
mAs; mean	13.5 (13.3-13.7)	14.7 (14.5-14.8)	14.9 (14.6-15.1)	15.4 (15.3-15.6)		
Field Diameter (cm) ; mean	27.7 (25.3-30.1)	28.0 (26.0-30.0)	27.7 (25.6-29.7)	31.1 (29.5-32.8)		
Angulation; mean	-3° (- 8° – + 2°)	11° (7°-15.0°)	0° (-0°-0°)	0° (0°-0°)		
Rotation; mean	-4° (-12°-+5°)	-4.0° (-10°-+2°)	-22° (-44°-1°)	-25° (-45°- -6°)		
Dose Hand (µSv); mean	10.7 (8.2-13.1)	17.9 (13.2-22.6)	23.5 (17.4-29.7)	36.7 (30.9-42.6)	34.2 (26.9-41.5)	54.6 (46.9-62.4)
Dose Thyroid region (µSv); mean	68.6 (-3.4-140.5)	42.6 (9.1-76.1)	13.8 (9.2-18.4)	23.6 (17.7-29.5)	83.2 (11.1-155.3)	66.2 (31.4-100.9)
Dose Gonads region (µSv); mean	17.8 (11.1-24.4)	20.8 (17.2-24.4)	16.1 (11.6-20.7)	26.4 (20.9-32.0)	34.3 (26.0-42.7)	47.2 (39.9-54.5)
Dose Thyroid Shielding (µSv); mean	1.7 (-0.1-3.4)	0.7 (0.2-1.2)	0.5 (0.3-0.6)	1.0 (0.7-1.3)	2.2 (0.4-3.9)	1.7 (1.1-2.3)
Dose Gonads Shielding (µSv); mean	1.3 (0.9-1.7)	1.5 (1.2-1.8)	1.3 (0.9-1.7)	2.1 (1.6-2.6)	2.6 (2.0-3.2)	3.6 (2.9-4.2)

Table 2. Continued.

Characteristics	Entrypoint		Progress View		Total	
	Thorax	Abdomen	Thorax	Abdomen	Thorax	Abdomen
Dose Hand Drape (μSv); mean	3.3 (2.4-4.2)	7.1 (4.1-10.0)	4.6 (3.5-5.8)	10.5 (6.3-14.8)	7.9 (6.1-9.8)	17.6 (11.9-23.4)
Dose Thyroid Drape (μSv); mean	94.7 (-22.1-211.6)	76.8 (14.4-139.3)	16.7 (8.7-24.7)	21.8 (18.3-25.3)	111.4 (-5.9-228.7)	98.6 (35-161.4)
Dose Gonads Drape (μSv); mean	33.8 (19.2-48.5)	34.3 (26.9-41.8)	26.4 (9.3-33.5)	37.8 (29.6-46.0)	60.2 (43.9-76.5)	72.1 (59.2-85.0)
Dose Thyroid Both (μSv); mean	0.06 (0.00-0.14)	0.05 (0.03-0.08)	0.02 (0.01-0.02)	0.13 (0.05-0.21)	0.08 (0.01-0.16)	0.18 (0.08-0.28)
Dose Gonads Both (μSv); mean	0.06 (0.00-0.13)	0.05 (0.02-0.08)	0.18 (0.12-0.25)	0.40 (0.24-0.56)	0.37 (0.28-0.46)	0.84 (0.55-1.13)

Note: Values between bracket represent 95% Confidence Interval

Table 3. Thorax group: percentages of dose difference compared to the setting without any radiation shielding. All percentages represent significant ($p < 0.05$) changes except the one marked with an asterisk (*).

	Couch / Ceiling Shielding	Lead drape Shielding	Couch / Ceiling and Lead drape Shielding
Hand			
Entrypoint	No difference	- 68.9%	No difference compared to lead drape shielding
Progress View		- 80.4%	
Total		- 76.8%	
Thyroid region			
Entrypoint	- 97.5%	+ 38.4%	- 99.8%
Progress View	- 96.6%	+ 13.8%	- 99.5%
Total	- 97.4%	+ 33.9%*	- 99.7%
Gonad region			
Entrypoint	- 93.2%	+ 90.3%	- 97.9%
Progress View	- 91.6%	+ 59.3%	- 98.4%
Total	- 92.4%	+ 75.3%	- 98.2%

Table 4. Abdominal group: percentages of dose difference compared to the setting without any radiation shielding. All percentages represent significant ($p < 0.05$) changes except the one marked with an asterisk (*).

	Couch / Ceiling Shielding	Lead drape Shielding	Couch / Ceiling and Lead drape Shielding
Hand			
Entrypoint	No difference	- 60.4%	No difference compared to lead drape shielding
Progress View		- 71.3%	
Total		- 67.8%	
Thyroid region			
Entrypoint	- 98.4%	+ 80.5%	- 99.9%
Progress View	- 95.8%	- 7.7%*	- 99.8%
Total	- 97.4%	+ 49.0%	- 99.8%
Gonad region			
Entrypoint	- 92.8%	+ 65.2%	- 98.9%
Progress View	- 92.0%	+ 42.9%	- 98.7%
Total	- 92.4%	+ 52.8%	- 98.9%

form of radiation protection. Compared to the mean dose with couch & ceiling protection of the scatter radiation model the live doses were 86.2 and 82.4% higher for the thyroid and gonad region without any difference in the hand dose.

Discussion

Interventional tools are continuously improving. Low dose at no compromise to high quality imaging and accuracy is an important topic. The recently developed interventional tool using CBCT-guidance has proven to be accurate and uses less radiation dose for the patient compared to CT-guidance, however there is to our knowledge currently no data on the scatter radiation dose for the interventional radiologist in CBCT-guidance [8-12]. The results of this study provide information on the radiation dose for the radiologist using CBCT-guidance and demonstrate that additional adequate lead protection can reduce the dose significantly.

In our study, the mean radiation dose ranges from 34.2 to 83.2 μSv per procedure and radiation dose rates ranges from 0.06 to 0.67 $\mu\text{Sv}/\text{sec}$; all without any radiation protection. Many studies are performed on scatter radiation dose during interventional procedures, but these concern fluoroscopic interventions or CT-fluoroscopy guided interventions.

A recent study by Martin et al. [1] reviewed the staff dose over the last 20 years. He concluded that there is a wide range of radiation dose to the hand and thyroid reported in the literature. The reported mean scatter dose in his review is 350 μSv per procedure for the hand and approximately 97.5 μSv for the thyroid. Percutaneous procedures result in the highest dose, however these procedures were not the majority of the interventions. During procedures with percutaneous access the reported mean hand dose is 920 μSv . These procedures were mainly transjugular intrahepatic portosystemic shunts (TIPS), biliary drainages and nephrostomy procedures. These high operator radiation dose are the result of long fluoroscopy times but not due to the radiation beam geometry [13-15]. In CBCT-guidance the fluoroscopy time short, resulting in a lower radiation dose to the interventional radiologist. However the wide range of the C-arm geometry can result in high backscatter radiation during CBCT-guidance. This is the same in coronary interventional procedures where the radiation beam projections have a wide range in C-arm geometry with high backscatter radiation for the cardiologist, especially in the beam projection where the tube is nearest to the operator [2,16]. Häusler et al. [2] reported a mean personal dose of 82.5 μSv with shielding per coronary procedure. Depending on the beam projection the maximum radiation dose rate is reported between

0.83-3.3 $\mu\text{Sv}/\text{sec}$ for the head, waist and knee region [16], which is higher than our reported personal dose and dose rate. Reason for this is the longer fluoroscopy time during coronary procedures.

Needle guidance using conventional CT can be performed without any radiation dose to the operator and is considered to be accurate and safe, but is however time consuming [3,17]. With the introduction of CT-fluoroscopy, first described in 1994 by Katada et al. [18], real-time visualization was possible making needle placement quicker, at least with the same accuracy, but resulting in a higher radiation dose to the radiologist [17]. There is a large variation in the reported scatter radiation dose during CT-fluoroscopy guidance procedures, due to different CT-fluoroscopy settings, use of needle guidance devices, lead drapes, operator experience and method and region of measurement [6]. The reported dose per CT-fluoroscopy guided procedure is between 7-2200 μSv and dose rate between 0.2-39.5 $\mu\text{Sv}/\text{sec}$ [3-6]. Using CBCT-guidance the highest dose rate is in progress view with the tube near to the interventional radiologist. This dose rate is 0.67 $\mu\text{Sv}/\text{sec}$, which is well in the lower part of the reported CT-fluoroscopy dose rate. In this position the gonad region is behind the tube, which in itself absorbs the dose but the thyroid region is in the peak scatter region.

Compared to the live cases we found a considerable difference in dose especially for the thyroid and gonad region. A probable explanation for this is that the calculated doses are, despite being clinical representative measurement points, in fact static points. During a live case the operator will move and the use of shielding is not always maximal. Therefore the measurement in the scatter radiation model with shielding is definitely lower because here optimal shielding was always present. However, the extrapolated dose without any form of shielding still results in a very low scatter radiation dose for the operator. To reach the maximal annual dose limit an interventional radiologist can perform approximately 240 cases a year. Considering this, the model without shielding overestimated the dose and the true scatter radiation dose will be in the lower half between the dose without shielding and with shielding. Despite the quite low doses in the model without the shielding, the use of shielding is always recommended.

Using radiation shielding (couch and ceiling) the scatter dose can be reduced by 25-99% [2,16,19,20]. In our study we found dose reductions comparable to the reported upper limit in the literature. Disposable lead drapes are reported to reduce the scatter dose, but this was during CT-fluoroscopy guided procedures

[4,21,22]. Using only disposable lead drapes we found that the total scatter dose is even higher for the thyroid and gonad region than without any shielding. Probably this is because the drapes are only horizontally on top of the patient and result in more backscatter because of the automatic fluoroscopy settings of the system. Using both the disposable lead drapes and the couch / ceiling shielding the additional effect of the lead drapes is significant. Also the dose to the patient can be altered due to these disposable lead drapes, but this should be investigated separately.

It should be emphasized that the scatter radiation dose to the radiologist reported in this study represents the dose outside a protective lead gown. Because of the ALARA (as low as reasonably achievable) principle, the interventional radiologists wore appropriate lead aprons and thyroid shielding despite the fact that scatter dose during CBCT-guidance procedures was low. Because of these protective measurements the dose will be further reduced. Lead gloves for the hands are available, but they are not commonly used during the procedures because this decreases the touch and feel of the operator which is generally considered not desirable.

A possible comment to this study is the validity of the assumption that the phantom is a real patient. This type of phantom is however widely used to measure patient dose and operator dose; therefore we believe the results of this study are representative and in line with published data [4,16,19]. Also one can comment that for comparison of the extrapolated radiation dose we used a relatively small live cases group. Our reported scatter radiation dose is also only suitable for patient with a BMI of 22-26 kg.m⁻². Nowadays multiple vendors offer commercially available CBCT-guidance solutions. Our finding concerns only one vendor. Comparison with other vendor systems should be performed to determine the difference in dose between the other systems.

Furthermore experienced CBCT-guidance users produced the data for the scatter dose calculation. In first time users with a learning curve in using CBCT-guidance the dose will probably be higher in the beginning.

We expect that the scatter radiation dose can be even lower in the future by adjusting the fluoroscopy settings (e.g. kV, mAs and lowering the pulserate) [19,23]. Also asymmetrical collimation could contribute but is currently not available in this system. When performing a procedure with the needle trajectory at the edge of the imaging field little to no collimation can be used.

Conclusion

We determined the radiation dose for the interventional radiologist based on a scatter radiation model and clinical cases. The mean scatter radiation dose without shielding in the scatter model was 53.3 μSv , which is quite low compared to the reported scatter radiation dose. Compared to the clinical cases (mean dose 24.0 μSv), the scatter model without shielding overestimated the radiation dose. Based on the model without shielding approximately 240 cases a year can be performed staying below the yearly limit. The best significant dose reduction of 98.6% can be achieved by a combination of lead drape and ceiling/couch shielding.

Acknowledgements

We are grateful of the support of B.J. Klok, clinical physics employee University Medical Centre Utrecht for supplying the phantom.

References

1. Martin CJ. A Review of Radiology Staff Doses and Dose Monitoring Requirements. *Radiat Prot Dosimetry* 2009; 136(3):140-157.
2. Häusler U, Czarwinski R, Brix G. Radiation exposure of medical staff from interventional x-ray procedures: a multicentre study. *Eur Radiol* 2009; 19:2000-2008
3. Paulson EK, Sheafor DH, Enterline DS, McAdams HP, Yoshizumi TT. CT Fluoroscopy-guided Interventional Procedures Techniques and Radiation Dose to Radiologists. *Radiology* 2001; 220:161-167.
4. Neeman Z, Dromi SA, Sarin S, Wood BJ. CT Fluoroscopy Shielding Decreases in Scattered Radiation for the Patient and Operator. *J Vasc Interv Radiol* 2006; 17:1999-2004.
5. Teeuwisse WM, Geleijns J, Broerse JJ, Obermann WR, van Persijn van Meerten EL. Patient and staff dose during CT guided biopsy, drainage and coagulation. *Br J Radiol* 2001; 74:720-726.
6. Buls N, Pagés J, de Mey J, Osteaux M. Evaluation of patient and staff doses during various CT Fluoroscopy guided interventions. *Health Phys* 2003; 85(2):165-173.
7. Racadio JM, Babic D, Homan R, Rampton JW, Patel MN, Racadio JM, Johnson ND. Live 3D guidance in the interventional radiology suite. *AJR Am J Roentgenol* 2007; 189(6):W357-W364.
8. Braak SJ, van Strijen MJ, van Leersum M, van Es HW, van Heesewijk JP. Real-Time 3D fluoroscopy guidance during needle interventions: technique, accuracy, and feasibility. *AJR Am J Roentgenol* 2010; 194(5):W445-W451.
9. Lee WJ, Chong S, Seo JS, Shim HJ. Transthoracic fine-needle aspiration biopsy of the lungs using a C-arm cone-beam CT system- diagnostic accuracy and post-procedural complications. *Br J Radiol* 2011 Oct 18 [epub ahead of print] DOI: 10.1259/bjr/64727750
10. Hwang HS, Chung MJ, Lee JW, Shin SW, Lee KS. C-arm cone-beam CT-guidance percutaneous transthoracic lung biopsy Usefulness in evaluation of small pulmonary nodules. *AJR Am J Roentgenol* 2010; 195:W400-W407
11. Braak SJ, van Strijen MJ, van Es HW, Nievelstein RA, van Heesewijk JP. Effective dose during needle interventions: cone-beam CT guidance compared with conventional CT guidance. *J Vasc Interv Radiol* 2011; 22(4):455-461.
12. Hirota S, Nakao N, Yamamoto S, Kobayashi K, Maeda H, Ishikura R, Miura K, Sakamoto K, Ueda K, Baba R. Cone-Beam CT with Flat-Panel-Detector Digital Angiographic system early experience in abdominal interventional procedures. *Cardiovasc Intervent Radiol* 2006; 29(6):1034-1038.
13. Williams JR. The interdependence of staff and patient doses in interventional radiology. *Br J Radiol* 1997; 70:498-503.

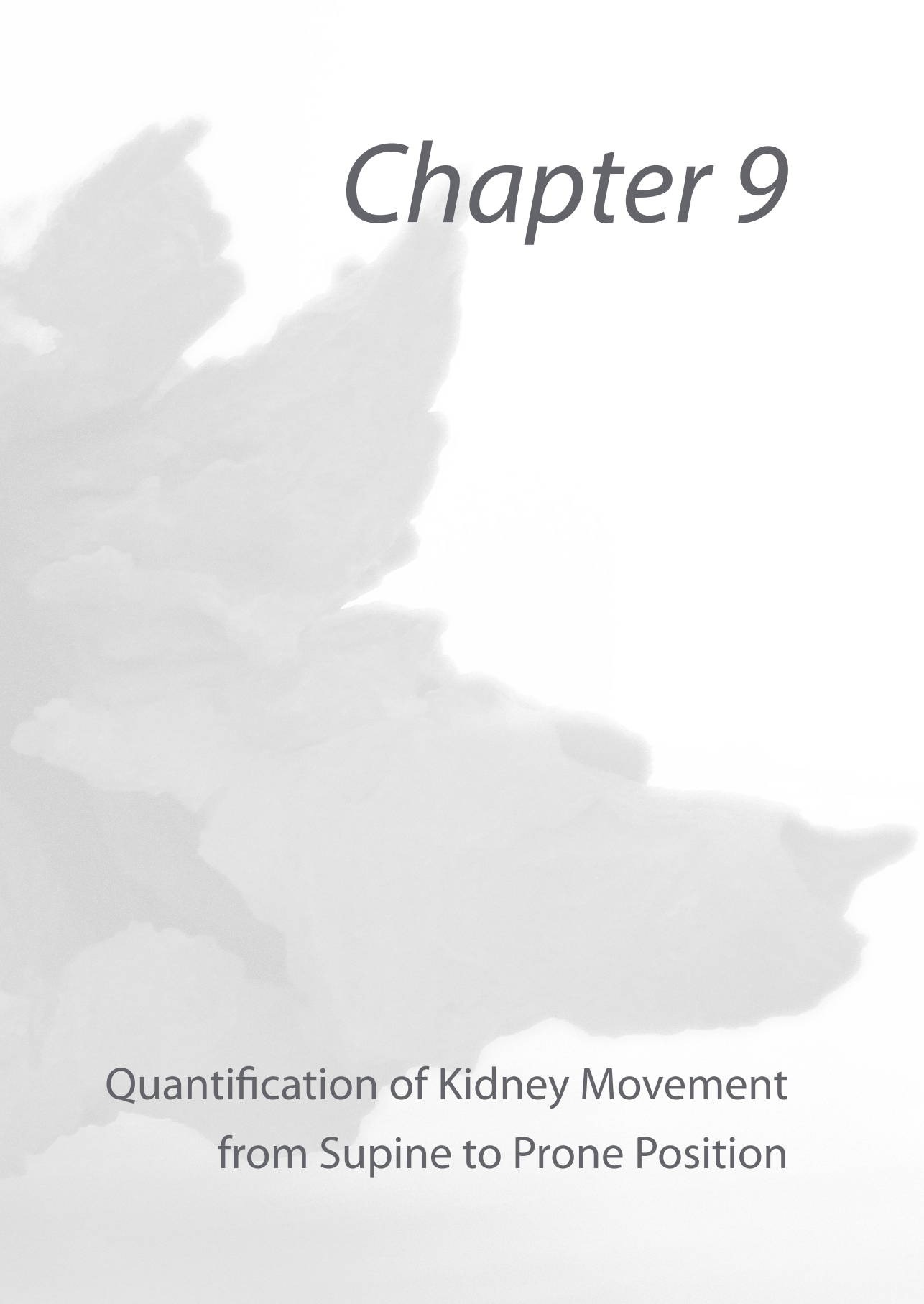
14. Ginjaume M, Pérez S, Ortega X. Improvements in extremity dose assessment for ionising radiation medical applications. *Radiat Prot Dosimetry* 2007; 125(1):28-32.
15. Whitby M, Martin CJ. A study of the distribution of dose across the hands of interventional radiologists and cardiologists. *Br J Radiol* 2005; 78:219-229.
16. Morrish OWE, Goldstone KE. An investigation into patient and staff doses from X-ray. *Br J Radiol* 2008; 81:35-45.
17. Silverman SG, Tuncali K, Adams DF, Nawfel RD, Zou KH, Judy PF. CT Fluoroscopy-guided Abdominal Interventions Techniques, Results, and Radiation Exposure. *Radiology* 1999; 212:673-681.
18. Katada K, Anno H, Takeshita G, Ogura Y, Koga S, Ida Y, Nonomura K, Kanno T, Ohashi A, Sata S, Shibata Y. Development of Real Time CT Fluoroscopy. *Nippon Acta Radiologica* 1994; 54:1172-1174.
19. Kuon E, Schmitt M, Dahm JB. Significant reduction of radiation exposure to operator and staff during cardiac interventions by analysis of radiation leakage and improved lead shielding. *Am J Cardiol* 2002; 89:44-49.
20. Marx MV, Nikiason L, Mauger EA. Occupational radiation exposure to interventional radiologists a prospective study. *J Vasc Interv Radiol* 1992; 3:597-606.
21. Stoeckelhuber BM, Leibecke T, Schulz E, Melchert UH, Bergmann-Koester CU, Helmberger T, Gellissen J. Radiation Dose to the Radiologist's Hand During Continuous CT Fluoroscopy-Guided Interventions. *Cardiovasc Intervent Radiol* 2005; 28:589-594.
22. Nawfel RD, Judy PF, Silverman SG, Hooton S, Tuncali K, Adams DF. Patient and Personnel Exposure during CT-fluoroscopy guided interventional procedures. *Radiology* 2000; 216:180-184.
23. Vetter S, Faulkner K, Strecker EP, Busch HP. Dose reduction and image quality in pulsed fluoroscopy. *Radiat Prot Dosimetry* 1998; 80:299-301.



David B. Meek • Sicco J. Braak • Marco J.L. van Strijen • Johannes P.M. van Heeswijk

Department of Radiology, St. Antonius Hospital, Nieuwegein, The Netherlands

Submitted European Radiology



Chapter 9

Quantification of Kidney Movement
from Supine to Prone Position

Abstract

Objectives

To quantify kidney movement as result of patient transfer from supine to prone position and to investigate if Body Mass Index (BMI) influences these movements.

Materials and Methods

New software is able to merge upper abdominal supine CT-scan with upper abdominal prone cone beam CT (CBCT) scan. Retrospective analysis was performed on merged volumes of 43 patients (30 men, mean age 66.9 ± 8.2 yr, mean BMI 27.3 ± 3.9 kg/m²) using needle guiding software. Kidney movement was assessed in four directions: deformation, rotation, 2D and 3D translation.

Results

There was a mean rotation of -2 ± 4 degrees in coronal plane and -6 ± 9 degrees in sagittal plane ($P = .01$ and $P = .01$ respectively). BMI influenced the dorsal and cranial translations significantly ($r = 0.317$; $P = .046$ and $r = 0.427$; $P = .002$ respectively). The 3D translation was 2.65 ± 1.50 cm and BMI also influenced the 3D translation significantly ($r = 0.413$; $P = .008$).

Conclusions

Our study demonstrated that quantifying kidney movement in a merged scan is feasible. There is a significant rotation of the length axis in coronal and sagittal view from supine to prone position and BMI influences cranial, dorsal and 3D translation.

Introduction

Kidney movement is an important issue in procedures performed in endourology, radiotherapy and image guided interventions such as biopsies, drainages and thermal ablative techniques.

Patient positioning plays a pivotal role in how the kidney is approached and is an important factor in the safety of a percutaneous approach. For instance, the prone position was previously the standard position in percutaneous nephrolithiomy procedures (PCNL) [1]. Valdivia et al [2] were the first to describe PNL in a modified supine position (Galdakao-Modified Supine Valdivia position) to benefit the procedure in obese and respiratory compromised patients. Specific patient characteristics such as the stones' complexity, their size, their location in the renal collecting system and the presence of staghorn calculi have lead to modifications in the standard positions. These include the reverse lithotomy position [3], prone split-leg position [4, 5], lateral decubitus position [6-8] and the modified lateral position ("Barts" technique) [9].

A recent global review of the Clinical Research Office of the Endourological Society (CROES) by Valdivia et al [10] stated that despite PCNL being widely adopted, it lacks a standardized technique. Moreover, they stated that operation time and stone-free rates favor prone PCNL, while patient safety favors supine PCNL so that the choice of patient position should be tailored to individual patient characteristics and the surgeon's preference. The debate on which position to use is mainly due to the complex relationship between patient positioning and kidney movement.

In October 2006 a newly developed interventional system was introduced in our radiology department. The system is based on a flat panel detector C-arm system (Allura FD20, Philips Healthcare, Best, The Netherlands), capable of acquiring CBCT. This system is also equipped with needle planning software; XperGuide® (Phillips, Healthcare, The Netherlands) which combines CBCT with fluoroscopy and needle planning software making needle interventions possible with a predefined trajectory. [11]

Furthermore it is possible to import previously acquired DICOM data (e.g. CT or MRI) into the workstation where these volumes can be merged with an acquired CBCT. In general an upper abdominal CT is made in supine position, whereas for kidney biopsy a CBCT is usually made in prone position. By merging these data

sets it is possible to quantify, analyze and interpret kidney movement due to the transfer from supine to prone position. Measuring the effect of this transfer on kidney movement could possibly lead to a prediction of kidney movement during the change in patient positioning, especially when the body mass index (BMI) is taken into account. Predicting kidney movement prior to intervention could benefit procedure time, sterility, costs and eventually patient's outcome. The objects of this study were:

1. To quantify kidney movement between the transfer from supine to prone position using a calibrated merged CBCT/CT volume concerning: deformation, 2D translation, rotation (in coronal and sagittal view) and 3D translation;
2. To correlate BMI to these quantifications.

Materials and methods

Patient population

We pre-selected 63 upper abdominal CBCT-scans. Inclusion criteria were: CBCT-scan obtained in prone position, upper abdominal supine CT-scan available prior to the CBCT-scan (<6 months) and at least one kidney fully shown on both scans with appropriate spatial resolution. In total we included 43 patients. We could not determine the BMI of three patients due to missing data on weight and length. Baseline characteristics of our study population are shown in *Table 1*.

Table 1. Characteristics of our study population including age, sex, BMI, the amount of left or right kidney's studied and the time between the CT- and CBCT-scan in years.

Characteristic (N=43)	Value
Age (y), Mean \pm SD	66.9 (\pm 8.2)
Sex, M/F	30/13
Body Mass Index [N=40] (kg/m ²), Mean \pm SD	27.3 (\pm 3.9)
Kidney (No.), Left/Right	21/22
Time between CT and CBCT (y), Mean \pm SD	0.1 (0.18)

Merging method

In order to merge the CBCT-scan with the CT-scan we selected both the scans in the merging window on the workstation. The merging window offers an automated merging tool and manual merging tools. To accurately merge

the imported CT-scan with the CBCT-scan, we preferred the manual merging tools. As stable reference points we used the vertebral column which is clearly visible on the CT-scan as well as the CBCT-scan (*Figure 1*). Individual vertebral characteristics such as osteophytes were used as an additional reference point. It is imperative to match the overlay from all three viewpoints (e.g. coronal, sagittal and axial) to establish a merged CBCT/CT volume as accurately as possible. In total 43 scans were merged.

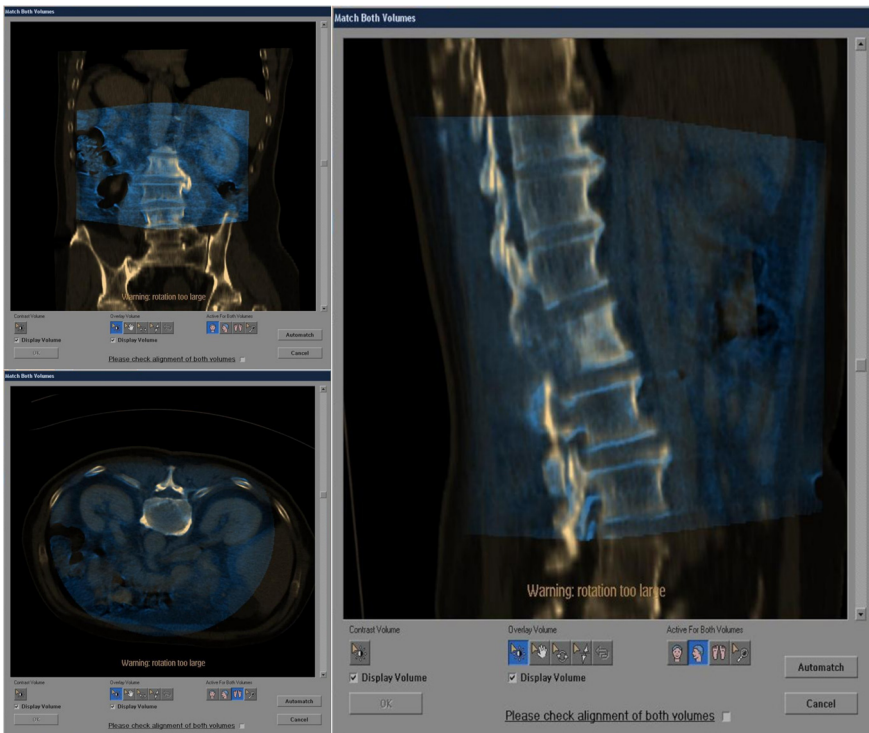


Figure 1. Merging window in coronal, sagittal and axial view, displaying the CBCT-scan (blue) and CT-scan (yellow). The vertebral bodies were used to accurately merge the two volume data sets because of its stable consistency within the patient and its good visibility in both scans.

Image analysis

To analyze kidney movement in the calibrated merged CBCT/CT volume we considered the kidney as an ellipsoidal object. In this ellipsoidal object we defined three axes: one major length axis from the upper pole (UP) to the lower pole (LP) and two transverse perpendicular width axes crossing in the exact middle of the major length axis. A model of this object is shown in *Figure 2*.

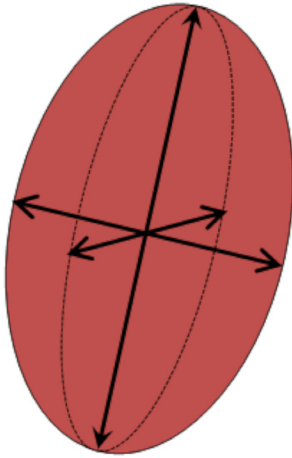


Figure 2. Ellipsoid model. Note that the two width axis are perpendicular to each other.

The workstation's software was then used to draw line tracks to represent the axis in the merged CBCT/CT volume. In order to do so, the UP and LP points were determined in axial view by marking the most cranial noticeable kidney tissue (UP point) and the most caudally noticeable kidney tissue (LP point). Between these two markings a line was automatically drawn by the workstation. This line track was revised in all three viewpoints until the line track represented the length axis of the kidney at its best. Thereafter the exact middle of the length axis was marked with a green dot (*Figure 3*). The first width axis runs from a tangent line that represents the medial limit of the kidney, runs through the green dot and terminates on a tangent line representing the lateral limit of the kidney. This line track is drawn perpendicularly to the medial tangent line. In the same way, a line track was drawn perpendicularly to the first width axis (*Figure 4*) to represent the second width axis. A total of six line tracks were drawn in the merged CBCT/CT volume, one length axis with two width axes in the same kidney times two (*Figure 5*).

Data acquisition

Once a line track is planned, the software displays the X, Y and Z-coordinates of the beginning and end points of this line and its total length in cm. The software can implement alterations and automatically display the new coordinates and length of the altered line track. Moreover, it can determine the distance in cm between beginning or end coordinates which do not belong to the same needle track.



Figure 3. The first visible kidney tissue of the lower pole (A) and upper pole (B) in axial view was marked in the calibrated CBCT/CT volume. A line track was automatically drawn by the system. This line track was revised in all three views (sagittal, coronal and axial) until it represented the length axis of the kidney at its best. Thereafter the exact middle was marked with a green dot (C).

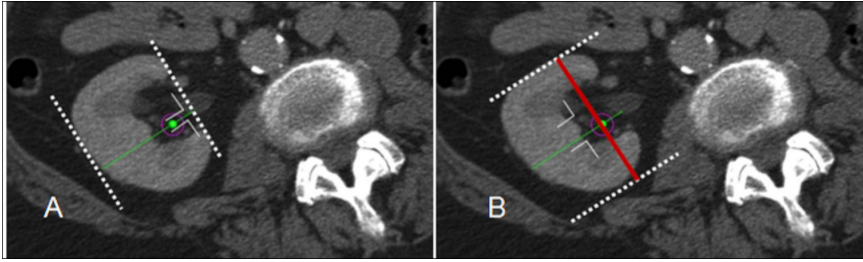


Figure 4. In the axial view in the exact middle of the length axis (green dot), the first width axis (green line) was planned perpendicular between two tangent lines representing the medial and lateral contours of the kidney (dotted lines) (A). The second width axis was drawn perpendicular to the first width axis (red line) until the contours of the kidney were reached (dotted lines) (B).

The three intra renal axes were compared to quantify deformation. The volume of the kidney was calculated using the following formula: volume in $\text{cm}^3 = (4/3 \times \pi \times (1/2 \text{ length-axis (cm)}) \times (1/2 \text{ first width-axis (cm)}) \times (1/2 \text{ second width-axis (cm)}))$. Figure 6 and 7 illustrates how rotation, 2D and 3D translation were measured using the axes and the coordinates of the UP and LP. We would like to emphasize that 2D translations are a projection of a 3D translation vector.

3D translation of the UP and LP was assessed using the determined distance between both UP and LP coordinates in all three planes: medial-lateral translation (dX), ventro-dorsal translation (dY) and cranio-caudal translation

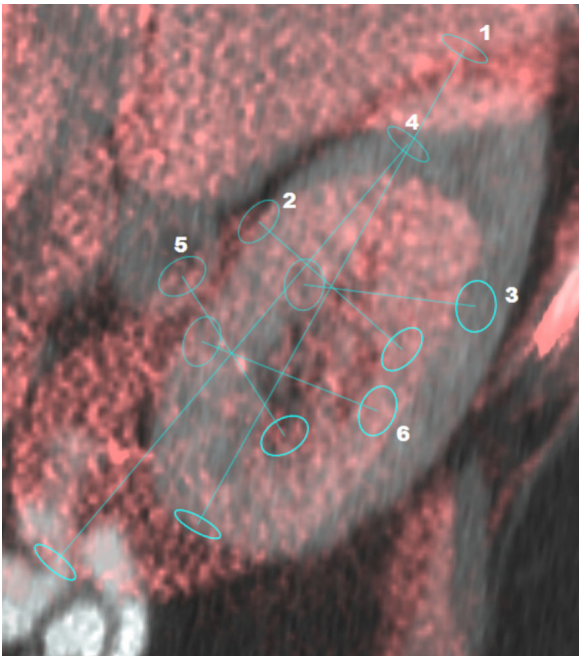


Figure 5. Merged CBCT/CT volume with all line tracks planned in sagittal plane. 1: Length axis CT, 2: First width axis CT, 3: Second width axis CT, 4: Length axis CBCT, 5: First width axis CBCT, 6: Second width axis CBCT.

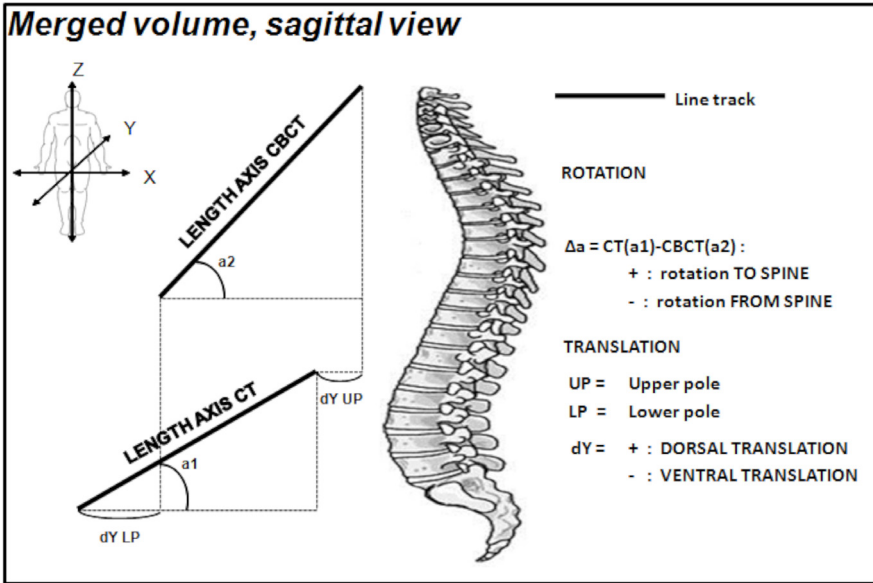


Figure 6. Ventral-dorsal translation and rotation measurement.

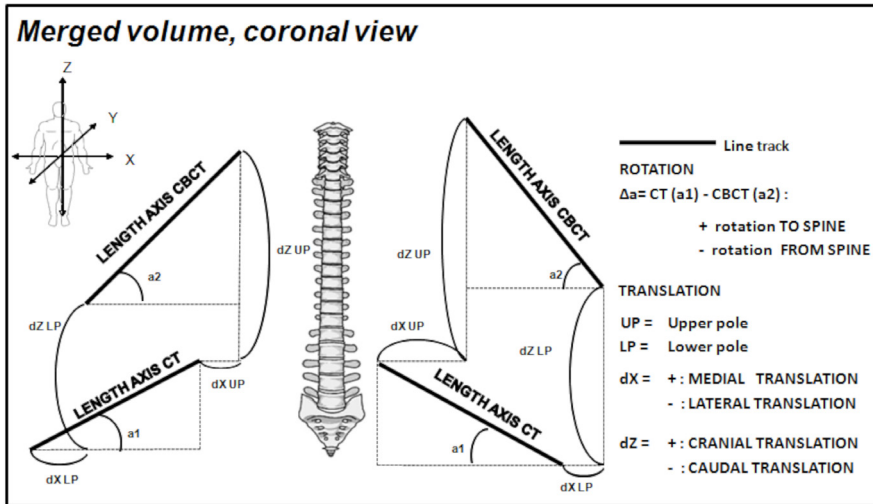


Figure 7. Medial-lateral, cranio-caudal and rotation measurement.

(dZ). The 3D translation of the UP and LP was calculated with the following formula: $3D \text{ translation (cm)} = \sqrt{((dX)^2 + (dY)^2 + (dZ)^2)}$. All line tracks were drawn three times. After collecting the data of one merged volume the planned line tracks were erased to minimize the memory effect. This process was repeated until the data of all 43 merged volumes was collected. The collected data was subsequently averaged for each subject.

Statistical analysis

All data is presented as mean \pm SD, unless otherwise indicated. Data was collected using Excel (version 2007; Microsoft, Redmond, Washington). For statistical analysis SPSS (version 17.0; SPSS, Chicago, Illinois) was used. Associations between variables were assessed using Spearman's correlation test or Pearson's correlation test where appropriate. A two-sided P-value $<0,05$ was considered significant.

Results

Deformation

Measurements of the lengths, widths and volumes of the kidneys are shown in *Table 2*. No significant difference was found between the axes and the volumes. There was a mean deformation of the kidney of $-0.92 \pm 6.20 \text{ cm}^3$. No correlation between BMI and any of the axes was identified.

Table 2. Mean length in cm and volume in cm^3 of the kidney in the merged scan, separated for CT and CBCT and their significance, followed by their differences (Δ) and significances with BMI.

	CT	CBCT	Sign.	Δ	Sign.
Length	11.74 \pm 1.16	11.78 \pm 0.95	.683	+0.04 \pm 0.60	.097
Width-1	5.21 \pm 0.69	5.20 \pm 0.67	.769	-0.11 \pm 0.33	.537
Width-2	5.85 \pm 0.70	5.76 \pm 0.77	.084	-0.08 \pm 0.31	.169
Volume	60.73 \pm 18.47	59.82 \pm 17.91	.337	-0.92 \pm 6.20	.461

2D translation and rotation

Table 3 shows data of the 2D translation of the UP and LP differentiated by the left and right kidney. There was a mean medial-lateral translation of $+0.11 \pm 0.44$ cm, which had no significant correlation with BMI. The ventro-dorsal translation was -0.22 ± 1.50 cm and the cranio-caudal translation was $+1.36 \pm 1.91$ cm. BMI influenced the dorsal and cranial translations significantly ($r= 0.317$; $P = .046$ and $r= 0.427$; $P= .002$ respectively). The rotation data shows that the angles of the length axes in coronal and sagittal plane between supine and prone position were significantly different (respectively, $P = .01$ and $P = .01$). There was a mean rotation of -2 ± 4 degrees in coronal plane and -6 ± 9 degrees in sagittal plane (*Table 4*). BMI had no correlation with this mean difference between the coronal and sagittal angles ($P = .236$ and $P= .540$ respectively).

Table 3. A: Mean 2D translations of the UP and LP differentiated by left or right kidney and their total in cm. **B:** Summed mean of the 2D translations in cm, its' correlation coefficient (r) and significances with BMI (B).

	UP			LP			Total	Mean	r	Sign
	Right	Left	Right	Left	Right	LP				
dX	+0.02±0.49	-0.00±0.52	+0.37±0.82	+0.03±0.50	+0.01±0.05	+0.20±0.69	+0.11±0.44	-0.129	.426	
dY	-0.99±1.46	-0.47±1.02	+0.73±2.40	-0.18±1.52	-0.74±1.25	+0.29±2.05	-0.22±1.50	0.317	.046	
dZ	+2.48±2.13	+0.76±1.88	+1.56±1.84	+0.55±1.60	+1.64±2.17	+1.07±1.78	+1.36±1.91	0.427	.002	
A	B									

Table 4. Mean coronal and sagittal rotations of the length axis in the CT- and in the CBCT-scan in degrees followed by their r and significances. Thereafter their differences (Δ) and its' significances with BMI.

	CT	CBCT	Sign	Δ	Sign
Coronal	78±6	80±7	.01	-2±4	.236
Sagittal	60±11	66±11	.01	-6±9	.540

Table 5. 3D translation of the UP and LP in cm, their mean together and its correlation coefficient (r) and significance with BMI.

	UP	LP	3D Mean (UP+LP)	r	Sign
3D Translation	2.75±1.51	2.55±1.58	2.65±1.50	0.413	.008

3D translation

The 3D translation was 2.65 ± 1.50 cm. BMI is positively correlated with the mean 3D translation ($r = 0.413$, $P = .008$) (Table 5).

Discussion

Until now, there are no studies available in the literature using a calibrated merged volume and needle planning software to measure kidney movement between supine and prone position of a patient, therefore no published literature is available for comparison. The only relevant studies found concern two-dimensional translations of the kidney as a result of respiration and measurements of normal kidney sizes.

Our results show that the 2D translations of the right kidney are larger than the left kidney. We hypothesized that this was due to the mass-effect of the intestines that would probably affect the more caudally located right kidney first. Concerning the total cranio-caudal translation for both kidneys together, the data indicates that a cranial translation took place ($+1.36 \pm 1.91$ cm). Furthermore, the cranio-caudal translations are larger than the medial-lateral and ventro-dorsal translations. It is the dominant 2D translation in both kidneys. Additionally, BMI is positively correlated with the cranial and dorsal translation. Our results are comparable to the results of the supine respiration-induced study by Draney et al. [12] They demonstrated that the right kidney was part of a greater translation than the left kidney during respiration (cranial 1.32 ± 0.07 cm versus 1.01 ± 0.54 cm and dorsal -0.63 ± 0.34 cm versus -0.23 ± 0.17 cm), indicating that we could not attribute the larger translations of the right kidney solely to mass effect. Moreover, Brandner et al [13] found that the cranio-caudal translation (mean: 1.2 cm) is the predominant translation compared to the medial-lateral (mean: 0.16 cm) and ventro-dorsal (mean: 0.53 cm) translation during respiration in the supine position.

According to our data there is a significant rotation of the kidney in the coronal and sagittal plane. This indicates that there is a significant rotation of the kidneys' length axis from the spine in the coronal and sagittal plane during the patients' transfer from supine to prone position. BMI did not influence these rotations significantly. No studies concerning the rotation of the kidneys have been found.

In our study the differences in the deformation of the kidney were not significant and the mean differences between the axes were small (maximum mean 0.11 cm and maximum SD 0.60 cm). We assumed that the mass effect of the intestines during the transfer to prone position could be responsible for the difference with the mainly ventro-dorsally placed second width axis, although the difference is not significant ($P = 0.084$). According to Glodney et al. [14], BMI is an independent positive influencing factor of pole to pole kidney length, cortical width and parenchymal width. However, in our study BMI does not influence the kidneys deformation.

BMI is positively correlated with the three-dimensional translation ($P = .008$). An increasing BMI, results in increased 3D translations ($r = 0.413$).

There are limitations to our study. The merging process and the planning of the line tracks are operator dependent, which can lead to a different interpretation of the kidneys' outline. To reduce the line track planning bias we therefore performed the process three times. On addition, the studies of Draney et al. [12] and Brandner et al. [13] showed the inevitable effect of respiration on two-dimensional translations of the abdominal organs. Apart from the two-dimensional translations, respiration has probably also influenced our quantifications of the kidneys' deformation, rotations and three-dimensional translation. Determining the position of the diaphragm to correct our quantifications was not possible, therefore we could not rule out the influence of breathing. However, we assume this effect to be small because both examinations were performed on inspiration.

Future imaging studies concerning kidney movement as a result of a patient positioning should meticulously develop a method to minimize the influence of breathing. All patients should receive clear and brief breathing instructions prior to the acquisition of both scans. For this purpose breath-hold monitoring devices have been developed [15]. Shyn et al. [16] and Carlson et al. [17] described the use of the same breath-hold monitoring device that successfully improves both PET/CT image registration and depiction of mobile target lesions in the lung and upper abdomen.

In our opinion reliable automatic merging is not possible in the current system. Technical innovations could improve the reliability of the automatic merging of both scans. In the future a process of automated measurements of the kidneys' volume based on Hounsfield-units and automated contour detection,

discriminating the kidney from the surrounding structures, could be possible. Besides endourology, kidney movement also plays a role in radiotherapeutic planning strategies. The kidneys are the dose-limiting organs for radiotherapy for gastrointestinal cancers, gynaecological cancers, lymphomas and sarcomas of the upper abdomen [18]. Moreover, organ motion is unequivocally important in the daily radiotherapeutic planning. If our method is applied to a merged scan consisting of scans (MRI or CT) obtained in different patient positions, it is possible to analyze organ motion as a result of these transfers. These analyzes could lead to changes pre-interventional planning of radiotherapy, endourology, surgery and interventional procedures such as biopsy, drainages or minimally invasive therapies (e.g. ablation), saving costs and benefitting a patients outcome.

References

1. Alken P, Hutschenreiter G, Gunther R, Marberger M (1981) Percutaneous stone manipulation. *J Urol* 125:463-466
2. Valdivia Uria JG, Valle Gerhold J, Lopez Lopez JA et al (1998) Technique and complications of percutaneous nephroscopy: Experience with 557 patients in the supine position. *J Urol* 160:1975-1978
3. Lehman T, Bagley DH (1988) Reverse lithotomy: Modified prone position for simultaneous nephroscopic and ureteroscopic procedures in women. *Urology* 32:529-531
4. Grasso M, Nord R, Bagley DH (1993) Prone split leg and flank roll positioning: Simultaneous antegrade and retrograde access to the upper urinary tract. *J Endourol* 7:307-310
5. Scarpa RM, Cossu FM, De Lisa A, Porru D, Usai E (1997) Severe recurrent ureteral stricture: The combined use of an antegrade and retrograde approach in the prone split-leg position without X-rays. *Eur Urol* 31:254-256
6. Kerbl K, Clayman RV, Chandhoke PS, Urban DA, De Leo BC, Carbone JM (1994) Percutaneous stone removal with the patient in a flank position. *J Urol* 151:686-688
7. Gofrit ON, Shapiro A, Donchin Y et al (2002) Lateral decubitus position for percutaneous nephrolithotripsy in the morbidly obese or kyphotic patient. *J Endourol* 16:383-386. Doi:10.1089/089277902760261437
8. Karami H, Arbab AH, Rezaei A, Mohammadhoseini M, Rezaei I (2009) Percutaneous nephrolithotomy with ultrasonography-guided renal access in the lateral decubitus flank position. *J Endourol* 23:33-35. Doi:10.1089/end.2008.0433
9. Papatsoris AG, Zaman F, Panah A, Masood J, El-Husseiny T, Buchholz N (2008) Simultaneous antegrade and retrograde endourologic access: "the barts technique". *J Endourol* 22:2665-2666. Doi:10.1089/end.2008.0283
10. Valdivia JG, Scarpa RM, Duvdevani M et al (2011) Supine versus prone position during percutaneous nephrolithotomy: A report from the clinical research office of the endourological society percutaneous nephrolithotomy global study. *J Endourol* 25:1619-1625. Doi:10.1089/end.2011.0110
11. Braak SJ, van Strijen MJ, van Leersum M, van Es HW, van Heesewijk JP (2010) Real-time 3D fluoroscopy guidance during needle interventions: Technique, accuracy, and feasibility. *AJR Am J Roentgenol* 194:W445-51. Doi:10.2214/AJR.09.3647
12. Draney MT, Zarins CK, Taylor CA (2005) Three-dimensional analysis of renal artery bending motion during respiration. *J Endovasc Ther* 12:380-386. Doi:10.1583/05-1530.1
13. Brandner E, Wu A, Chen H et al (2006) Abdominal organ motion measured using 4D CT. *Int J Radiat Oncol Biol Phys* 65:554-560

14. Glodny B, Unterholzner V, Taferner B et al (2009) Normal kidney size and its influencing factors - a 64-slice MDCT study of 1.040 asymptomatic patients. *BMC Urol* 9:19. Doi:10.1186/1471-2490-9-19
15. Lee S, Yang DS, Choi MS, Kim CY (2004) Development of respiratory motion reduction device system (RMRDs) for radiotherapy in moving tumors. *Jpn J Clin Oncol* 34:686-691. Doi:10.1093/jjco/hyh125
16. Shyn PB, Tatli S, Sainani NI et al (2011) Minimizing image misregistration during PET/CT-guided percutaneous interventions with monitored breath-hold PET and CT acquisitions. *J Vasc Interv Radiol* 22:1287-1292. Doi:10.1016/j.jvir.2011.06.015
17. Carlson SK, Felmlee JP, Bender CE et al (2005) CT fluoroscopy-guided biopsy of the lung or upper abdomen with a breath-hold monitoring and feedback system: A prospective randomized controlled clinical trial. *Radiology* 237:701-708. Doi:10.1148/radiol.2372041323
18. Dawson LA, Kavanagh BD, Paulino AC et al (2010) Radiation-associated kidney injury. *Int J Radiat Oncol Biol Phys* 76:S108-15. Doi:10.1016/j.ijrobp.2009.02.089



M.J.L. van Strijen • S.J. Braak

Department of Radiology, St. Antonius Hospital, Nieuwegein, The Netherlands

Submitted for publication

Chapter 10

Cone beam CT and Real Time 3D
Needle Guidance for Biopsy and
Needle Interventions:

a Pictorial of the Technique and Clinical Indications

Introduction – Cone-beam CT

Although conventional interventional radiology (IR) is associated with mainly two dimensional x-ray imaging and predominantly for vascular work, the scope of IR is expanding continuously towards a higher diversity in vascular and non-vascular procedures, and towards more complex 3D imaging. This phenomenon is partly due to the innovative nature of this clinical field, but may also be attributed to technical developments in medical imaging. While rotational capabilities of the C-arm have initially been used for 3D rotational angiography [1], the introduction of faster graphics boards and especially the introduction of flat panel detectors have made the equipment now capable of performing cone-beam CT imaging [2,3,4]. This emerging technology can be very useful for needle-guided interventions in the angiosuite.

Technique

A cone-beam CT (CBCT) volume is acquired by a rotational scan ($\geq 180^\circ$) of the C-arm of a fluoroscopy flat panel system. Compared to conventional CT imaging there are some important differences. In general, CT makes use of a so-called fan beam, whereas CBCT uses the entire cone-shaped beam. On a single slice helical CT scanner the detector acquires 2-dimensional line projections. In conventional CT-scanners a volume-CT is made by changing a stationary circular rotation around the patient to a helix by simultaneously moving the table through the X-ray beam. In CBCT the table remains stationary in often one single rotation, because the cone shape of the bundle on the detector already provides a scan volume, instead of only one slice. The stationary rotation in CBCT is needed as the rotation of the C-arm is much slower compared to the rotation of the tube built in a conventional CT scanner.

The size of the detector determines the dimensions of the CBCT. When beam and 2D-detector are rotated around the body (in C-arm technology usually a single rotation up to 360°) a volume is acquired with dimensions defined by the size of the detector. The 3D volume is reconstructed by using special reconstruction algorithms [5]. Since the resolution of the individual detectors in a flat panel is higher than the resolution of a conventional CT detector, in theory images with higher spatial resolution can be obtained. Due to current technical limitations

of the detector cone-beam CT volumes have lower contrast resolution (varying between 5HU and 20HU, depending on the different manufacturers) compared to conventional CT systems. Apart from that this technique is more subject to artefact formation like movement (due to slower rotation), noise and beam hardening because of the cone-beam acquisition (*Figure1*).

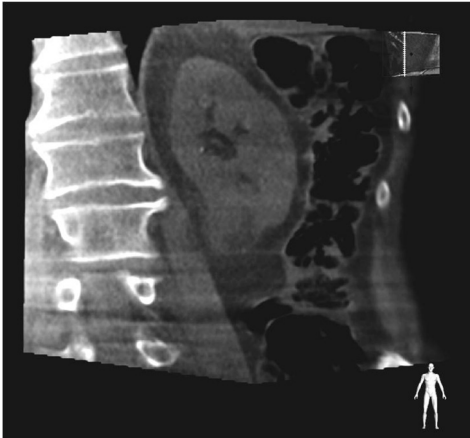


Figure 1. typical example of a cone-beam CT volume. Although some artefacts are present the quality is definitely sufficient to perform CBCT needle guidance.

Combining cone-beam CT and 3D needle guidance

A cone-beam CT volume can be used for checking the result of an interventional procedure or quick imaging in case of sudden complications during an intervention (e.g. bleeding, stent migration). Combined with dedicated software the volume can also be used to make a virtual needle path planning prior to a percutaneous needle-based intervention. Philips Healthcare (Best, The Netherlands) was the first to develop a working system and called the technique of real-time needle guidance XperGuide. Currently more vendors have these options available with different proprietary names (Siemens: I-guide, GE: Innova). By also identifying important and vital surrounding anatomical structures a possible safe window for placement of a needle or determining a needle path for performing a procedure is feasible [6,7].

Merging cone-beam CT with pre-interventional CT and MR

Although the image quality of CBCT is sufficient for performing the needle path planning, additional information from pre-interventional CT or MR images may sometimes be required or can be very helpful in hard to visualize structures.

Especially the unique soft tissue information of MR scans can sometimes be very helpful for needle path planning or targeting. In these cases it is possible to import DICOM-images in the system. The imported volume is registered to a CBCT volume based on anatomical landmarks, after which the needle planning can be performed on the merged volume. This technique is very helpful in needle interventions in soft tissue lesions or lesions only visible on contrast enhanced CT (Figure 2).

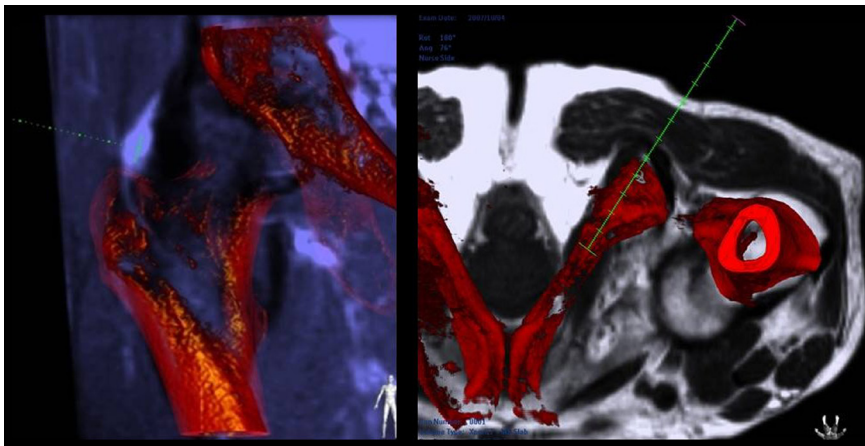


Figure 2. Two examples of merging previous acquired MR images with a cone-beam CT volume. On the left the imaging characteristics of a tendinitis are superimposed on the CBCT. On the right a bone metastases only visible on MR which is used for needle path planning on the CBCT.

Cone-beam CT needle guidance - the procedure

The first step in performing a procedure is positioning the patient in such a way that the target area will lie within the foreseen scan volume. Due to the limited physical dimensions of the detector and the C-arm this requires some careful planning. In addition, attention should be paid to position the patient in such a way that the C-arm is able to rotate around the patient uneventfully. For acquiring a cone-beam CT volume two basic C-arm positions are possible: patient head position (propeller scan, usually 240° rotation) or the C-arm alongside the table (nurse position/roll scan, usually 180° rotation). Better image quality is achieved by performing a scan with as many degrees of rotation as possible, where a larger number of projections (images) help reduce the artefacts as much as possible. Depending on the angiosystem characteristics usually the propeller scan is quicker in acquisition and provides therefore better image quality. After the acquisition the CBCT volume is reconstructed, and with dedicated

needle guidance navigation software a virtual needle path can be drawn in the volume. Special software links the planned virtual 3D path to the C-arm, after which real-time feedback is provided between the motion of the C-arm and the virtual planning. This feature allows automatic positioning of the C-arm in the exact desired angle that is for optimal real-time needle guidance based on the planned needle path. During the procedure separate additional volume acquisitions can be made for verifying the position of a needle or the progress of the intervention, for instance in the event of organ or patient movement. A diagnostic or therapeutic intervention is usually concluded by a check CBCT, for verification of the needle position and for checking possible complications (e.g. bleeding, pneumothorax), that need treatment while the patient is still on the table.

Guiding devices

The fluoroscopy image, with or without a CBCT-volume slice overlay, provides only 2D information on the needle position and angulation. For providing positional information in the other dimension several different tools and techniques are available. Apart from the freehand technique, with the inherent uncertainty of maintaining the needle position while manoeuvring, several guiding devices are available. The use of a guiding laser, preferably situated at the caudal end of the table, can provide additional angulation information (SimpliCT, Neorad AS, Norway). The Seestar device (Apriomed, Sweden) and Simplify (Neorad, Norway), originally designed for conventional CT-guidance, are very useful tools for needle guidance providing a solid base for guiding needles (*Figure 3*). New devices are currently under development and also the first robotic-assisted devices are under evaluation (Isys Medizintechnik Austria).



Figure 3. Overview of guiding devices for CBCT needle guidance. From left to right: SimpliCT (Neorad), Simplify (Neorad), Seestar (Radi Medical), and Isys device (Isys Medizintechnik)

Clinical indications

Diagnostic biopsy

In general the technique of CBCT needle guidance is suitable for all patients with lesions inaccessible for US guided intervention, and in whom a CT or MR guided needle placement is indicated. One of the important pre requisitions is that the patient is able to lay still for the entire procedure, or that appropriate measures can be taken to ensure that the patient maintains the same positions all along the procedure (proper fixation of the relevant anatomy, conscious sedation or general anaesthesia with full muscle relaxation). This is needed as the accuracy of the needle position relies on complete immobilisation after the acquisition of the scan used for planning the needle path. Currently no automatic movement compensation techniques are available. Possible solutions movement compensation currently under investigation are the use of optical systems for detecting patient movement, the use of fiducials, and intelligent image analysis algorithms providing real time adjustment of the CBCT volume and needle path relative to the live fluoroscopy.

Thorax

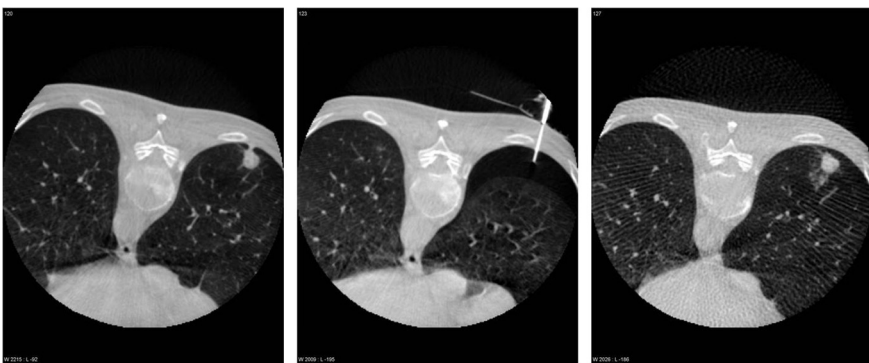
In the thoracic cavity this technique can be used for diagnostic biopsies in the lung parenchyma, mediastinal structures, and in the surrounding soft tissues and skeletal anatomy. Ultrasound guided biopsy is impossible for intrapulmonary lesions and bone, and visibility of mediastinal structures is limited where the precarious nature of these interventions requires good visibility instead. And although ultrasound can be used for pleural based masses, the benefit of performing these procedures in the angiosuite lie in the fact that complication management is much easier in a more dedicated environment. Compared to conventional CT, CBCT guidance proves to be quicker and uses less radiation dose [8] although there is a distinct learning curve for physicians new to the technique.

Movement of the target during the procedure is largest in the basal parts of the lungs and needs including a part of the diaphragm in the CBCT volume for identification of the moment it coincides with the visible part of the diaphragm on the overlying fluoroscopy. Possible complications include pneumothorax (to be avoided by limiting needle sizes and transpleural movement of the needle

within one breath hold, to avoid tearing of the pleura), mediastinal haemorrhage etc. In our experience we also see that especially peripherally located lesions are also referred, as these are difficult to reach with bronchoscopy.

In our institution we mainly use a 17G coaxial technique, taking biopsies with short length 18G thru cut devices. To prevent a pneumothorax as much as possible it is important to position this guiding needle outside of the pleural space to prevent tearing of the pleura in breathing (less important in the apical lung). Since the amount of soft tissue of the thoracic wall is limited quite often a guiding or stabilizing device is helpful for fixing the coaxial needle, but also quite often we use a freehand technique, especially in somewhat larger lesions also faintly visible on fluoroscopy. Breathing instructions are used to position the level of inspiration in accordance with the initial planning CBCT [9].

A post procedural pneumothorax can be identified directly on the CBCT after completing the intervention as well as parenchymal haemorrhage. In our experience these are nearly always small and self-limiting. If the pneumothorax is too extensive direct treatment by suction with a blunt tipped needle connected to a large syringe with three-way stopcock and occlusive dressing can prevent the insertion of chest tube in the majority of cases (*Figure 4*). In our 5-year experience we have performed a bronchial embolisation for parenchymal bleeding in only one patient. The number of patients with a pneumothorax is considerably lower than figures reported in literature [9-12]. Because of proper planning we never had an accidental intercostal bleeding.



Figures 4. XperGuide example of a coaxial 18G lung biopsy. From left to right: planning CBCT, check CBCT with large pneumothorax and very low-dose check CT after aspiration.

Abdominal

The indications for using CBCT guidance in the abdomen is comparable to the indications in the thorax. Lesions located deep in the abdomen, poorly visible with ultrasound or difficult to reach because of adjacent critical anatomic structures. CBCT is especially useful for needle guidance for lesions under the diaphragm (e.g. adrenal mass, subphrenic abscess etc.) because of the angulated needle paths. Patients for abdominal interventions are usually placed in a prone position, as most important organs and lesions in the retroperitoneal space can be safely approached from posterior (*Figure 5*). In the upper abdomen we face the same problem as in the basal lungs, where breathing movement can cause misalignment of needle and target. The technique used to overcome this is the same as described under lung biopsies. The limited contrast resolution can be a problem for identifying liver lesions, but in this situation overlay imaging using previously acquired contrast enhanced high resolution CT or MRI scans is feasible. By comparing CBCT and the available conventional CT scans we noticed that a considerable shift in the upper abdominal organs can be caused by switching from supine to prone position. Deformation of liver anatomy can be observed and has to be taken into account when performing liver biopsies. Kidneys can rotate around longitudinal and transverse axis, to an extent that is related to body mass index of the patient [research in progress, submitted for publication]. These deformations and displacements are especially important when the CBCT is used in combination with previously acquired conventional CT images or MRI. In these cases it is important to focus only on the target organ on the most recent CBCT, and less on the surrounding structures when matching these data sets. In mesenteric procedures bowel movement can pose a problem where keeping the procedure as short as possible (to prevent shift of the target) or using supportive medication can be the solution.

Pelvic

In pelvic interventions CBCT needle guidance is mainly used for biopsying lymphadenopathy in the deep perivascular regions, pre-sacral biopsy and abscess drainage in deep locations. Again, this is especially useful when the penetration of ultrasound is insufficient or the visualization window is small.

One of the challenges in pelvic interventions can be the drainage of pelvic fluid collections or abscesses. Quite often these fluid collections are in difficult to reach



Figure 5. Example of a retroperitoneal mass between the aorta and the inferior vena cava. These hard to reach lesions can be safely biopsied by using the potentially high accuracy of cone-beam CT guidance.

positions with important overlying vital structures. A good overview is crucial just as well as proper needle guidance. Sometimes in perivascular lymph node biopsy it is necessary to use an approach where fluid dissection or lifting obstructive tissue by using a guiding needle is mandatory.

Bone

Bone is impossible to visualize with ultrasound, CT again has the limitation of gantry tilt and small working space in the gantry. Contrast resolution of CBCT for bone interventions is excellent, especially overlying fluoroscopy over the reconstructed volume. Therefore in case of bone biopsy for suspected metastasis, vertebroplasty/cementoplasty, and thermo ablation treatment for instance in osteoid osteoma or painful metastases CBCT needle guidance is a very useful tool.

Vascular

When combining CBCT volumes with vascular procedures a whole new field of hybrid imaging procedures becomes feasible. We have previously published our initial experience in using this technique together with DSA to effectively treat type II endoleaks [13] (Figure 6). Also CBCT needle guidance can be used for difficult vascular access, for performing vascular interventions and treating vascular pathology with limited use of contrast by using CBCT for registering for instance CTA or MRA for roadmapping [14]. Another type of procedures currently under investigation is embolisation of vascular lesions by again combining angiographic information and soft tissue information on tumour size (liver metastases).



Figure 6. Endoleak treatment using CBCT guidance. The availability of DSA at the same time enables depiction of the complex feeding vessel anatomy in this type IIB endoleak.

Cone-beam CT and diagnostic biopsy: results

In our hospital this technique has now been used in over 600 procedures with an indication for CT guided biopsy or intervention, with low complication rate [7]. This new needle guidance technology is considered valuable, since an accomplished 100% technical success in terms of reaching the correct target position is feasible and has been described in our first 150 patients. The use of live fluoroscopy on top of CBCT guidance has resulted in a significant reduction of procedure time. In addition, the open architecture of the C-arm not only provides a lot of working space but also results in a less claustrophobic experience by the patient.

Therapeutic needle interventions

RFA and cryo ablation

This technique is also useful for placing needles in renal cell tumours to perform thermal ablations. In clinical practice using real time needle guidance and CBCT proves to be a lot quicker than using CT or MR. There is also a considerable time gain in comparison with procedures using a laparoscopic approach. In laparoscopy dorsally located tumours can be a separate complicating factor, since the kidney has to be surgically dissected completely and lifted for access. In a prone position the CBCT needle guidance procedure can be performed easily and specifically dorsally located tumours are easily accessible. Despite

the present needle artefacts on control CBCT's the formation of the ice ball in cryo-ablation can be visualized sufficiently during the treatment.

Cone-beam CT and radiation dose

Extensive dose measurements in our initial patients have shown that a considerable reduction in radiation dose for the patient can be achieved by using this technique instead of conventional CT. The dose reduction varied between 13-43% depending on the anatomical location [7]. Apart from the initial CBCT acquisition for planning a typical needle path CBCT procedure consists of at least a check CBCT after the needle intervention. Further dose reductions are possible by consistently using the recently introduced horizontal collimation for the check CBCT (smaller volume, only in the direct area of interest). The largest reduction of patient dose is attributed to the CBCT compared to a conventional CT. Some of total dose reduction is unfortunately compensated by the higher dose caused by fluoroscopy compared to single CT shots, but not when CT fluoroscopy is being used. The total fluoroscopy time with these procedures is limited and seldom exceeds 3 minutes.

Expanding the horizon of 3D needle guidance

As described above various clinical applications are now feasible replacing the use of conventional CT. Especially difficult anatomical positions, that are cumbersome to visualize using ultrasound, or procedures requiring a dynamic monitoring of needle progression may benefit from this technique. Some examples of challenging procedures where XperGuide was used successfully are the treatment of iliac aneurysm treatment, celiac plexus block, trigeminal nerve ablation, drainage of peri-aortic fluid collections in the mediastinum, and pre-operative tumor localisation in small lung tumours by using fiducials and localisation wires (*Figure 7*).

Limitations

Apart from higher accuracy for needle placement and the considerable reduction in dose for the patient there are also minor disadvantages, that need additional effort of the operator or will probably be solved by ongoing research and development. When using overlay imaging the exact position of the organs of the upper abdomen can vary considerably in prone or supine



Figure 7: CBCT in placing a localisation wire in a small lung nodule in a patient with lung carcinoma. A localized resection of the area surrounding the localisation wire was performed the same day by using video assisted thoracoscopy (VATS).

position, causing considerable differences between the diagnostic CT scan and the cone-beam CT during the planning stage of the intervention. Currently there is also not yet an active movement compensation available. Patients unable to lie still for a limited period of time are a problem for using this technique, and movement caused by breathing needs active manual counter movement compensation by the interventional radiologist. Proper fixation or the use of general anaesthesia with muscle relaxation are possible solutions. Apart from that very obese patients may be too large for proper positioning and prevent unobstructed rotation of the C-arm. Architectural redesign will lead the way here, but is currently limited by dose issues when enlarging the distance between tube and detector. Further improvement of image quality can be achieved by better artefact correction/reduction.

Future improvements

A lot of effort is put in facilitating this technique and make it more widely available for interventional work. It is to be expected that in the next years the flat panel technology will be replacing the conventional image intensifier technique in a vast amount of hospitals, thereby opening the doorway to CBCT guided procedures. Also the focus will be on enhancing image quality by using sophisticated reconstruction algorithms and volumetric information based on fewer projections.

The use of already acquired images will further reduce dose for the patient and will help in enhancing image quality and accuracy of this technique. Accuracy and speed of the procedure will further improve by using robotic assistance for needle guidance. Additional software tools currently under development will help expand new approaches to existing interventional techniques (ablation planner software combined with needle guidance, embolisation guidance) or enable the development of new techniques (virtual ablations, no contrast no radiation interventions based on electromagnetic device tracking in combination with registered previously acquired image data sets, *Figure 8*).

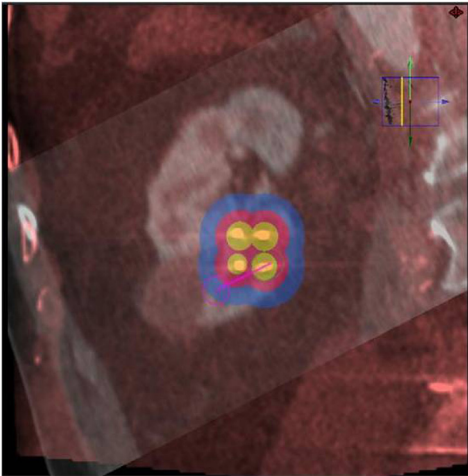


Figure 8: CBCT needle guidance with use of the ablation planner tool. With this tool not only the needles can be planned, but also the area affected by the ablation. In this example previously acquired conventional CT (in grey) is used as an overlay for the CBCT (in red). The different zones surrounding the needles graphically represent the isotherms belonging to this type of needle.

Conclusion

Cone-beam CT and 3D needle guidance are promising new techniques in the angiosuite, replacing conventional CT guided procedures with equal or higher accuracy and less dose for the patient. These technical developments may enable us to further expand the spectrum of clinical applications in the field of interventional radiology.

References

1. Anxionnat R, Bracard S, Macho J, Da Costa E, Vaillant R, Launay L, Troussset Y, Romeas R, Picard L. 3D angiography clinical interest. First applications in interventional neuroradiology. *J Neuroradiol* 1998; 25:251-262.
2. Jaffray DA, Siewerdsen JH, Wong JW, Martinez AA. Flat-panel cone-beam computed tomography for image-guided radiation therapy. *International journal of radiation oncology, biology, physics* 2002; 53(5):1337-1349.
3. Siewerdsen JH, Moseley DJ, Burch S, Bisland SK, Bogaards A, Wilson BC, Jaffray DA. Volume CT with a flat-panel detector on a mobile, isocentric C-arm: pre-clinical investigation in guidance of minimally invasive surgery. *Med Phys*. 2005 Jan;32(1):241-54.
4. Ritter D, Orman J, Schmidgunst C, Graumann R. 3D soft tissue imaging with a mobile C-arm. *Comput Med Imaging Graph*. 2007 Mar;31(2):91-102.
5. Gupta R, Grasruck M, Suess C, Bartling SH, Schmidt B, Stierstorfer K, Popescu S, Brady T, Flohr T. Ultra-high resolution flat-panel volume CT: fundamental principles, design architecture, and system characterization. *Eur Rad* 2006; 16:1191-1205.
6. Racadio JM, Babic D, Homan R, Rampton JW, Patel MN, Racadio JM, Johnson NM. Live 3D Guidance in the Interventional Radiology Suite. *AJR Am J Roentgenol*. 2007 Dec;189(6):W357-64
7. Braak SJ, van Strijen MJ, van Leersum M, et al. Real-Time 3D fluoroscopy guidance during needle interventions: technique, accuracy, and feasibility. *AJR Am J Roentgenol* 2010; 194(5):W445-51.
8. Braak SJ, van Strijen MJ, van Es HW, Nivelstein RAJ, van Heesewijk JPM. Effective dose during needle interventions: cone-beam CT guidance compared with conventional CT guidance. *J Vasc Interv Radiol* 2011; 22:W455-461.
9. Braak SJ, Herder GJM, van Heesewijk JPM, van Strijen MJ. Pulmonary Masses: Initial Results of Cone-Beam CT-Guidance for Percutaneous Lung Biopsy. *Cardiovasc Intervent Radiol* 2011; 7 December, Epub ahead of print
10. Heck SL, Blom P, Berstad A. Accuracy and complications in computed tomography fluoroscopy-guided needle biopsies of lung masses. *Eur Radiol* 2006; 16:1387-1392
11. Hiraki T, Mimura H, Gobara H et al. CT fluoroscopy-guided biopsy of 1,000 pulmonary lesions performed with 20-gauge coaxial cutting needles: diagnostic yield and risk factors for diagnostic failure. *Chest* 2009; 136:1612-1617
12. Duncan M, Wijesekera N, Padley S. Interventional radiology of the thorax. *Respirology* 2010; 15:401-412

13. van Bindsbergen L, Braak SJ, van Strijen MJL, de Vries JPPM. Type II endoleak embolization post-EVAR with use of real-time 3D fluoroscopic needle guidance. *J Vasc Interv Radiol* 2010; 21:1443-1447
14. Kobeiter H, Nahum J, Becquemin JP. Zero-contrast thoracic endovascular aortic repair using image fusion. *Circulation* 2011 Sep 13;124(11):e280-2.



Summary
General Discussion
Implications

Summary

With the introduction of flat panel detectors and faster computer technology cone-beam CT guidance (CBCT) is now feasible. CBCT-guidance is a stereotactic needle guidance technique for interventions, combining 3D soft-tissue cone-beam CT imaging, navigation needle planning software, and real-time fluoroscopy. CBCT-guidance is possibly a very good alternative for needle interventions.

For evaluating this new technique we studied four aspects of CBCT-guidance:

- Accuracy in phantoms with comparison to fluoroscopy guidance and CT-guidance.
- Clinical applications of CBCT-guidance.
- Radiation dose aspects of CBCT-guidance.
- Clinical aspects of the merging capability of CBCT-guidance technique.

Because CBCT-guidance is based on overlay imaging of CT-images and fluoroscopy we decided to compare the results of CBCT-guidance to conventional fluoroscopy guidance and to CT-guidance in two phantom studies. Conventional fluoroscopy for needle guiding is especially useful and feasible in visible fluoroscopic anatomic structures. In a spine phantom for vertebroplasty the accuracy of needle placement was significantly better using CBCT-guidance than when using the conventional fluoroscopy method. Also the fluoroscopy time was lower with CBCT-guidance and therefore the dose for the operator was lower as well, but both procedure time and patient dose were higher (**Chapter 1**).

The study described in **Chapter 2** compared the accuracy of CBCT-guidance to CT-guidance in a different phantom. We determined the accuracy of needle placement to small targets (2.3 mm) in three different trajectories; easy (in plane straight down), medium (in plane angulated) and hard (out of plane and angulated). Furthermore a distinction in the results was made based on the experience of the operators. The results showed that CBCT-guidance is the preferred modality for more difficult procedures with angulated needle paths or in small targets. This is contributable to significantly higher accuracy combined with comparable procedure times. Also the results suggest a learning curve

is definitely present in this new technique, especially in performing needle placement in double angulated needle paths.

The general performance of CBCT needle guidance in a clinical setting (**Chapter 3**), CBCT guidance in pulmonary biopsies (**Chapter 4**) and CBCT guidance in renal biopsies (**Chapter 5**) are described respectively. In **Chapter 4** we report the outcome for sensitivity (90%), specificity (100%), PPV (100%), NPV (66.7%) and accuracy (91.7%) in biopsying lung lesions. The results using CBCT-guidance for biopsying renal masses that are hard to identify with US are presented in **Chapter 5**. The sensitivity, specificity, PPV, NPV, and accuracy of biopsying renal masses were 91.7%, 100%, 100%, 89.5%, and 95.1% respectively. In all interventions a 100% technical success (within the predefined 5 mm safety margin) was achieved (**Chapter 3**).

The mean interventional procedure time was 25.2 minutes and the mean fluoroscopy time was 2 minutes 49.5 seconds. These results indicate that CBCT-guidance in routine clinical setting definitely does have technical advantages. For difficult to reach lesions, for example lesions in the lower thoracic regions, in subphrenic locations or in the upper pole of the kidneys, CBCT-guidance offers a good and accurate alternative method to perform the needle procedure with. The availability of real-time fluoroscopic overlay makes it possible to biopsy moving targets more accurately than with step-and-shoot modalities. Of course it is possible to use conventional CT-guidance for these needle interventions, but this often requires longer fluoroscopy times, larger volumes to scan to follow the needle path and higher experience and dexterity of the operator. Furthermore due to the C-arm configuration the workspace is larger and patient accessibility is better in CBCT-guidance compared to CT-guidance (even when there is a dedicated large bore intervention CT). Because CBCT-guidance is based on an interventional C-arm configuration there is the possibility to use it for angiography as well.

In **Chapter 6** we described the use of both CBCT needle guidance and angiography in patients with a complex type II endoleak after endovascular abdominal aneurysm repair (EVAR). With CBCT guidance a direct puncture of the endoleak nidus was performed and after angiography through the puncture needle we embolized the endoleak with glue. The digital subtraction angiography (DSA) depicted the feeding vessels and the amount of glue and pressure that should be needed to treat. All patients were treated successfully. Based on the results of

Chapters 3-6 we conclude that CBCT-guidance is a safe and accurate method to perform a needle intervention in a clinical setting.

When introducing a new technique for needle interventions using ionizing radiation the question always arises how much the dose will be for the patient and the operator. In **Chapter 7** we report a significant dose reduction (13 to 42%) of CBCT-guidance compared to procedures using conventional CT-guidance (7.6-16.1 mSv versus 13-20.4 mSv). To quantify the operator dose a phantom study measuring the dose for the hand, thyroid region and gonad region was performed without using any protection, with the use of disposable lead aprons, the use of couch and ceiling mounted lead shielding and a combination of all (**Chapter 8**). Furthermore, dose measurements were made during clinical cases. The hand dose in the model was 34.2 μ Sv - 54.6 μ Sv (thoracic / abdominal procedures respectively), The doses for thyroid and gonad regions were 83.2 μ Sv and 34.3 μ Sv in the thoracic, and 66.2 μ Sv and 47.2 μ Sv in the abdominal group. Based on the scatter model and the results of the measurements of the clinical cases the mean scatter radiation is quite low compared to the reported scatter radiation dose. However, the model without protection overestimates the dose, and approximately 240 cases a year can be performed without exceeding the yearly limit. The best significant dose reduction (98.2%-98.9%) can be achieved by a combination of lead drape and ceiling/couch shielding.

Another important feature underlining the multimodality capability of the system is the ability to import previously acquired DICOM data (e.g. CT or MRI). Merging this with a low dose CBCT makes it possible to create a combined volume that provides excellent visibility of the target and no need for repeated contrast administration. A disadvantage of this function is that previous DICOM data usually is obtained in supine position and quite often the CBCT-guidance procedure is performed in prone position. This position change can cause considerable shifts in internal organs, especially in the upper abdomen. Based on the available data of renal interventions a retrospective analysis of the change of kidney position was determined and the results are described in **Chapter 9**.

In the last **Chapter (10)** CBCT-guidance technique is evaluated in different types of procedures and different anatomic locations. Tips and tricks are provided based on our experience in over 600 performed procedures.

General discussion and implications:

CBCT needle guidance is a promising new interventional tool with high accuracy and specific advantages compared to conventional CT scanners. One might wonder if in the near future it will replace conventional CT guided interventions completely?

In most hospitals in Europe the workload on the CT scanners available is considerable, and the possibilities to reserve time for interventions is limited. Some dedicated centres (mainly academic) have dedicated interventional CT scanners available, but in most other hospitals these procedures have to fit into a regular daily schedule. If an accidental finding, needing immediate treatment and is easy to perform in the same session on the CT scanner, there is no need or rationale to move the patient to the angio suite. In these cases it's better to perform the procedure (usually abscess drainage) immediately following the diagnostic scan, especially if an (near) axial approach can be used. In some cases though, the approach is difficult to perform because of steep needle angulations and difficult to reach locations, and the trouble of having to move the patient will pay off in the benefits associated with using a CBCT-guidance. Another important reason to perform interventional procedures with CBCT-guidance is the fact that the angio suite is dedicated and equipped for sterile and even complex procedures where most of the CT-suites usually are not (disregarding dedicated intervention CT suites). The room is designed and intended to perform interventions under sterile conditions, the required materials are at hand and the personnel involved specifically trained. Also there is a benefit in the geometry, where patient accessibility is much better in the working space in C-arm configurations. Apart from CBCT-guidance the presence of fluoroscopy, the ability to perform angiography and the integration of interventional ultrasound turns this into a multimodality system. The hybrid imaging definitely facilitates the direct management of possible complications. For instance the post lung biopsy pneumothorax is easier to manage in the angio suite than in the CT scanner, because of the ability of fluoroscopy to overview the complete pneumothorax in all directions and the effect from drainage can be monitored in real-time.

In case of an intractable bleeding there is always the possibility to directly convert to a conventional angiographic embolization procedure, again with

the benefit of working in a dedicated intervention suite with embolization materials at hand.

Although ultrasound remains the method of choice because of the lack of ionizing radiation, the imaging characteristics and the field of view can make it hard to overview the complete trajectory of the wire or drain in drainage procedures. Combining it with fluoroscopy provides an overview of the wire or drain trajectory. By moving these kinds of procedures to an angio suite with CBCT, CBCT-guidance and integrated ultrasound not only every procedure is feasible but a reduction on the workload of CT and ultrasound is a beneficial effect as well.

CBCT-guidance is a relatively new concept that can pose a challenge for the interventional radiologist to become familiar with. Changing one's working routine can require some effort at first, especially since we know from the results in Chapter 1 and 2 that a learning curve with this new method is inevitable. The accuracy and speed, as well as the beneficial effects of dose reduction for operator and patient will make this investment worthwhile. For a radiologist who already has or soon will have this technique available in his or her department, we believe that hands-on courses, proctoring and e-learning are essential, also since these are now available. When replacing outdated equipment many hospital administrations will now choose this new equipment with CBCT because of the aforementioned benefits, and because this equipment is now becoming state-of-the-art in interventional radiology.

This new technique not only has advantages. There are definitely also some disadvantages and current limitations. The main challenge for these types of procedures is accidental patient movement after acquisition of the volume and during the needle positioning. This becomes noticeable during the procedure when fluoroscopically identifiable structures are no longer overlaying the CT volume, and in case of minor movements in the plane of the table can be overcome by manual adjustments of the overlay position or gentle movements of the table. Obviously this can be prevented as much as possible by making the patient as comfortable as possible, providing proper fixation of the anatomic region or maybe even the use of general anaesthesia.

Another relative limitation is the available space in the C-arm, where larger patients can restrict the movement of the arm. Currently this can be solved by using a different approach (runway approach), or by using a roll movement with

the C-arm positioned sideways instead of a propeller movement at the head of the table. The redesign and development of larger C-arms has started already and it is only a matter of time for new geometry to overcome this limitation.

Future perspectives

After the introduction of CBCT-guidance in our department only very few CT-guided interventions are performed nowadays. It's our conviction that with the combination of conventional fluoroscopy, cone-beam CT, needle guidance software, and merging capabilities another step is made to full, hybrid imaging and that this will be the future of performing dedicated interventions.

Developments are still continuing at a rapid pace though, and there are some issues in improving the user interface, usability and technical aspects. The merging function is still laboursome and difficult at times. The option to do this automatically is available but is not sufficiently reliable in our experience. One of the main reasons for this is the fact that many procedures are performed in a different patient position than the previous acquired CT- or MRI data. For the kidneys we have described and quantified this movement between prone and supine positions. Probably there will be software in the future taking this into account, also enabling the dynamic plastic deformation and relative position of this anatomy into account as well.

The visualization and overlay of both the fluoroscopy image and the CBCT-slice breathing movement can be overcome by comparing the position of the diaphragm and giving the patient breathing commands to make the position of the diaphragm to coincide with the CBCT image. Automated motion detection, not available yet, could make the intervention easier and more accurate. Several different options using different methods are currently being investigated and will probably result in further improvements of needle guidance in the near future. Lowering the radiation dose will always be of great importance. Although CBCT guidance already results in a lower dose to the patient compared with conventional CT guidance, further improvements are not only desirable but also definitely feasible. One of the easiest changes would be the use of asymmetrical collimation, needed when working in the outer quadrants of the viewing field. Changing the table position to center the area of interest is already feasible, but does require special adjustments with parallax distortion in mind.

In a routine procedure fluoroscopy accounts for approximately 55% of the dose administered to the patient. Further adjustments in fluoroscopy technique are therefore also desirable.

Needle positioning in the current setup of the procedure is still very much dependant on the operator. We mainly used a fixation tool for the coaxial needle on the patient (Seestar, Apriomed Sweden) and recently evaluated a laser guidance tool (SimpliCT, Neorad, Sweden). Both of them have a clear benefit in providing additional stability to the needle [1]. A new development in this area is the recent introduction of a robot arm to assist in needle guidance and further reduce the dose for the operator because of the remote operation [2].

In the field of ablation procedures a new development is the use of pre intervention tumour segmentation and ablation planner software. Ablation is a well-established method for treatment of primary cancers or metastases [3]. The effect of an ablation relies heavily on proper needle positioning as well as predicting the ablation zone (extending the tumour boundaries, safety margin). These additions to the system are already being investigated and evaluated in a clinical setting and the results of these studies are expected soon.

One option which is not yet feasible, but subject to extensive research already is the ability to use electromagnetic (EM) needle navigation, [4], further reducing dose and improving accuracy.

General conclusion

CBCT-guidance is a hybrid imaging guidance technique and is being used in a clinical setting more frequently. With this technique, CT-like imaging and accurate needle guidance is available in the interventional suite. CBCT-guidance is especially useful in hard to reach lesions with an indication for CT guided intervention, but probably will not replace the use of ultrasound if ultrasound guidance is feasible. Combining the CBCT-guidance system with ultrasound (whether or not combined with EM-tracking) results in a multimodality system in a dedicated intervention room that will be ideal for all interventions. Because of good accuracy, the added functionality for importing previous exams and the expected future developments (e.g. tumor segmentation, ablation planner and EM tracking) CBCT-guidance will claim its place in the expanding field of interventional oncology.

References

1. Kroes M, Braak SJ, van Strijen MJL, Busser W, Hoogeveen YL, de Lange F, SchultzeKool L. Abstract No. 68: Laser Guidance in combination with Needle Path Planning reduces Fluoroscopy Time and Patient Radiation Dose in Cone-beam CT Needle Interventions. *JMIR* 2012; page S31.
2. Korb W, Kornfeld M, Birkfellner W, Boesecke R, Figl M, Fuerst M, Kettenbach J, Vogler A, Hassfeld S, Kornreif G. Risk Analysis and Safety Assessment in Surgical Robotics: A Case Study on a Biopsy Robot. *Minim Invasive Ther Allied Technol* 2005; 14(1):23-31.
3. Webb H, Lubner MG, Hinshaw JL. Thermal Ablation. *Semin Roentgenol* 2011; 46:133-141
4. Nagel M, Hoheisel M, Petzold R, Kalendar WA, Krause UHW. Needle and Catheter Navigation using Electromagnetic Tracking for Computer-assisted C-arm CT Interventions. *Proc. of SPIE* 2007; 6509:J1-J9.

Appendix

Samenvatting (summary in Dutch)

Authors and affiliations

Review committee

List of publications

Acknowledgements (dankwoord)

Curriculum Vitae

Samenvatting

Door de introductie van flat panel detectoren en snellere computertechnologie is het mogelijk om cone-beam CT (CBCT) te gebruiken voor 'naaldnavigatie'. CBCT-geleiding is een stereotactische naaldgeleiding techniek voor interventies. Hierbij wordt er gebruik gemaakt van de combinatie van 3D weke delen cone-beam CT, naald-navigatiesoftware voor traject planning en real-time fluoroscopie. CBCT-geleiding is mogelijk een zeer goed alternatief voor naaldinterventies.

Om deze nieuwe techniek te evalueren onderzochten wij vier aspecten van CBCT-geleiding:

- Nauwkeurigheidbepaling van CBCT-geleiding op fantomen, dit in vergelijking met conventionele fluoroscopie en in vergelijking met CT-geleiding.
- Klinische toepassingen van CBCT-geleiding.
- De stralingsdosis van CBCT-geleiding voor de patient en radioloog.
- Klinische aspecten van de fuserende toepassing bij de CBCT-geleidings techniek.

Omdat CBCT-geleiding gebaseerd is op een combinatie van CT-gelijkende beelden en fluoroscopie hebben we besloten om de resultaten van deze techniek separaat te vergelijken met conventionele fluoroscopie-geleiding en met CT-geleiding. Interventies met conventionele fluoroscopie zijn vooral nuttig en haalbaar bij zichtbare structuren onder doorlichting. In een wervelkolomfantoom voor vertebroplastiek onderzochten wij onder andere de nauwkeurigheid van het plaatsen van de naalden. De nauwkeurigheid van de plaatsing was significant beter gebruikmakend van CBCT-geleiding dan bij de conventionele fluoroscopie methode. Daarnaast was de fluoroscopietijd korter bij CBCT-geleiding en daarmee de dosis voor de interventie radioloog lager, maar de proceduretijd was langer en de dosis voor de patiënt waren hoger (**hoofdstuk 1**).

De studie beschreven in **hoofdstuk 2** vergelijkt de nauwkeurigheid van CBCT-geleiding ten opzichte van CT-geleiding in een ander fantoom. De nauwkeurigheid van de plaatsing van de naald naar kleine doelen (2,3 mm) werd

bepaald door drie verschillende moeilijkheidsgraden: eenvoudig naaldtraject (in het scanvlak recht naar beneden), middelmatig (in het vlak onder een hoek) en moeilijk (buiten het scanvlak en onder een hoek (dubbel schuin)). Daarnaast werd onderscheid gemaakt door de resultaten op basis van de ervaring van de radiologen met CBCT-geleiding te vergelijken. De resultaten toonden aan dat CBCT-geleiding de voorkeur heeft voor middelmatige en moeilijke procedures. Dit vanwege de significant betere nauwkeurigheid bij vergelijkbare proceduretijd. Daarnaast doen de resultaten vermoeden dat er een leerproces aanwezig is bij deze nieuwe techniek, met name bij het uitvoeren van moeilijke procedures.

De resultaten van CBCT naaldgeleiding worden respectievelijk beschreven in de algemene klinische setting (**hoofdstuk 3**), bij longbipten (**hoofdstuk 4**) en bij nierbipten (**hoofdstuk 5**). In **hoofdstuk 4** rapporteren wij bij longbipten een sensitiviteit van 90%, specificiteit van 100% en een positief voorspellende waarde (PVW) van 100%. De negatief voorspellende waarde (NVW) bedroeg 66,7% en de nauwkeurigheid 91,7%. De resultaten van nierbipten met behulp van CBCT-geleiding, welke niet echogeleid benaderd kunnen worden, zijn beschreven in **hoofdstuk 5**. De sensitiviteit, specificiteit, PVW, NVW en de nauwkeurigheid waren respectievelijk 91,7%, 100%, 100%, 89,5% en 95,1%.

Bij alle interventies werd een 100% technisch succes bereikt (binnen de vooraf gedefinieerde 5 mm veiligheidsmarge). De gemiddelde procedure tijd was 25,2 minuten en de gemiddelde fluoroscopietijd was 2 minuut 49,5 seconden (**hoofdstuk 3**). Al deze resultaten impliceren een voordeel van CBCT-geleiding in de dagelijkse klinische praktijk. Bij moeilijk bereikbare laesies zoals laesies laag thoracaal, subfrenisch of in de bovenzijde van de nier, biedt CBCT-geleiding een goede en nauwkeurige alternatieve methode om de procedure uit te voeren. Door de overprojectie van het fluoroscopie beeld over een cone-beam CT snede is het mogelijk om bewegende doelen nauwkeurig te bipteren in tegenstelling tot de step-and-shoot modaliteiten. Uiteraard is het mogelijk om conventionele CT-geleiding te gebruiken voor dit soort interventies, maar dit vereist vaak meer fluoroscopietijd, grotere volumes welke gescand moeten worden om het gehele naaldtraject te visualiseren (dus meer dosis voor de patient) en meer ervaring en behendigheid van de interventie radioloog. Verder is door de C-arm configuratie de werkruimte en de toegankelijkheid

rond de patient beter bij CBCT-geleiding ten opzichte van CT-geleiding (zelfs bij speciale interventie CT-scanners met grote doorgang). Omdat CBCT-geleiding gebaseerd is op een interventie C-boog, is het tevens mogelijk om gecombineerd gebruik te maken van 'standaard' angiografie.

In **hoofdstuk 6** beschrijven we het gebruik van zowel CBCT-geleiding en angiografie bij patiënten met een complexe type II endoleak na endovasculaire abdominale aneurysma reparatie (EVAR). Met behulp van CBCT geleiding werd een directe punctie verricht in het centrum van het endoleak. Na angiografie werd het endoleak geemboliseerd door middel van weefsellijm. De digitale subtractieangiografie (DSA) visualiseerde de aanvoerende arteriën verantwoordelijk voor het endoleak en bepaalde mede de hoeveel weefsellijm en druk die nodig was om het endoleak te emboliseren. Alle patiënten werden met succes behandeld.

Op basis van de resultaten van hoofdstukken 3-6 concluderen wij dat CBCT-geleiding een veilige en nauwkeurige methode is om een naaldinterventie uit te voeren in een klinische setting.

Bij de introductie van een nieuwe techniek (voor naaldinterventies) gebruik makend van ioniserende straling is het belangrijk te weten wat de dosis zal zijn voor de patiënt en de radioloog. In **hoofdstuk 7** wordt een significant lagere dosis (13 tot 42%) beschreven tijdens CBCT-geleiding ten opzichte van soortgelijke procedures met behulp van conventionele CT-geleiding (respectievelijk 7,6-16,1 mSv versus 13-20,4 mSv). Om de stroostralingsdosis te kwantificeren voor de interventie radioloog werd er met behulp van een fantoom een stroostralingsmodel gemaakt om de dosis voor de hand, schildklierregio en gonadenregio te bepalen. Hierbij werd er ook gekeken naar het effect van stralingsbescherming door middel van wegwerp looddoeken, het gebruik van tafel/plafond afscherming en een combinatie van beide (**hoofdstuk 8**). Naast de dosis bepaling op basis van het fantoom werden er ook metingen verricht tijdens klinische casussen. De handdosis in het stroostralingsmodel was 34,2 - 54,6 mSv (resp. thoracale / abdominale procedures), de dosis voor de schildklierregio en gonadenregio waren 83,2 en 34,3 mSv bij thoracale interventies en 66,2 en 47,2 mSv bij abdominale interventies. Gebaseerd op het stroostralingsmodel en de resultaten tijdens de klinische casussen is de

gemiddelde stroomstraling tijdens een CBCT-geleidings procedure vrij laag in vergelijking met de gerapporteerde stroomstraling in de literatuur. Hoewel de resultaten van het stroomstralingsmodel zonder bescherming de dosis overschat (ten opzichte van de klinische casussen), kunnen er ongeveer 240 casussen per jaar worden uitgevoerd zonder de jaarlijkse dosislimiet te overschrijden. De beste significante verlaging van de stroomstralingsdosis (98,2% - 98,9%) wordt bereikt door een combinatie van de wegwerp looddoeken en de plafond/tafel afscherming.

Een ander belangrijk kenmerk welke de multimodaliteits mogelijkheden onderstreept van het systeem is de mogelijkheid om eerder verworven onderzoeken (bijv. CT of MRI) te importeren in het systeem. Door deze samen te voegen met een lage dosis CBCT is het mogelijk om een gecombineerd volume te maken met goede zichtbaarheid van het doel en herhaalde toediening van contrast is niet nodig. Een nadeel van deze functie is dat de eerder verworven onderzoeken meestal worden uitgevoerd in rugligging en dat de CBCT-geleiding procedure vaak wordt uitgevoerd in buikligging. Deze positie verandering kan leiden tot aanzienlijke verschuivingen van de interne organen vooral in de bovenbuik. Op basis van de beschikbare gegevens van de nierinterventies is er een retrospectieve analyse uitgevoerd van de verplaatsing van de nieren door de positie verandering. Deze resultaten zijn beschreven in **hoofdstuk 9**.

In het laatste **hoofdstuk (10)** wordt de CBCT-geleidings techniek geëvalueerd in verschillende soorten procedures en anatomische locaties. Tevens worden er aanbevelingen bij het gebruik van CBCT-geleiding gedaan op basis van onze ervaring in meer dan 600 uitgevoerde procedures.

Appendix

Samenvatting (summary in Dutch)

Authors and affiliations

Review committee

List of publications

Acknowledgements (dankwoord)

Curriculum Vitae

St. Antonius Hospital, Nieuwegein, The Netherlands

Department of Radiology

Dr. J.P.M. van Heesewijk, dr. M.J.L. van Strijen, dr. H.W. van Es, T.Th.C. Overtoom, M. van Leersum, **S.J. Braak**, D. Meek

Department of Pulmonology

Dr. J. Herder

Department of Urology

Dr. H.H.E. van Melick, M.G. Onaca

Department of Vascular Surgery

Dr. J.P.P.M. de Vries, L. van Bindsbergen

Department of Clinical Physics

E. Meijer

Philips Healthcare, Best, The Netherlands

K. Zuurmond, H.C.J. Aerts

University Medical Center Utrecht, Utrecht, The Netherlands

Department of Radiology

Prof. dr. W.P.Th.M. Mali, dr. R.A.J. Nievelstein

University Medical Center St. Radboud, Nijmegen, The Netherlands

Department of Radiology

Prof. dr. L.J. SchulzeKool, dr. J.J. Futterer, dr. W.K.J. Renema, dr. Y.L. Hoogeveen, dr. F. de Lange, M.J. Arntz, W.M.H. Busser

Appendix

Samenvatting (summary in Dutch)

Authors and affiliations

Review committee

List of publications

Acknowledgements (dankwoord)

Curriculum Vitae

Review committee

Prof. dr. J.C. Grutters

Department of Pulmonology
St. Antonius Hospital
Nieuwegein, The Netherlands

Prof. dr. ir. J.J.W. Lagendijk

Department of Radiotherapy
University Medical Center Utrecht
Utrecht, The Netherlands

Prof. dr. F.L. Moll

Department of Surgery
University Medical Center Utrecht
Utrecht, The Netherlands

Prof. dr. L. Schultze Kool

Department of Radiology
University Medical Center St. Radboud
Nijmegen, The Netherlands

Further members of the opposition committee:

Prof. dr. M.A.A.J. van den Bosch

Department of Radiology
University Medical Center Utrecht
Utrecht, The Netherlands

Prof. dr. J.P.J. van Schaik

Department of Radiology
University Medical Center Utrecht
Utrecht, The Netherlands

Dr. E.P.A. Vonken

Department of Radiology
University Medical Center Utrecht
Utrecht, The Netherlands

Appendix

Samenvatting (summary in Dutch)

Authors and affiliations

Review committee

List of publications

Acknowledgements (dankwoord)

Curriculum Vitae

List of publications

C.M. Vernooij, **S.J. Braak**, B.H. Verweij en S.T.F.M. Frequin. *Een acute dwarslaesie op basis van een spontaan acuut spinaal subduraal hematoom*. Tijdschr Neurol Neurochir 2008;109:27-31.

S.J. Braak, C.A. de Witt, F.J.M. Disch, T.T.C. Overtoom en J.J. Westermann. *Percutaneous embolization on hereditary hemorrhagic telangiectasia patients with severe epistaxis*. Rhinology 2009;(47)2:166-171.

J.W.M. Aarts, **S.J. Braak** en M.F. Boomsma. *Neuroradiology case of the week, mixed laryngocele*. http://www.urmc.rochester.edu/radiology/education/materials/neuroradiology_case/

B.Verhoeven, M. Besselink en **S.J. Braak**. *Mesenteric thrombosis. Snapshot in surgery*. BJS 2009.

S.J. Braak, M.J.L. van Strijen, M. van Leersum, H.W. van Es en J.P.M. van Heesewijk. *Real-time 3D fluoroscopy guidance during needle interventions: Technique, Accuracy & Feasibility*. AJR 2010;194(5):W445-451.

L. van Bindsbergen, **S.J. Braak**, M.J.L. van Strijen en J.P.P.M. de Vries. *Type II endoleak embolization post-EVAR with use of real-time 3D fluoroscopic needle guidance*. JVIR 2010; 21:1443-1447.

S.J. Braak, M.J.L. van Strijen, H.W. van Es, J.P.M. van Heesewijk en R.A.J. Nievelstein. *Effective dose during needle interventions: cone-beam CT-guidance compared to CT-guidance*. JVIR 2011; 22:455-461.

S.J. Braak, G.J.M. Herder, J.P.M. van Heesewijk, M.J.L. van Strijen. *Pulmonary Masses: Initial Results of Cone-Beam CT-Guidance with Needle Planning Software for Biopsy*. CVIR 2011 [epub ahead of print]

S.J. Braak, H.E. van Melick, M.G. Onaca, J.P.M. van Heesewijk, M.J.L. van Strijen. *3D Cone-Beam CT Guidance in Renal Biopsy: Results in 43 Patients with Suspected Renal Masses*. European Radiology 2012 [epub ahead of print]

R. Peters, O. Peters, **S.J. Braak**, J. Verschakelen. *Pathology of the Thymus on CT-imaging*. JBR 2012 [Epub ahead of print]

S.J. Braak, K.Zuurmond, Hans C.J. Aerts, M. van Leersum, T.Th.C. Overtom, J.P.M. van Heesewijk, M.J.L. van Strijen. *Accuracy study of needle placement in percutaneous vertebroplasty: Cone-beam CT-Guidance versus conventional fluoroscopy*. Accepted pending revision CVIR.

WMH Busser, **SJ Braak**, MJ Arntz, WKJ Renema, JJ Futterer, MJL van Strijen, YL Hoogeveen, F de Lange, LJ SchultzeKool. *Cone-beam CT guidance provides superior accuracy for complex needle paths compared to CT guidance*. Submitted AJR.

S.J. Braak, M.J.L. van Strijen, E. Meijer, C.F.P. van Swol, J.P.M. van Heesewijk, W.P.Th.M. Mali. *Operator Radiation Exposure in Cone-beam CT guidance*. Submitted JVIR.

D. Meek, **S.J. Braak**, M.J.L. van Strijen, H.W. van Es, J.P.M. van Heesewijk. *Quantification of kidney movement in supine and prone position by merging conventional CT and cone beam CT images*. Submitted European Radiology

M.J.L. van Strijen, **S.J. Braak**. *Cone-beam CT and real time 3D needle guidance for biopsy and needle interventions: a pictorial of the technique and clinical indications*. Submitted for publication.

List of presentations

Oral presentation Dutch Radiological Society, annual meeting, Kaatsheuvel, November 2006.

The fate of the external carotid artery after carotid artery stenting.

Poster presentation 7th International HHT Scientific Conference, Capri, April 2007.

Percutaneous embolization in 12 patients with hereditary hemorrhagic telangiectasia and severe epistaxis.

Oral presentation Dutch Radiological Society, annual meeting, Rotterdam, September 2007.

Percutaneous embolization in 12 patients with hereditary hemorrhagic telangiectasia and severe epistaxis.

Oral presentation SMIT, Vienna, August 2008.

Real time 3D-fluoroscopy guidance during needle interventions: result of the first 61 patients.

Oral presentation SMIT, Vienna, August 2008.

Effective Dose during Needle Interventions: Real Time 3D Fluoroscopy Guidance versus CT-guidance.

Oral presentation SMIT, Vienna, August 2008.

Real Time 3D Fluoroscopy Guidance merged with MR images: a promising new technique.

Oral presentation Dutch Radiological Society, annual meeting, Rotterdam, Oktober 2008.

Real time 3D-fluoroscopy guidance during needle interventions: result of the first 85 patients.

Oral presentation Dutch Radiological Society, annual meeting, Rotterdam, Oktober 2008.

Considerable reduction of the effective dose during needle interventions: real-time 3D fluoroscopy guidance versus CT fluoroscopy.

Oral presentation RSNA, Chicago, December 2008.

Effective dose during Needle Interventions: Real time 3D-fluoroscopy guidance versus CT fluoroscopy.

Oral presentation ECR, Vienna, March 2009.

Live 3D-fluoroscopy guidance during needle interventions Clinical Implications & Benefits.

Poster presentation Dutch Surgical Society, annual meeting, Veldhoven, Mei 2009.

Type II endoleak embolisatie met real-time 3D-fluoroscopische naaldgeleiding.

Poster presentation CIRSE, Lissabon, September 2009.

Type II endoleak embolisation with real-time 3D-fluoroscopy guidance.

Oral presentation Dutch Radiological Society, annual meeting, Amsterdam, September 2009.

Type II endoleak embolisatie met real-time 3D-fluoroscopische naaldgeleiding.

Oral presentation Dutch Urology Society, annual meeting, Nieuwegein, May 2010.

3D needle guidance with cone-beam CT: results in 41 patients with a suspicion on renal cell carcinoma.

Oral presentation RSNA, Chicago, December 2010.

Radiation dose for interventional radiologists in 3D cone-beam CT guidance.

Appendix

Samenvatting (summary in Dutch)

Authors and affiliations

Review committee

List of publications

Acknowledgements (dankwoord)

Curriculum Vitae

Iedereen die heeft bijgedragen aan de totstandkoming van dit proefschrift wil ik hiervoor heel hartelijk danken. Een speciaal woord van dank verdienen in ieder geval de volgende personen:

*

Alle 'XperGuide' patiënten, zonder U voor mij geen promotie. Hartelijk dank voor uw medewerking!

Prof. dr. W.P.Th.M. Mali, geachte promotor, vanaf onze eerste ontmoeting ongeveer anderhalf jaar geleden heb ik met name één ding van u geleerd: 'niet te veel uitweiden, gewoon kort maar krachtig'. Het is een eer dat u mijn promotor wilde zijn, hartelijk dank!

Dr. M.J.L. van Strijen, geachte co-promotor, beste Marco, interesse in wetenschap had ik al, maar door jou ben ik begonnen en meegenomen in het XperGuide project. Bijna vanaf het prille begin ben ik betrokken geweest bij de procedures. Wat ik bijzonder gewaardeerd heb is het meedenken over studieprojecten, het nalezen en corrigeren van mijn manuscripten, fantoomstudies o.a. in de avonduren, bezoeken aan Philips Healthcare, meegaan/begeleiden tijdens (inter-)nationale presentaties, de workshops, gesprekken in Houten en promotie-ontwikkeling-etentjes. Eigenlijk het totale palet. Maar niet alleen heb jij mij begeleid in mijn promotie maar ook ben je een van mijn 'oud bazen' en heb jij mij vele knepen van het vak geleerd. Mijn bijzondere grote dank!

Dr. J.P.M. van Heesewijk, geachte co-promotor, beste Hans, als co-assistent beoordeelde jij mij met de aanvullende opmerking "is geschikt voor een opleidingsplaats Radiologie" en zie hier, mijn promotieboek en ondertussen collega Radioloog. Tijdens mijn gehele promotietraject ben jij altijd zeer betrokken en geïnteresseerd geweest. Jij was altijd bereid om mee te denken en een kritische noot te plaatsen daar waar nodig. Onder andere jou snelle correcties en hulp bij het engels heb ik zeer gewaardeerd. Bedankt dat jij als mijn oud opleider ook mijn co-promotor wil zijn.

De leden van de beoordelingscommissie, Prof. dr. L. Schultze Kool, Prof. dr. F.L. Moll, Prof. dr. ir. J.J.W. Lagendijk en Prof. dr. J.C. Grutters, dank voor het lezen, beoordelen en goedkeuren van mijn proefschrift.

Paranimfen drs. J.J.F. Bütterhoff, Jordi en mr. ir. R.X.J. Blokzijl, Xander, ik vind het een hele eer dat jullie tijdens mijn dissertatie naast mij staan. Ondertussen alweer 16 jaar bevriend. Dat dit weer een van de mooie herinneringen mag worden!

De mede-auteurs, respectievelijk prof. dr. Willem P.Th.M. Mali, dr. Rutger-Jan Nievelstein, dr. J.P.M. (Hans) van Heesewijk, dr. Marco J.L. van Strijen, dr. H. Wouter van Es, Tim Th.C. Overtoom, Mark van Leersum, David Meek, dr. Judith Herder, dr. Harm H.E. van Melick, Mircea G. Onaca, dr. Jean-Paul M. de Vries, Lars van Bindsbergen, Erica Meijer, Prof. dr. Leo J. SchulzeKool, dr. Jurgen J. Futterer, dr. W. Klaas Jan Renema, dr. Yvonne L. Hoogeveen, dr. Frank de Lange, Mark J. Arntz, Wendy M.H. Busser, Kirsten Zuurmond, Hans C.J. Aerts, zeer veel dank voor het meedenken en (mee-) schrijven van manuscripten en voor het meedoen aan verschillende studies, soms tot laat in de avond.

Radiologen St. Antonius Ziekenhuis, locatie Nieuwegein. Beste Hans Casparie, Tim Overtoom, Hans van Heesewijk, Marc van Leersum, Thomas Bollen, Wouter van Es, Jiri Zapletal, Marco van Strijen, Jan-Albert Vos. Ik voelde me direct thuis in Nieuwegein. Ik heb het als een voorrecht gezien om door jullie te worden opgeleid. Bedankt voor de mooie opleidingsjaren!

Assistenten radiologie St. Antonius Ziekenhuis (i.h.b. Thomas Bollen, Daniel van den Heuvel, Diana van der Linden, Judith Hemmer, Linda Koobs, Martijn Boomsma, Jeroen Prette, Michiel van Werkum, Julius Sala), naast het helpen van elkaar heb ik de sfeer en gezelligheid altijd zeer prettig gevonden. Hopelijk zie ik jullie nog vaak op verschillende congressen.

Collega specialisten en assistenten St. Antonius Ziekenhuis, zonder jullie verwijzingen geen Xperguide procedures en dus geen studie materiaal. Bedankt.

XperGuide-team en andere van Philips Healthcare, in het bijzonder Rinie Evenaar, Erik van Ommen, Alessandro Radaelli, Angelique Balguid, Kirsten Zuurmond, Hans van Garderen, Sjirk Boon, Cindy Crawl, Martine van Alfen en Bart Carelsen, ik heb altijd een zeer prettige samenwerking ervaren. Jullie waren betrokken en bereid om aanpassingen aan het systeem te doen. Jullie hulp bij de live casus / workshops en (dosis) berekeningen waren zeer prettig en we hadden gezellige (internationale) borrels/etentjes. Bedankt voor alles.

Laboranten en medewerkers van de afdeling radiologie St. Antonius Ziekenhuis, bedankt voor de fijne samenwerking. Ik heb iedere dag met veel plezier gewerkt in het St. Antonius Ziekenhuis en dit kwam mede door jullie.

Maatschap, assistenten en laboranten Ziekenhuis Groep Twente (ZGT), iedere dag ga ik met veel plezier naar mijn werk. De prettige werkomgeving, sfeer, betrokkenheid, collegialiteit is erg fijn. Ik hoop nog heel veel jaren met jullie te mogen samenwerken.

De sponsors Philips Healthcare, C.R. Bard inc., Guerbet Group, Bayer BV, de raad van bestuur Ziekenhuis Groep Twente (ZGT), St. Antonius Ziekenhuis (raad van bestuur), Microtek Medical BV, Galil-medical, MML-medical, Apriomed AB, iSYS Medizintechnik GmbH, Neorad AS., mijn grote dank voor uw bijdrage aan de tot standkoming van mijn dissertatie

Marja Kool, secretaresse afdeling Radiologie UMCU, bedankt voor alle hulp, het beantwoorden van mijn talloze vragen en de organisatie rondom mijn promotie.

Lieve vrienden en in het bijzonder Jaarclub Cambrinus, bedankt voor de interesse en steun. Dit heeft mij altijd een goed en vertrouwd gevoel gegeven. Sinds het begin van onze vriendschap zijn we een steeds hechtere vriendenclub geworden. Ik hoop dat wij nog veel mooie dingen met elkaar mogen meemaken.

Pap, mam, broer, Klazien, Carmen en Maurits S., ook jullie waren altijd zeer geïnteresseerd in mijn bezigheden en ontwikkelingen op het werkvlak en promotie. Bedankt voor de liefde, zorg en steun.

Drs. Drs. M.H. Braak-Gorny, lieve Helen, ik ben trots op je! Op een mooie toekomst!

*

Appendix

Samenvatting (summary in Dutch)

Authors and affiliations

Review committee

List of publications

Acknowledgements (dankwoord)

Curriculum Vitae

Sicco Jurjen Braak was born on June 16th 1978 in Utrecht, The Netherlands. He grew up in Groenekan, a small village nearby Utrecht. After graduating in 1996 at the college 'Het Nieuwe Lyceum' in Bilthoven, he started a study in Medical Technical Informatics at the University of Utrecht, because initially he was not admitted to the study of medicine.

Two months later he could still start his medical training at the Vrije Universiteit Amsterdam. In his second year he switched to the University of Utrecht. During his study of medicine he was an active member of his student society *Unitas Studiosorum Rheno-Traiectina*, for which he was Rector Senatus in 1999-2000. After graduating from medical school in 2004, he travelled 3 months in the United States and Canada with his girlfriend Helen. Hereafter he worked for three months at Falck Nutec, Maasvlakte Rotterdam, as a teacher in nautical first aid / medical care. Subsequently he worked for over a year at the Department of Emergency Care at Mesos Medical Center Utrecht, The Netherlands. In December 2005 he started as non-training resident in Radiology in the St. Antonius Hospital Nieuwegein, The Netherlands. Hereafter he started in March 2006 as a resident-in-training in Radiology under supervision of J.P.M. van Heesewijk, MD, PhD. During his residency he started in 2007 his PhD project at the Department of Radiology, St. Antonius Hospital Nieuwegein supervised by M.J.L. van Strijen, MD, PhD, J.P.M. van Heesewijk, MD, PhD and W.P.Th.M. Mali, MD, PhD (Professor in Radiology at the University Medical Center Utrecht). The results of his research presented in this thesis were published in several international scientific journals and presented at national and international conferences. In March 2011 he started as a radiologist at the Ziekenhuis Groep Twente (ZGT) in Almelo / Hengelo, The Netherlands. He lives in Utrecht and is married to Helen Braak-Gorny since 2005.